# Mathematical Modeling of Kidney Function During Pregnancy

by

Melissa Maria Stadt

A thesis
presented to the University of Waterloo
in fulfillment of the
thesis requirement for the degree of
Master of Mathematics
in
Applied Mathematics

Waterloo, Ontario, Canada, 2022

## Author's Declaration

This thesis consists of material all of which I authored or co-authored: see Statement of Contributions included in the thesis. This is a true copy of the thesis, including any required final revisions, as accepted by my examiners.

I understand that my thesis may be made electronically available to the public.

## Statement of Contributions

This thesis contains one research work that has been published in a scientific journal. The author lists for the paper and contributions made by myself and my coauthors are as follows:

**Adaptive changes in single-nephron GFR, tubular morphology, and transport in a pregnant rat nephron: modeling and analysis**

Melissa M. Stadt[1], Anita T. Layton[1,2]
**1** Department of Applied Mathematics, University of Waterloo, Waterloo, Ontario, Canada
**2** Department of Biology, Cheriton School of Computer Science, and School of Pharmacology, University of Waterloo, Waterloo, Ontario, Canada

M.M. Stadt ran the simulations, wrote compute code, analyzed data, interpreted results, prepared figures as well as drafted and revised the manuscript. A.T. Layton conceived and designed the research project, analyzed data, interpreted results as well as drafted and revised the manuscript.

## Abstract

During pregnancy, major adaptations must occur in the maternal body to be able to support the rapidly developing fetus and placenta. Adaptations occur in almost all tissues and organs. These changes are dynamic, complex, and not fully understood. In particular, due to the altered requirements of an expanded plasma volume and increased electrolyte needs of the fetus and placenta, major adaptations must occur in the kidneys. The goal for this thesis is to investigate the functional implications of the pregnancy-induced adaptations that happen in the kidneys by developing and analyzing computational models. In particular, we first developed pregnancy-specific epithelial transport models of a single nephron in a mid- and late pregnant rat to quantify how individual renal adaptations in morphology, hemodynamics, and transporter activity affect handling of electrolytes and volume along the nephron. Our results predict which transport adaptations are essential for a healthy pregnancy as well as predict transport adaptations that have not been investigated experimentally. We then developed full pregnancy-specific kidney models that includes heterogeneity in the nephron populations for a more accurate accounting of whole kidney function during pregnancy. Additionally, we developed models for renal function in a hypertensive female rat to analyze the effects of hypertension as well as hypertension with pregnancy on nephron transport.

Our results suggest that increased $Na^+$ transporter expression along the distal segments in female rats when compared to males may better prepare females for the demands of pregnancy. During pregnancy, it appears that significantly increased activity of distal segment $Na^+$ transporters with increased proximal tubule size are key in ensuring $Na^+$ retention occurs. $K^+$ retention is likely achieved through decreased distal segment $K^+$ secretion as well as increased activity of the $K^+$ pump. Together these changes allow the maternal body to retain sufficient $Na^+$ and $K^+$ for fetal cell function. During hypertension, similar relative changes in transporter activity in males and females results in similar transport properties. Specifically, $Na^+$ load is shifted to the distal segments requiring altered transporter expression to avoid excess natriuresis.

**Acknowledgements**

First I would like to thank my supervisor Dr. Anita Layton who introduced me to the world of mathematical physiology and has been a consistent support to push me to my full potential. She is always there to answer my many questions and gives ample opportunities for me to learn and grow as a researcher. I am looking forward to several more years of working together.

I would also like to thank my committee members, Dr. Brian Ingalls, Dr. Siv Sivaloganathan, and Dr. Anita Layton who took the time to review my thesis.

Thank you to my lab mates: Delaney Smith, Stéphanie Abo, Mehrshad Sadria, William Bell, Anderson White, Chris West, and Shervin Hakimi who have been a great encouragement as well as good company. I have learned something from each of them. I would also like to thank the many other colleagues and people who have been with me throughout my master's work.

Lastly, I would like to thank my family who have been a consistent support in everything I ever set out to do.

## Dedication

This thesis is dedicated to my family: mom, dad, and sisters Emily and Jessica.

# Table of Contents

# List of Figures

# List of Tables

# Chapter 1

# Introduction

Historically, females have largely been excluded from clinical trials and basic research studies due to concerns of running clinical trials on women of childbearing age as well as a lack of wide-spread knowledge about the impact of sex as a biological variable [24, 89]. This has resulted in highly male-centric physiology and biomedical research results. However, in recent years, as more emphasis on sex-specific research has increased, significant sex differences have been found in key structural and morphological differences in most physiological systems [24, 74, 78, 89].

A clear major difference between males and females is the ability of the female body (during child-bearing age) to undergo pregnancy and fully develop a fetus and placenta. Pregnancy clearly has major implications for reproductive organs, but most (if not all) physiological systems undergo major changes during a pregnancy. Pregnancy is arguably the ultimate non-pathological stress test that the body may ever undergo within a lifetime. In order to support a healthy pregnancy, the maternal body must adapt in a precisely coordinated and dynamic way. This is essential to support the supply of nutrients, electrolytes, and oxygen for the fetus and placenta. When these adaptations do not occur properly, this may lead to a complications which can have major short- and long-term health effects on both the mother and fetus [95]. In the past few decades, mathematical modeling has been used to study and provide key insights into a broad range physiological systems and applications in medicine [67]. Many of these models, however, have only been based on only male or not sex-specific data. This has left as serious gap in knowledge about female physiology. Recently, a few groups have made an effort to develop *sex-specific* models of physiological systems [74]. These include models of the circadian rhythms [3], the hypothalamic-pituitary-adrenal axis [102], kidney function [30, 59–61, 83, 110], blood pressure regulation [7, 8, 82], and liver metabolism [33]. However, much more work is yet to be

done as discussed in Ref. [74].

With so few sex-specific models, even fewer have been built to represent what occurs during a pregnancy [2]. This is a serious knowledge gap since the study of pregnancy and its related pathologies has historically been limited due to the fetal risks and ethical implications of running clinical trials on pregnant women. However, this limitation may be overcome, in part, by using computational modeling to test hypotheses and investigate the efficacy of potential therapies for gestational diseases *in silico* with the use of pregnancy-specific models.

An organ that has particularly benefitted from study through computational modelling is the kidney. In recent years, researchers have successfully developed models that can provide an accurate prediction of what is happening in the kidneys [73, 75, 121]. The kidneys are complex and have multifactorial functions to be able to not only filter out metabolic wastes, but maintain body volume and electrolyte homeostasis, among other important regulatory mechanisms. In recent years, it has been shown that there are significant differences in male and female kidneys [94, 103, 112]. Subsequent computational modeling efforts were made to investigate the functional implications of these renal sex differences [58–60, 83].

In the studies presented in this thesis, we expand on the previous work using female-specific computational models of kidney function to investigate what happens to the kidneys during pregnancy. The adaptations the kidneys undergo during pregnancy are highly complicated, with many competing factors. Thus using computational modelling can help put together what has been found in experimental literature and unravel what the functional implications of such pregnancy-induced changes are. In the following chapters we present the first pregnancy-specific kidney models as well as the analysis we conducted. In these studies we seek to answer the questions: How do the kidneys of a pregnant rat adapt to support the solute and volume demands of the fetus and placenta? Which adaptations may be the most important in maintaining the altered electrolyte and volume homeostasis found in pregnancy? How does hypertension-induced altered renal transport effect kidney function in a non-pregnant female versus a pregnant female? We seek to answer and develop hypotheses for each of these questions using the computational models described in the following chapters.

## 1.1 Outline of thesis

In Chapter 2 we discuss relevant background of kidney and pregnancy physiology. This starts with a review of the kidney's role in volume and electrolyte homeostasis, nephron

function, and basic renal anatomy. Additionally, we discuss relevant changes that happen in a maternal body during pregnancy. These are the motivating factors for the remaining studies. In Chapter 3 we detail how nephron epithelial transport is modeled in a superficial nephron via conservation equations and models of solute and volume transport in various cell types. We then discuss how the superficial nephron model is developed into a whole kidney model by considering heterogeneous nephron populations. The last part of Chapter 3 is a review of sex-specific computational models of kidney function which are the basis for this study. Chapter 4 is largely based on our published models of a superficial nephron in a mid- and late pregnant rat (see Ref. [109]). In this study we discuss how we made pregnancy-specific epithelial transport models of a pregnant rat superficial nephron based on experimental literature results that have shown pregnancy-induced adaptations in renal morphology, transporter abundance, and hemodynamics. We then used these models to quantify which adaptations have the largest impact on renal solute handling when compared to a non-pregnant rat using sensitivity analysis. In Chapter 5 we extend the superficial nephron model to a multiple nephron model as well as investigate the functional implications of hypertension on kidney function in a non-pregnant and mid-pregnant rat. Chapter 6 provides a summary of the results of this thesis as well as discuss the limitations and directions for future work.

# Chapter 2

# Physiology Background

Kidney function is highly complex, tightly regulated, and plays an important role in many mechanisms. How the kidneys ensure that the body has the right composition of blood to perform essential functions is a massive area of study. During pregnancy, many changes occur that alter how most physiological systems function. In Section 2.1 we review kidney physiology that is relevant to the studies in the following chapters. In Section 2.2 we highlight some major adaptations that occur during pregnancy that are relevant to kidney function. These areas of physiology are the motivating factors for the studies presented in the following chapters.

## 2.1 Kidney Physiology

Kidneys are commonly known for being filters for our blood, but they play a key role in regulating many body functions. The kidneys are located near the back side of the abdomen with one kidney on each side of the spine [40]. Despite making up <1% of total body weight, the kidneys are essential for regulating body homeostasis. The importance of the kidneys can be observed especially in those with end-stage renal disease, a debilitating condition that severely decreases quality of life with little that can be done outside of rigorous dialysis or a kidney transplant [1].

Some of the functions of the kidneys are regulation of the excretion of metabolic waste products, water and electrolyte homeostasis, acid-base balance, long-term blood pressure, red blood cell production, and more [40]. Indeed, entire books can (and have, e.g., see Ref. [40]) be written about kidneys and their functions. In this study we will focus on the

kidney's role in water and electrolyte homeostasis. Here I will highlight key functions and anatomy of the kidneys that are relevant to the background of this study.

### 2.1.1 Volume and Electrolyte Homeostasis

Tight regulation of solute and volume homeostasis is essential for healthy body function. Many of the body's functions serve to ensure that the extracellular fluid osmolality is contained within a normal range. Since many disease states can alter mechanisms that finely balance intake and output of water and solutes, disordered body fluid make up is one of the most common issues found in clinical medicine [114].

Water makes up about 55-65% of total body weight [114]. This total body water is distributed between the intracellular and extracellular fluid compartments. It has been approximated that about 2/3 of the total body water is in the intracellular fluid, while the remaining 1/3 is in the extracellular fluid. About 1/4 of the extracellular fluid is contained in the blood plasma. Since most of the biological membranes are permeable to water, water largely flows across membranes into the compartment with the higher osmolality. Total body water is dependent on a balance between intake and excretion. Intake is regulated physiologically by the thirst mechanism while excretion is mostly done through urinary excretion which is regulated by the kidneys [114].

The balance of $Na^+$ and water are closely linked. $Na^+$ is important for maintaining normal cellular homeostasis, blood pressure, and regulating fluid and electrolyte balance since it is the major solute in the extracellular fluid, thus driving osmolality (and hence water flow into compartments). $Na^+$ also plays an crucial role in excitability of muscle and nerve cells due to the dependence on appropriate electrochemical potential gradients.

Another tightly regulated electrolyte is $K^+$. Disorders of $K^+$ balance, both high (hyperkalemia) and low (hypokalemia) $[K^+]$ in the blood plasma is a serious side effect of many disorders [42, 43, 51, 134, 135]. The kidneys are the main mechanisms to regulate total-body $K^+$ balance [51, 55]. The kidney regulates body water and solute homeostasis via complex mechanisms through the renal plasma flow through the glomerulus and then tightly regulated transport in the nephrons (see Section 2.1.3; Fig. 2.1).

### 2.1.2 Anatomy

The kidneys receive over 1 L/min of blood (or about 20% of cardiac output) via the renal arteries. This blood flows into the glomeruli (plural of glomerulus), which are tightly

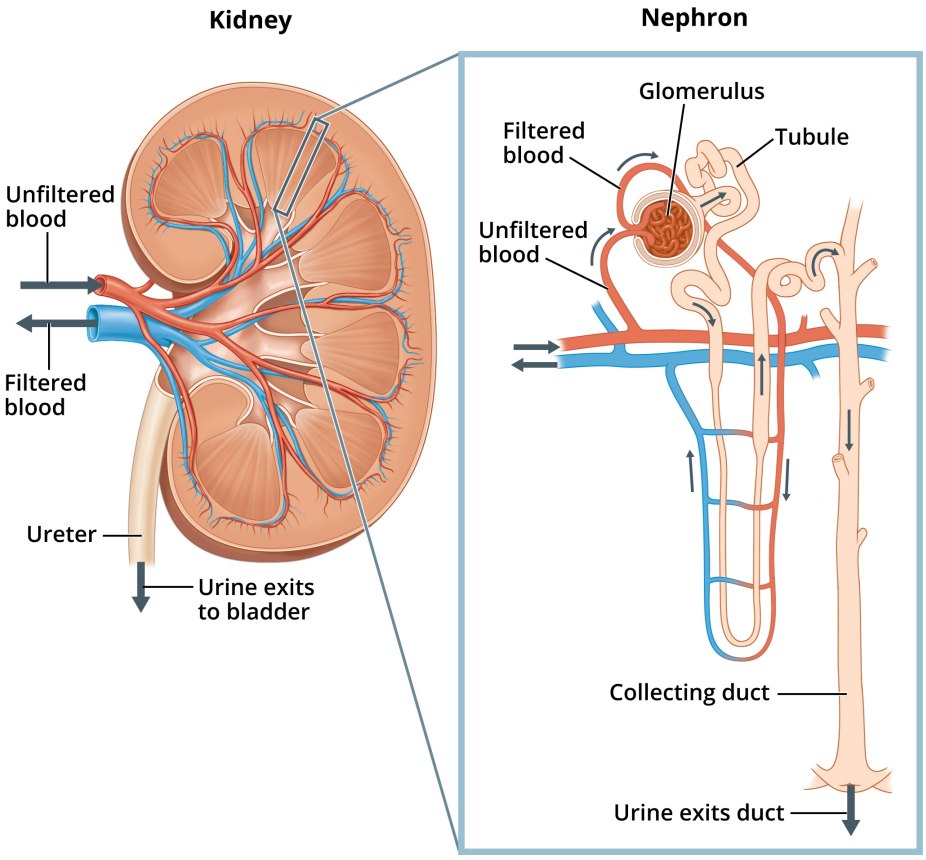


Figure 2.1: Diagram of a kidney and a close up of a nephron in the kidney. Figure used from National Institute of Diabetes and Digestive and Kidney Diseases, National Institutes of Health.

interconnected clusters of capillaries. Each glomerulus is surrounded by a capsule called Bowman's capsule. Solutes and volume are filtered from the glomerulus into Bowman's capsule. The fluid filtered is called filtrate and is essentially made up of the blood plasma without the proteins. Notably electrolytes such as $Na^+$, $K^+$, and $Cl^-$ are all freely filtered meaning that their concentrations in the filtrate are essentially the same as in the blood plasma. The filtrate goes into tiny tubules, which are called the nephrons (see Section 2.1.3). The nephrons are the functional units of the kidney. A diagram of a kidney and a nephron is given in Fig. 2.1.

The kidneys have two major regions; the cortex (outer region) and the medulla (inner region). These regions have different structural and functional properties. The glomeruli are located in the cortex. In the cortex, the segments of the nephrons are generally convoluted. In contrast, in the medulla, the tubules and vessels are tightly lined up and are in almost parallel arrangements. Each kidney also has a ureter which delivers urine to the bladder to be excreted. The ureter and the attached tubules are topologically outside of the body so that what is not reabsorbed from the tubules is excreted as waste in urine.

### 2.1.3 Nephrons

The functional unit of the kidney is the nephron. In a healthy human kidney, it is estimated that there are around 1 million nephrons. Rats are estimated to have about 36,000 nephrons. Starting at the Bowman's capsule (capsule around the glomerulus), nephrons are made up of a single layer of epithelial cells which vary depending on cell type. Different segments have different cell types that are specialized in fine-tuning the filtrate so that what is remaining at the end of the nephron is waste that is delivered to the bladder to be excreted in urine. Along the nephrons, solutes and volume are secreted and reabsorbed in a specialized way largely depending on the active and passive transporters in each cell, permeability, and the electrochemical gradient driven by the various cations and anions (see Section 2.1.4 for details about epithelial transporters). These processes are regulated by a combination of hormonal, neural, and intrarenal signals to ensure the body fluid is maintained at the correct balance [40]. A schematic diagram of a nephron is given in Fig. 2.2.

#### Nephron segments

As discussed above, the nephrons regulate its luminal fluid concentrations and flows through transport processes. This happens via reabsorption (removing solutes or volume) and se-

cretion (adding solutes) via various transport mechanisms along the nephron. These mechanisms can be via passive or active transport so that the contents of volume and solute in the fluid in the final urine is significantly different from the initial filtrate from the glomerulus. The segments of the nephron listed from the start to the end are: the proximal convoluted tubule, the proximal straight tubule, the descending thin limb of Henle's loop (or in short, the descending limb), the ascending thin limb of Henle's loop, the thick ascending limb of Henle's loop (a.k.a., thick ascending limb), the distal convoluted tubule, the connecting tubule, the cortical collecting duct, and the outer- and inner-medullary collecting ducts. A schematic diagram of a nephron and different cell types is in Fig. 2.2.

The first segment of the nephron is the proximal convoluted tubule. This segment is the longest nephron segment, is located in the cortex, and is convoluted. It is followed by the proximal straight tubule (also known as the S3 segment) which descends towards the medulla. The proximal convoluted tubule and proximal straight tubule will together be referred to as the "proximal tubule". The proximal tubule is where most reabsorption of volume and each of the freely filtered solutes occurs. Approximately 2/3 of the filtered load of $Na^+$, $K^+$, and fluid is reabsorbed in the proximal tubule.

The next segment is the descending thin limb of Henle's loop. We will refer to this as the descending limb. This segment is in the medulla and then loops into what is then called the thin and thick ascending limb of Henle's loop. In short these segments are referred to as the the thin and thick ascending limbs. These segments are notably different, especially in water permeability. In the descending limb, the membrane is permeable to water, thus is a place of major water reabsorption. The increased water reabsorption causes the luminal fluid to be more concentrated. This transport is largely passive. In contrast, the opposite happens in the ascending limb. The ascending limb is mostly impermeable to water. The thick ascending limb has major transporters such as the $Na^+$-$K^+$-$2Cl^-$ symporter which drives $Na^+$, $K^+$, and $Cl^-$ reabsorption. In total the ascending limb reabsorbs about 25% of the filtered $Na^+$. In summary, the descending limb reabsorbs water, but not electrolytes and the ascending limb absorbs electrolytes, but not water.

At the end of the ascending limb is the macula densa. The cells of the macula densa sense the luminal fluid content and generate signals that regulate renal function. After the macula densa is the distal convoluted tubule and then the connecting tubules. Due to the low amount of fluid left in the tubule relative to the initial filtrate, these segments do much of the fine-tuning to determine what will be excreted from the body.

The distal convoluted tubule is entirely within the cortex. The distal convoluted tubule is often considered in two parts. In the first part, the $Na^+$-$Cl^-$ cotransporter regulates the $Na^+$ and $Cl^-$ reabsorption, but in the last approximately 1/3 of the distal convoluted

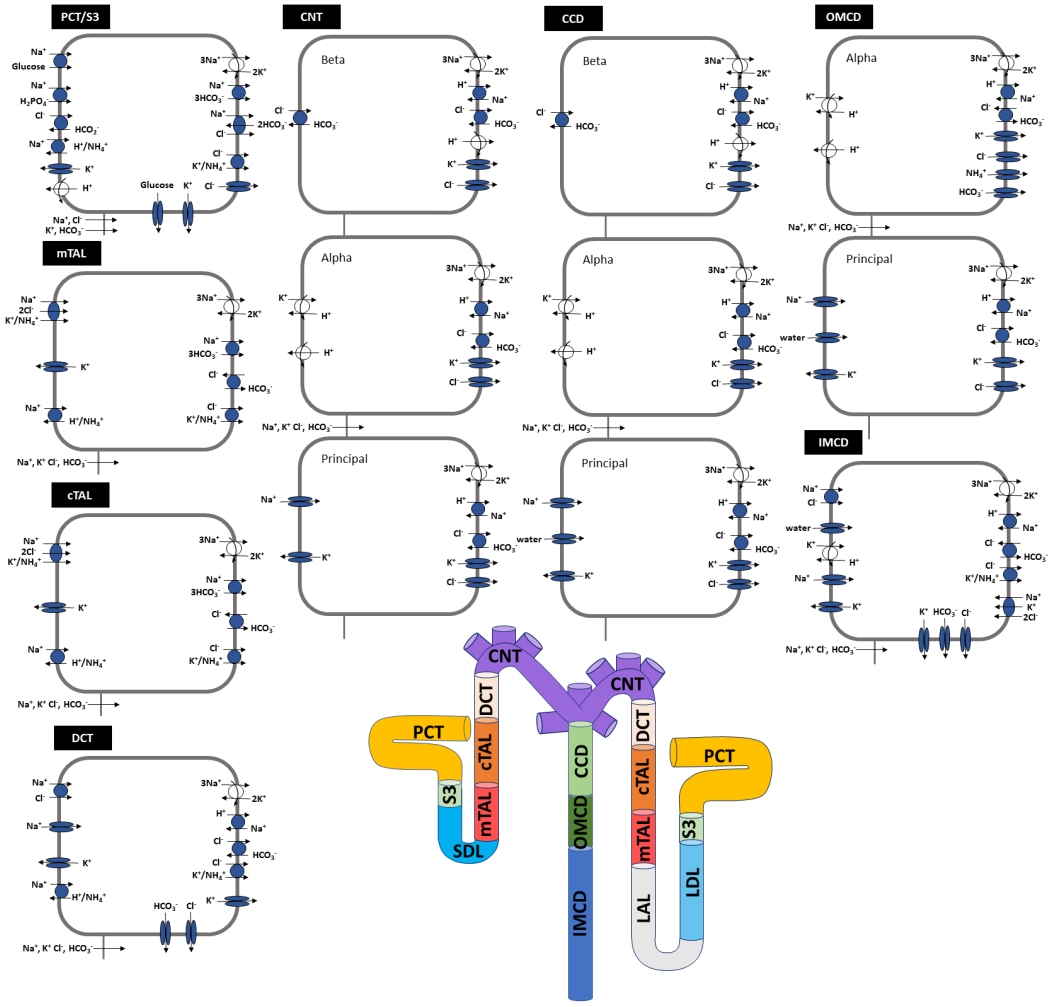


Figure 2.2: Schematic diagram of the nephron cells. The diagram displays main $Na^+$, $K^+$, and $Cl^-$ transporters as well as aquaporin water channels. Alpha and Beta indicate $\alpha$ and $\beta$ intercalated cell types. The nephron figure shows a superficial nephron and juxamedullary nephron (includes LAL and LDL). The shorter nephron (left side) is the superficial nephron and longer is a representative juxtamedullary nephron. PCT, proximal convoluted tubule; S3, proximal straight tubule; LDL, thin descending limb; LAL, thin ascending limb; mTAL, medullary thick ascending limb; cTAL, cortical thick ascending limb; DCT, distal convoluted tubule; CNT, connecting tubule; CCD, cortical collecting duct; OMCD, outer medullary collecting duct; IMCD, inner medullary collecting duct. Cells and nephron diagram adapted from Ref. [80].

tubule, the epithelial $Na^+$ channel regulates much of the $Na^+$ reabsorption in this segment [133].

The connecting tubule has multiple cell types: the principal and $\alpha-$ and $\beta-$intercalated cells[1]. The principal cells make up the majority (about 60%) of the cell types along this segment and largely mediate $Na^+$ and water reabsorption as well as $K^+$ secretion [69]. The $\alpha$-intercalated cells are known to express the $H^+$-ATPase transporter which secretes $H^+$ into the lumen, while the $\beta$ intercalated cells secrete $HCO_3^-$ via a $Cl^-$-$HCO_3^-$ exchanger known as Pendrin (See Fig. 2.2) [69, 116]. Functionally, this means that the principal cells play a key role in fine-tuning the water volume, $Na^+$, $K^+$, and $Cl^-$ concentrations of the filtrate while the intercalated cells play a key role in acid-base balance.

The connecting tubules coalesce with other nephrons to then come together in the collecting ducts. The collecting ducts are often considered in three parts depending on their regions: the cortical, outer-medullary, and inner-medullary collecting ducts. Along the collecting duct, the filtrate is close to urine and final fine-tuning occurs. In a similar way to the connecting tubule, the cortical, and outer-medullary regions of the collecting duct have intercalated cells (see Fig. 2.2).

#### Superficial and juxtamedullary nephrons

There are different nephron types in the kidneys. Specifically, these are called the superficial and juxtamedullary nephrons. The superficial nephrons make up about 66% of the total nephron population in rats. The glomeruli of superficial nephrons are at the top of the cortex and the loops of Henle only reach the outer medulla. The other type of nephrons are the juxtamedullary nephrons. The glomeruli of the juxtamedullary nephrons are lower in the cortex and have loops of Henle that reach into the inner medulla at various depths. When considering a full kidney, both nephron types should be considered (see Chapter 3). A diagram showing the differences between the superficial and juxtamedullary nephrons is given in Fig. 2.2.

### 2.1.4 Transporters

Along the nephrons, transport occurs via either the transcellular or paracellular route. The heterogeneity in the different segments along the nephron is due to the transporters located on the cells and the permeability of the paracellular space. A schematic diagram of

[1] $\alpha-$ and $\beta-$intercalated cells are also often called Type A and Type B intercalated cells, respectively

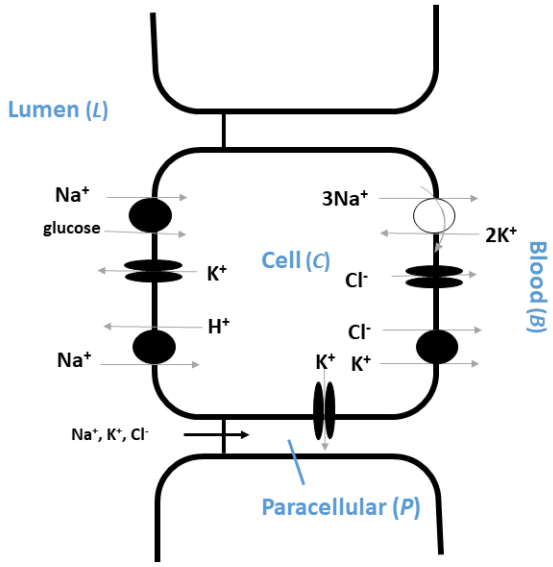


Figure 2.3: Schematic diagram of arbitrary epithelial cells along the nephron. Paracellular transport occurs in the paracellular space. Transcellular transport occurs in the cell membranes.

the paracellular space and cellular membranes is given in Fig. 2.3. A schematic diagram of the different cell types along the nephron with the various transporters and permeabilities is given in Fig. 2.2.

### Paracellular and transcellular transport

Paracellular transport occurs through the space between the epithelial cells called tight junctions. In the tight junctions there are proteins called claudins and occuludins that determine the permeability of the paracellular barrier in the various segments along the nephron. Paracellular transport occurs via net diffusion which depends on the concentration gradient of a particular solute as well as (for ions, i.e., charged molecules) the electrical potential difference. In other words, the solutes move down its electrochemical potential gradient.

Transcellular transport is a two-part process. First, the solute or water crosses the apical membrane of the cell (the cellular membrane that faces the lumen). Then, the solute or water leaves the cell through the basolateral membrane (membrane facing away from

the lumen). Various transporters and channels expressed on the cell mediate this transport. Transport can be passive, meaning it does not require energy, or active, meaning it requires energy. Transport that requires energy is generally moving a solute against its electrochemical potential gradient while passive transport moves a solute with its electrochemical potential gradient.

### Channels and transporters

Channels are small proteins with a "hole" through the center that allows for water or specific solutes to diffuse through them based on their structure. Common channels along the nephron are the $K^+$ channels, $Na^+$ channels, and water channels (often called aquaporins). Transport through channels is passive and is driven by the electrochemical gradient.

Transporters bind solutes and move them across a membrane. There are many types of transporters along the nephron, but we will highlight a few here. Cotransporters (also known as symporters) move multiple solutes across a membrane together. Another type of transporter is an exchanger (also known as an antiporter) which move solutes in the opposite directions across a membrane. For example, the $Na^+$-$K^+$-$2Cl^-$ cotransporter located in the thick ascending limb of the nephron is an important cotransporter that moves one $Na^+$ ion, one $K^+$ ion, and 2 $Cl^-$ ions out of the lumen into the cell. A key exchanger is the $Na^+$-$H^+$ exchanger which moved $Na^+$ out of the lumen into the cell in exchange with a $H^+$ going out of the cell into the lumen.

Primary active transporters require energy to move solutes up their electrochemical potential gradient. These transporters generally use energy from the hydrolysis of adenosine triphosphate (ATP) so that these transporters are known as ATPases. For example, the $Na^+$-$K^+$ pump known as the $Na^+$-$K^+$-ATPase is located on the basolateral side of every cell type along the nephron (and is located in most cells in the body). $Na^+$-$K^+$-ATPases pump three $Na^+$ ions out of the cell and two $K^+$ ions into the cell. This transport works against the $Na^+$ and $K^+$ electrochemical gradients and allows for the cell to maintain high intracellular [$K^+$] and low intracellular [$Na^+$]. Since volume largely "follows" the $Na^+$ gradient, the low intracellular [$Na^+$] also plays an integral role in maintaining cell volume.

In summary, the nephrons are highly specialized and regulated through various segments that play different parts to ultimately determine (when healthy) the amount of secretion and reabsorption of specific solutes in each segment so that what is excreted through urine is waste to ensure proper balance. This is is a complex process which computational modelling can serve to unravel to provide insights into renal function (see Chapter 3).

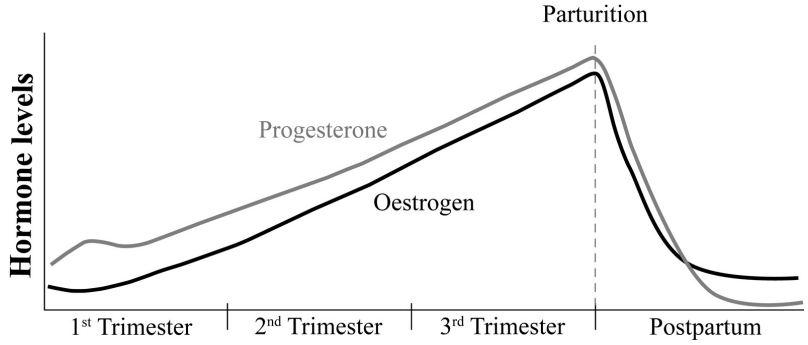


Figure 2.4: Approximate estrogen and progesterone levels during human pregnancy in the three trimesters. Note that post-partum period is not to scales as hormone levels reach pre-pregnancy levels at approximately five days post-partuirition. Figure used from Vink et al. [115].

## 2.2 Motivation: Pregnancy-induced adaptations

The maternal body undergoes vast changes to almost all organs and tissues during pregnancy [95]. These changes are dynamic, multi-factorial, and are often competing, which makes studying pregnancy physiology especially complicated. In the following sections we highlight key maternal adaptations that are relevant to this study. Specifically, we highlight maternal adaptations that effect the kidneys or that the kidneys play a role in maintaining.

### 2.2.1 Hormonal changes

During pregnancy, a placenta is formed which supports and protects the rapidly developing fetus. Additionally, the placenta mediates many maternal physiological functions by secreting hormones and growth factors into the maternal body [28, 95]. These hormones include prolactin, steroids, and neuroactive hormones. In particular, during pregnancy, plasma levels of estrogen and progesterone are at the highest levels found in a healthy woman. Specifically, during pregnancy, estradiol levels increase to about 50-fold non-pregnant levels and serum progesterone levels rise from about 1-20 ng/mL during non-pregnancy, but to about 100-200 ng/mL by the end of pregnancy [72]. Approximate estrogen and progesterone levels in the three trimesters and post-parturition are shown in Fig. 2.4.

The renin-angiotensin-aldosterone system (RAAS) is a regulatory hormone system that is significantly altered during pregnancy. The RAAS is a hormonal cascade that ulti-

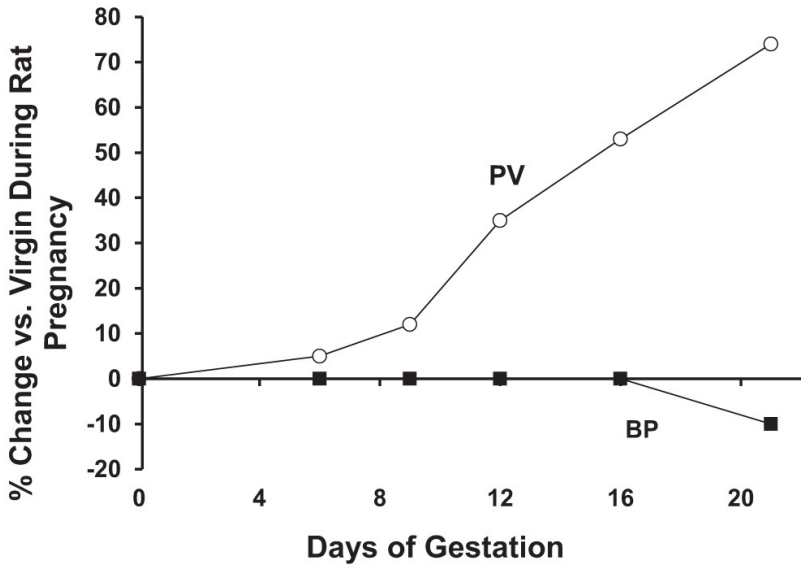


Figure 2.5: Time course of plasma volume (PV) during pregnancy and blood pressure (BP) given as a percent change from the non-pregnant value. Figure used from West et al. [129].

mately leads to production of the substrate angiotensinogen along with several enzymes and products [16,39,101]. Angiotensin II is the bioactive product generated by this cascade and is a key regulator in several mechanisms that affect blood pressure and $Na^+$ excretion [16, 39, 101]. During pregnancy, all components of the RAAS are significantly upregulated [87, 129]. This RAAS activation is likely the primary effector of the plasma volume expansion and $Na^+$ retention (see Sections 2.2.2 and 2.2.3) found in pregnancy [129]. The upregulated RAAS has implications on various functions in the maternal body, including kidney function.

Other regulatory systems are majorly altered during pregnancy. These changes all have effects on the function of various organs and tissues in the maternal body. We chose to highlight the RAAS as well as progesterone and estrogen because these are all known to effect renal function, which is the overall focus of this study. However, we note that many other hormone systems within the body are altered during pregnancy [95].

### 2.2.2 Plasma volume expansion

In order to sufficiently perfuse the placenta and fetus, a significant plasma volume expansion is required for a healthy pregnancy for both mother and fetus in most mammals, including

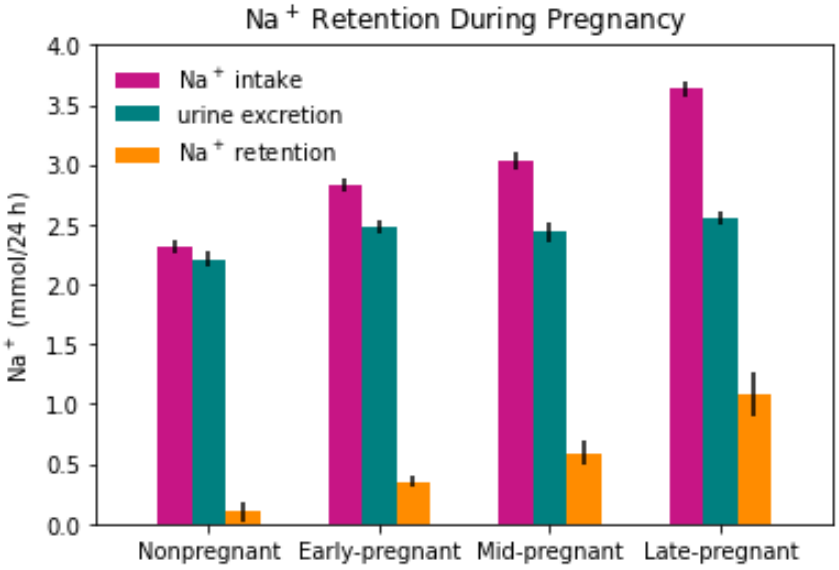


Figure 2.6: $Na^+$ intake and urine excretion during the different stages of pregnancy. Net $Na^+$ retention is indicated. Figure created using data from West et al. [125].

rats and humans [23,31,35,84,129]. See Fig. 2.5 for approximate continual plasma volume expansion in a rat. It is likely that the activated RAAS (see Section 2.2.1) is the primary effector of the pregnancy-induced plasma volume expansion and $Na^+$ retention (see Section 2.2.3) [129]. Remarkably, blood pressure typically decreases during pregnancy, despite this large volume change [31,129]. This is due to the multitude of changes that happen in the maternal cardiovascular system. The importance of the plasma volume expansion can be shown in that pregnancy disorders, such as gestational hypertension and preeclampsia, as well as fetal growth restriction are all strongly associated with a failure to expand plasma volume [23,26,50,104,129].

### 2.2.3 Electrolyte retention

In a non-pregnant rat, almost all $Na^+$ intake is excreted through urine. In contrast, beginning from early pregnancy, net $Na^+$ retention occurs [9,14,32,53,84,125,127]. Specifically, this means that while during pregnancy both $Na^+$ intake and urinary $Na^+$ excretion increase, the increase in urinary $Na^+$ excretion does not match the increase in intake, hence the maternal body retains $Na^+$. This is illustrated in Fig. 2.6. Since the kidneys regulate $Na^+$ homeostasis in the body, major adaptations must occur (see Section 2.2.4). This $Na^+$

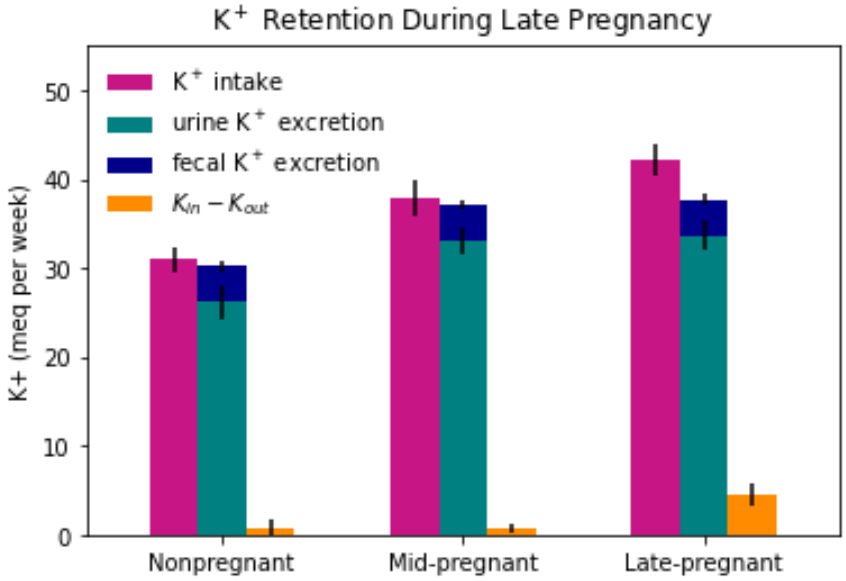


Figure 2.7: $K^+$ intake, excretion (fecal and urine), and retention for NP, MP, and LP rats. $K_{in}$ denotes $K^+$ intake and $K_{out}$ is the sum of urinary $K^+$ excretion and fecal $K^+$ excretion. Figure created using data from Churchill et al. [32].

retention is a crucial driver of the plasma volume expansion described previously because $Na^+$ and volume homeostasis are tightly related.

Another key electrolyte is $K^+$. Starting from late-pregnancy, net $K^+$ retention occurs. In a non-pregnant rat, over a day, 90% of all $K^+$ intake is excreted through urine, while the remaining 10% is excreted through feces. This again is not the case in late pregnancy as there is a significant $K^+$ retention [32,131]. Pregnancy-induced adaptations in the kidneys are the major drivers of this $K^+$ retention (see Section 2.2.4). Fig. 2.7 shows data that supports $K^+$ retention.

Much of this retained $Na^+$ and $K^+$ can be found in the feto-placental unit [9,32,131]. It is likely that $Na^+$ and $K^+$ are retained significantly because $Na^+$ and $K^+$ are essential electrolytes for cell function within the body, hence the fetus needs sufficient $Na^+$ and $K^+$ for proper cell function.

### 2.2.4 Renal adaptations

To regulate the electrolyte and volume retention required in pregnancy (see Sections 2.2.2 and 2.2.3), the kidneys undergo major adaptations in morphology [15,53,62], hemodynamics [19–21], and nephron transport [4,19,31,35,53,63,66,68,99,125–128,130–132].

One of the first gestational renal adaptations observed is the major increase in the glomerular filtration rate (GFR). GFR has been found to increase by about 40-50% in humans during pregnancy [23, 34] and about 30% in rats [19–21]. This phenomenon is remarkable as there are no other non-pathological states that sustain such a high increase in GFR for a significant amount of time. Even an early prominent renal physiologist, Dr. Homer Smith, remarked, "To a renal physiologist, a pregnant woman is a very interesting phenomenon. I do not know any other way to increase the filtration rate by 50% or better for prolonged periods." [108]. That marked increase in filtration must be matched by appropriate changes in nephron transport. Otherwise, the excessive water and electrolyte loss will likely prove fatal.

Further studies found that the kidney increases in volume during pregnancy [15,49,53, 62]. In particular, the proximal tubule lengthens [15, 49]. When taken in isolation, this should increase renal transport capacity.

Along the nephron segments, the activity of several key transporters have been found to change during pregnancy; such adaptations are complex and sometimes counterintuitive, when considered in isolation [35]. For example, Mahaney et al. [63] found that the activity of major $Na^+$ transporter, $Na^+$-$K^+$-ATPase is downregulated during pregnancy despite the large increase in $Na^+$ reabsorption. Other $Na^+$ transporters are also downregulated [68,128], while others are upregulated [47,125,126,130]. Upregulation of key water channels has also been found during mid-pregnancy (MP) and late-pregnancy (LP), likely facilitating increased water reabsorption [66, 99]. Renal adaptations are different during MP and LP. Specifically, during LP, net $K^+$ retention occurs in addition to $Na^+$ retention, which starts from early pregnancy (as discussed above). West et al. [131] found significant changes in $K^+$ transporters in the distal nephron segments during LP. $Na^+$ and $K^+$ transporter adaptations during pregnancy in the rat is discussed in a recent review by de Souza and West [35]. Details about pregnancy-induced renal adaptations and how they are studied using computational modeling are discussed in Chapters 4 and 5.

# Chapter 3

# Mathematical modeling of nephron epithelial transport

The computational models used in the following studies presented in this thesis are based on existing epithelial cell-based models of the nephrons [58–60, 75, 80]. In this chapter, I will describe the superficial nephron model in Section 3.1 which was later expanded into what is referred to as a multiple nephron model, meaning it captures heterogeneity within the nephron populations, and is described in Section 3.2. These equations are the baseline model equations used in each of the epithelial transport models used in the studies presented in the following chapters. How these models were developed into *pregnancy-specific* models or to model hypertension is discussed in Chapters 4 and 5.

## 3.1 Superficial nephron model

The cell-based epithelial transport models of a superficial nephron represent functionally distinct segments as follows: proximal convoluted tubule (PCT), proximal straight tubule (a.k.a. the S3 segment), short descending limb (SDL), thick ascending limb divided into the medullary and cortical parts (mTAL and cTAL, respectively), distal convoluted tubule (DCT), connecting tubule (CNT), and the collecting duct divided into the cortical and medullary segments: the cortical (CCD), outer-medullary (OMCD), and inner-medullary (IMCD) collecting ducts (see Fig. 2.2). These segments are listed in the order in which they appear in the nephron starting from Bowman's capsule. With the exception of the proximal tubule, each nephron segment is represented as a rigid tubule lined by a layer of epithelial

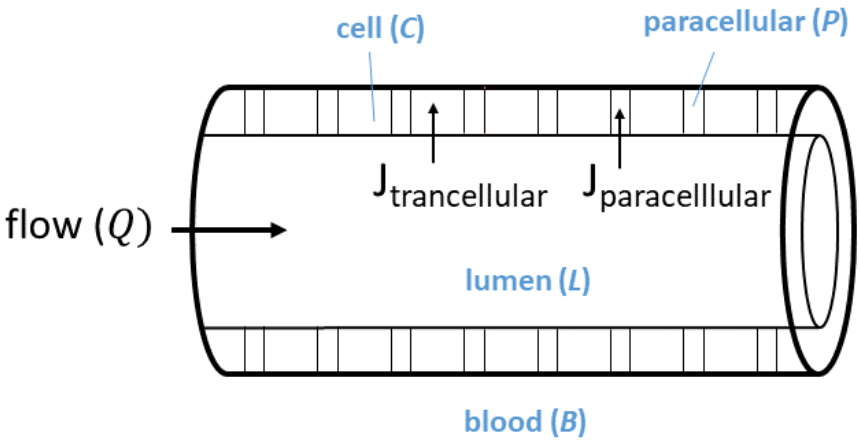


Figure 3.1: Schematic diagram of fluid flow in the nephron with paracellular and transcellular fluxes ($J_{\text{paracellular}}$ and $J_{\text{trancellular}}$, respectively).

cells, with apical and basolateral transporters that vary according to cell type. Each of the nephron segments have distinct transporters, permeabilities, and morphological properties. The model accounts for the following 15 solutes: $Na^+$, $K^+$, $Cl^-$, $HCO_3^-$, $CO_2$, $NH_3$, $NH_4^+$, $HPO_4^{2-}$, $H_2PO_4^-$, $H^+$, $HCO_2^-$, $H_2CO_2$, urea, and glucose. The model is made up of a large system of differential algebraic equations, formulated at steady state, and predicts luminal fluid flow, hydrostatic pressure, luminal fluid solute concentrations, cytosolic solute concentrations, membrane potential, and transcellular and paracellular fluxes.

### 3.1.1 Conservation equations

#### Conservation of volume

Consider a segment denoted by $i$, ($i$ = PCT, S3, etc.) at steady state. For a specific cell along the nephron the cellular, paracellular, and luminal space are represent by different compartments. Conservation of volume in the cellular and paracellular compartments is given by

$$J^i_{v,LC} + J^i_{v,BC} + J^i_{v,PC} = 0 \tag{3.1}$$
$$J^i_{v,LP} + J^i_{v,BP} + J^i_{v,CP} = 0 \tag{3.2}$$

where $J^i_{v,ab}$ denotes the transmembrane flux of volume from compartment $a$ to compartment $b$ where $a$ and $b$ are given as $L$, $B$, $P$ or $C$ which denote the lumen, blood, cellular, and paracellular compartments, respectively. In the lumen, for non-coalescing segments (i.e., not the CNT and IMCD, explained below), conservation of volume is given by

$$\frac{dQ^i}{dx} = 2\pi r^i \hat{J}^i_{v,L} \tag{3.3}$$

where $Q^i$ denotes the volume flow, $r^i$ is the luminal radius, and $\hat{J}^i_{v,L} \equiv J^i_{v,LC} + J^i_{v,LP}$ is the total volume flux. The luminal fluid flow is given by pressure-driven Poiseuille flow

$$\frac{dP^i}{dx} = -\frac{8\mu Q^i}{\pi (r^i)^4} \tag{3.4}$$

where $P^i$ is the hydrostatic pressure and $\mu$ is the luminal fluid viscosity.

### Flow-dependent tubular transport

All segments except the proximal tubule are non-compliant (i.e., the radius $r^i$ is a constant). In the proximal tubule, the flow-dependent transport for a compliant tubule is used. These questions were originally developed by Weinstein et al. [123] and are briefly described here.

The compliant luminal radius in the proximal tubule ($r_{\mathrm{PT}}$) is given by

$$r_{\mathrm{PT}} = r^0_{\mathrm{PT}} \left(1 + \mu_{\mathrm{PT}} \left(P_{\mathrm{PT}} - P^0_{\mathrm{PT}}\right)\right) \tag{3.5}$$

where $r^0_{\mathrm{PT}}$ is the reference radius, $P^0_{\mathrm{PT}}$ is the reference pressure, and $\mu_{\mathrm{PT}}$ characterizes tubular compliance. In the proximal tubule, luminal fluid flow modulates transporter density via mechanosensory function from torque of the epithelial microvilli [37], so then the microvillous torque is given by

$$\tau^{\mathrm{PT}} = \frac{8\mu Q^{\mathrm{PT}} l_{\mathrm{PT,mv}}}{r^2_{\mathrm{PT}}} \left(1 + \frac{l_{\mathrm{PT,mv}} + \delta_{\mathrm{PT,mv}}}{r_{\mathrm{PT}}} + \frac{l^2_{\mathrm{PT,mv}}}{2r^2_{\mathrm{PT}}}\right) \tag{3.6}$$

where $l_{\mathrm{PT,mv}} = 2.5$ $\mu$m is the microvillous length and $\delta_{\mathrm{PT,mv}} = 0.15\mu$m denotes the height above the microvillous tip where drag is considered. The values for these parameters are used from Refs. [80, 123]. Using this we compute

$$S_{\mathrm{torq}} = 1 + s\left(\frac{\tau_{\mathrm{PT}}}{\tau^0_{\mathrm{PT}}} - 1\right) \tag{3.7}$$

where $\tau^0_{\mathrm{PT}}$ is computed by evaluating (3.6) when $Q^{\mathrm{PT}}$ is the initial volume flow at the start of the PT and $r_{\mathrm{PT}}$ is the initial PT radius, $s = 1.3$ is a scaling factor in the proximal convoluted tubule and $s = 0.65$ in the S3 segment in each of the models. The density of the apical and basolateral transporters in the proximal tubules is then scaled by $S_{\mathrm{torq}}$ to capture the torque-modulated effects [37, 123].

### Coalescing segments

In the late segments of the nephron, specifically the CNT and IMCD coalesce with other nephrons. To capture this in the model, water and solute flows are scaled by the tubule population where $\omega^i$ (for $i =$ CNT or IMCD) denotes the fraction of the tubule remaining at a given spatial location where

$$\frac{d}{dx}\left(\omega^i Q^i\right) = 2\pi r^i \hat{J}^i_{v,L} \tag{3.8}$$

denotes the conservation of volume in the lumen.

The fraction of connecting tubules $\omega^{\mathrm{CNT}}$ remaining at the coordinate $x^{\mathrm{CNT}}$ (determined as the distance from the start of the connecting tubule) is given by

$$\omega^{\mathrm{CNT}}(x^{\mathrm{CNT}}) = 2^{-2.32 x^{\mathrm{CNT}}/L^{\mathrm{CNT}}} \tag{3.9}$$

where $L^{\mathrm{CNT}}$ is the connecting tubule length. The collecting ducts also coalesce in the inner medulla so that the fraction of collecting ducts at distance from the start, denoted by $x^{\mathrm{IMCD}}$ is given by

$$\omega^{\mathrm{IMCD}}\left(x^{\mathrm{IMCD}}\right) = 0.1\left(1 - 0.95\left(\frac{x^{\mathrm{IMCD}}}{L^{\mathrm{IMCD}}}\right)^2\right)\exp\left(-2.75\frac{x^{\mathrm{IMCD}}}{L^{\mathrm{IMCD}}}\right) \tag{3.10}$$

where $L^{\mathrm{IMCD}}$ is the length of the inner-medullary collecting duct. Equations (3.9) and (3.10) are derived in Layton et al. [81].

### Conservation of non-reacting solutes

For a given non-reacting solute $k$ (i.e., $k =$Na$^+$, K$^+$, Cl$^-$, $CO_2$, urea, or glucose), conservation of mass in the paracellular and cellular space is given by

$$J^i_{k,LC} + J^i_{k,BC} + J^i_{k,PC} = 0 \tag{3.11}$$

$$J^i_{k,LP} + J^i_{k,BP} + J^i_{k,CP} = 0 \tag{3.12}$$

respectively, where $J^i_{k,ab}$ denotes the transmembrane flux of solute $k$ from compartment $a$ to compartment $b$.

In the lumen, conservation is given by

$$\frac{d}{dx}\left(Q^i C^i_{k,L}\right) = 2\pi r^i \hat{J}^i_{k,L} \tag{3.13}$$

for non-coalescing segments and

$$\frac{d}{dx}\left(\omega^i Q^i C^i_{k,L}\right) = \hat{J}^i_{k,L} \tag{3.14}$$

for coalescing segments (i.e., the CNT and IMCD), where $\hat{J}^i_{k,L} \equiv J^i_{k,LC} + J^i_{k,LP}$ denotes that total flux of solute $k$, $\omega^i$ is as defined in (3.9) and (3.10) for the CNT and IMCD, respectively, and $C_{k,L}$ is the luminal concentration of solute $k$.

### Conservation of reacting solutes

For reacting solutes, conservation is imposed on the total buffers, so that in the cellular and paracellular compartments ($m = C$ or $P$) we have

$$\hat{J}^i_{CO_2,m} + \hat{J}^i_{HCO_3^-,m} + \hat{J}^i_{H_2CO_3,m} = 0 \tag{3.15}$$

$$\hat{J}^i_{A,m} + \hat{J}^i_{B,m} = 0 \tag{3.16}$$

where $\hat{J}^i_{k,m}$ is the total flux of solute $k$ into compartment $m$, so that in particular we have $\hat{J}^i_{k,C} \equiv J^i_{k,LC} + J^i_{k,BC} + J^i_{k,PC}$ and $\hat{J}_{k,P} \equiv J^i_{k,LP} + J^i_{k,BP} + J^i_{k,CP}$, $(A, B)$ is a buffer pair where $A$ denotes acid and $B$ denotes base. The pairs represented in this model are ($HPO_4^{2-}$, $H_2PO_4^-$), ($NH_3$, $NH_4^+$) or ($HCO_2^-$, $H_2CO_2$). In the lumen, for reacting solutes, we have that

$$\frac{d}{dx}\left(Q^i C^i_{CO_2,L} + Q^i C^i_{HCO_3,L} + Q^i C^i_{H_2CO_3,L}\right) = \hat{J}^i_{CO_2,L} + \hat{J}^i_{HCO_3,L} + \hat{J}^i_{H_2CO_3,L} \tag{3.17}$$

$$\frac{d}{dx}\left(Q^i C^i_{A,L} + Q^i C^i_{B,L}\right) = \hat{J}^i_{A,L} + \hat{J}^i_{B,L} \tag{3.18}$$

with the same notation as above. Additionally, conservation is imposed on the protons so that

$$\sum_k \hat{J}^i_{k,m} = 0 \tag{3.19}$$

for $k =$ $H^+$, $NH_4^+$, $H_2PO_4^-$, $H_2CO_3$, and $H_2CO_2$.

#### Conservation of charge

Since ions are charged solutes, across a cell membrane there are both internal and external conducting solutions therefore giving a potential difference across the membrane. It is assumed that within each compartment there is electroneutrality so that

$$\sum_k z_k C_{k,m} = 0 \tag{3.20}$$

where $z_k$ is the valence of solute $k$ and $C_{k,m}$ is the concentration of solute $k$ in compartment $m$ ($m = P$ or $C$). Also it is assumed that there is no net current into the lumen so that

$$\sum_k z_k F \left( J_k^{CL} + J_k^{PL} \right) = 0. \tag{3.21}$$

where $F$ denotes Faraday's constant, $L$ is the lumen, and $J_k^{CL}$ and $J_k^{PL}$ denote the flux of solute $k$ from the cellular and paracellular space to the lumen, respectively.

### 3.1.2 Membrane transport

#### Volume transport

For a membrane between compartments $a$ and $b$, for a segment $i$, volume flux is denoted by $J_{v,ab}^i$ and given by the Kedem-Katchalsky equation for water transport

$$J_{v,ab}^i = A_{ab}^i L_{p,ab}^i \left( \sigma_{ab}^i \Delta\pi_{ab}^i + \Delta P_{ab}^i \right) \tag{3.22}$$

where $A_{ab}^i$ denotes the membrane area, $L_{p,ab}^i$ denotes the hydraulic permeability, $\sigma_{ab}^i$ is the reflection coefficient,

$$\Delta\pi_{ab}^i = RT\Sigma_k \Delta C_{k,ab}^i$$

where $\Sigma_k \Delta C_{k,ab}^i$ is the osmolality difference where $C_{a,b}^i$ denotes the concentration gradient of solute $k$ along membrane $a, b$, $R$ is the ideal gas constant, $T$ is the thermodynamic temperature, and $\Delta P_{ab}^i$ is the hydrostatic pressure gradient.

#### Solute transport

Unlike transmembrane volume flux ($J_{v,ab}^i$; see Eq. (3.22)), transmembrane solute flux ($J_{k,ab}$) depends on electrodiffusion through channels, coupled transport through transporters, and

primary active transport across ATP-driven pumps (as discussed in Chapter 2). In general, for a solute $k$ across membrane $a, b$, solute flux $J^i_{k,ab}$ is given by

$$J^i_{k,ab} = \left(1 - \sigma^i_{k,ab}\right) \bar{C}^i_{k,ab} J^i_{v,ab} + J^i_{k,ab}(\text{electrodiffusive}) + J^i_{k,ab}(\text{coupled}) + J^i_{k,ab}(\text{ATP-driven}) \tag{3.23}$$

where the first term represents convective transport, $\sigma^i_{k,ab}$ is the reflection coefficient, and

$$\bar{C}^i_{k,ab} = \frac{C^i_{k,a} - C^i_{k,b}}{\ln C^i_{k,a} - \ln C^i_{k,b}} \tag{3.24}$$

is the mean membrane solute concentration where $C^i_{k,a}$ and $C^i_{k,b}$ denote the concentrations of solute $k$ in compartment $a$ and $b$ of segment $i$, respectively.

The second term in (3.23), $J^i_{k,ab}(\text{electrodiffusive})$, denotes solute transport via electrodiffusive flux. This is transport through channels. For ions, electrodiffusive flux is given by the Goldman-Hodgkin-Katz equation

$$J^i_{k,ab}(\text{electrodiffusive}) = h^i_{k,ab} \zeta^i_{k,ab} \left( \frac{C^i_{k,a} - C^i_{k,b} \exp\left(-\zeta^i_{k,ab}\right)}{1 - \exp\left(-\zeta^i_{k,ab}\right)} \right) \tag{3.25}$$

where $h^i_{k,ab}$ is the membrane permeability for solute $k$,

$$\zeta^i_{k,ab} = \frac{z_k F}{RT} \Delta V^i_{ab}$$

where $z_k$ is the solute valence, $F$ is Faraday's constant, $R$ is the ideal gas constant, $T$ is the thermodynamic temperature, and $\Delta V^i_{ab}$ denotes the electrical potential difference.

For an uncharged solute, the electrodiffusive flux is given by simple diffusion

$$J^i_{k,ab}(\text{electrodiffusive}) = h^i_{k,ab} \left(C^i_{k,a} - C^i_{k,b}\right) \tag{3.26}$$

since transport only depends on the concentration gradient (i.e., not on the electric potential).

The third term in (3.23), $J^i_{k,ab}(\text{coupled})$, denotes the total coupled transport of a solute $k$ across cotransporters and exchangers. The final term in (3.23), $J^i_{k,ab}(\text{ATP-driven})$, denotes the total transport via primary active transport (i.e., across ATPases). Transport via cotransporters, exchangers, and primary active transport is described below.

### Transporters

Transport via cotransporters, exchangers, and primary active transport are modeled based either on existing kinetic models for each transporter. Here we highlight a few key transporters and how they are modeled.

*Cotransporters and Exchangers.* Exchangers are transporters that transport two or more solutes in the opposite directions across a membrane. One example is the $Na^+/H^+$ exchanger isoform 3 (NHE3), which is located along the apical membrane of the proximal tubule and the thick ascending limb. NHE3 exchanges $Na^+$ from the lumen with intracellular $H^+$ or $NH_4{}^+$. That is there is competitive binding of intracellular $H^+$ and $NH_4{}^+$. Indeed, NHE3 plays a major role in both $NH_4{}^+$ secretion and $Na^+$ reabsorption in the proximal tubule. The model for NHE3 transport was developed by Weinstein et al. [117]. The model derivation is described below.

Following the same notation as in in Weinstein et al. [117], let $A$, $B$, $C$ denote $Na^+$, $H^+$, and $NH_4{}^+$, respectively, with $X$ denoting an empty transporter. Then let $a^i$ and $a^e$ denote the intracellular $[Na^+]$ and extracellular $[Na^+]$, respectively and analogously for $[H^+]$ and $[NH_4{}^+]$ (i.e., using lower case $b$ and $c$). Similarly let $x^i$, $x^e$ denote empty transporter density on the internal and external face of the membrane, respectively, and $ax$ is of the complex of $Na^+$ with a transporter, so that

$$K_a = \frac{a^i x^i}{(ax)^i} = \frac{a^e x^e}{(ax)^e} \tag{3.27}$$

where $K_a$ is an equilibrium constant for $Na^+$. Similarly letting $b$ denote the $[H^+]$ and $c$ denote $[NH_4{}^+]$ we have

$$K_b = \frac{b^i x^i}{(bx)^i} = \frac{b^e x^e}{(bx)^e}, \qquad K_c = \frac{c^i x^i}{(cx)^i} = \frac{c^e x^e}{(cx)^e} \tag{3.28}$$

where $K_b$ and $K_c$ are equilibrium constants. Next, assume that the total amount of carrier is conserved (denoted by $x_{\mathrm{T}}$) we get

$$x^i + (ax)^i + (bx)^i + (cx)^i + x^e + (ax)^e + (bx)^e + (cx)^e = x_T \tag{3.29}$$

and that there is zero net flux meaning

$$T_a(ax)^i + T_b(bx)^i + T_c(cx)^i = T_a(ax)^e + T_b(bx)^e + T_c(cx)^e, \tag{3.30}$$

where $T_k$ is the transport rate of solute $k$. Let

$$\alpha \equiv \frac{a}{K_a}, \qquad \beta \equiv \frac{b}{K_b}, \qquad \gamma \equiv \frac{c}{K_c} \tag{3.31}$$

be non-dimensionalized concentrations. Note that by (3.27) we have that

$$(ax)^i = \frac{a^i x^i}{K_a} = \frac{a^i}{K_a} x^i = \alpha^i x^i \tag{3.32}$$

and in the same way $(bx)^i = \beta^i x^i$ and $(cx)^i = \gamma^i x^i$. Then plugging this into (3.29) we have that

$$x^i \left(1 + \alpha^i + \beta^i + \gamma^i\right) + x^e \left(1 + \alpha^e + \beta^e + \gamma^e\right) = x_T. \tag{3.33}$$

In the same way, (3.30) can be written as

$$-x^i \left(T_a \alpha^i + T_b \beta^i + T_c \gamma^i\right) + x^e \left(T_a \alpha^e + T_b \beta^e + T_c \gamma^e\right) = 0. \tag{3.34}$$

Thus (3.33) and (3.34) give a $2 \times 2$ system of equations to solve for $x^i$ and $x^e$:

$$\begin{pmatrix} 1 + \alpha^i + \beta^i + \gamma^i & 1 + \alpha^e + \beta^e + \gamma^e \\ -\left(T_a \alpha^i + T_b \beta^i + T_c \gamma^i\right) & T_a \alpha^e + T_b \beta^e + T_c \gamma^e \end{pmatrix} \begin{pmatrix} x^i \\ x^e \end{pmatrix} = \begin{pmatrix} x_T \\ 0 \end{pmatrix}.$$

Let $\Sigma$ denote the determinant of the matrix so that

$$\Sigma = (1 + \alpha^i + \beta^i + \gamma^i)(T_a \alpha^e + T_b \beta^e + T_c \gamma^e) + (T_a \alpha^i + T_b \beta^i + T_c \gamma^i)(1 + \alpha^e + \beta^e + \gamma^e) \tag{3.35}$$

and then by using Cramer's rule we have that

$$x^i = x_T (T_a \alpha^e + T_b \beta^e + T_c \gamma^e)/\Sigma \tag{3.36}$$

$$x^e = x_T (T_a \alpha^i + T_b \beta^i + T_c \gamma^i)/\Sigma. \tag{3.37}$$

The flux of $Na^+$, $H^+$, and $NH_4{}^+$ across the NHE3 can now be computed. Let $J_a$ denote the outward flux of $Na^+$ across the NHE3 so that

$$J_a = T_a (ax)^i - T_a (ax)^e \tag{3.38}$$

which using (3.32) we get that

$$J_a = T_a \left(\alpha^i x^i - \alpha^e x^i - \alpha^e x^e\right). \tag{3.39}$$

Then substitute (3.36) and (3.37) into (3.39) to get

$$\begin{aligned} J_a &= T_a \left(\alpha^i x^i - \alpha^e x^e\right) \\ &= T_a \left[\alpha^i \left(x_T (T_a \alpha^e + T_b \beta^e + T_c \gamma^e)/\Sigma\right) - \alpha^e \left(x_T (T_a \alpha^i + T_b \beta^i + T_c \gamma^i)/\Sigma\right)\right] \\ &= \frac{x_T T_a}{\Sigma} \left[\alpha^i \left(T_a \alpha^e + T_b \beta^e + T_c \gamma^e\right) - \alpha^e \left(T_a \alpha^i + T_b \beta^i + T_c \gamma^i\right)\right] \\ &= \frac{x_T T_a}{\Sigma} \left[\alpha^i \left(T_b \beta^e + T_c \gamma^e\right) - \alpha^e \left(T_b \beta^i + T_c \gamma^i\right)\right] \\ &= \frac{x_T T_a}{\Sigma} \left[T_b \left(\alpha^i \beta^e - \alpha^e \beta^i\right) + T_c \left(\alpha^i \gamma^e - \alpha^e \gamma^i\right)\right]. \end{aligned}$$

In the same way we get that the net outward flux of $H^+$ and $NH_4{}^+$ are given by

$$J_b = \frac{x_T T_b}{\Sigma}\left[T_a\left(\beta^i\alpha^e - \beta^e\alpha^i\right) + T_c\left(\beta^i\gamma^e - \beta^e\gamma^i\right)\right] \tag{3.40}$$

$$J_c = \frac{x_T T_c}{\Sigma}\left[T_a\left(\gamma^i\alpha^e - \gamma^e\alpha^i\right) + T_b\left(\gamma^i\beta^e - \gamma^e\beta^i\right)\right] \tag{3.41}$$

respectively. Hence, using the internal and external concentrations of $Na^+$, $H^+$, and $NH_4{}^+$, translocation rates, and carrier amount can be used to compute the fluxes across the NHE3 antiporter can be computed. Weinstein et al. [117] fit the model parameters to experimental kinetics data since these values such as the translocation rate cannot be measured directly. Some assumptions were also made, specifically the translocation rates are fixed and both the internal and external binding affinities are taken to be equal. The NHE3 model is a type of model that has been extended to capture the transport of other exchangers and transporters including the $Na^+$-$K^+$-$2Cl^-$ and $K^+$-$Cl^-$ cotransporters [75].

*Non-equilibrium Thermodynamic Formalism.* The non-equilibrium thermodynamic formalism is used to determine fluxes for transporters where no kinetic model has been developed, largely due to the transporter not being fully characterized experimentally [44,75,124]. Weinstein [124] first developed this approach for modeling renal epithelial transport. We use the same notation as in Layton & Edwards [75] in our description below.

First, recall that diffusive flux is driven by the electrochemical potential gradient. If we consider a compartment $i$ for some solute $k$ the electrochemical potential can be given by

$$\mu_k^i = \mu_k^0 + RT\ln C_k^i + z_k F\Psi^i \tag{3.42}$$

where $\mu_S^0$ denotes the chemical potential of the pure solute in a reference state, $C_k^i$ is the concentration of solute $k$ in compartment $i$, $R$ is the ideal gas constant, $T$ is the thermodynamic temperature, and $\Psi^i$ is the electric potential in compartment $i$. Considering another compartment $j$ we can compute the electrical potential gradient by

$$\Delta\mu_k = \mu_k^i - \mu_k^j. \tag{3.43}$$

Solute is transported down its electrochemical potential gradient so that solute $k$ is transported from compartment $i$ into compartment $j$ if when $\Delta\mu_k < 0$, i.e., $\mu_k^j > \mu_k^i$. Note that we can write (3.43) as

$$\begin{aligned}
\Delta\mu_k &= \mu_k^i - \mu_k^j \\
&= (\mu_k^0 + RT\ln C_k^i + z_k F\Psi^i) - (\mu_k^0 + RT\ln C_k^j + z_k F\Psi^j) \\
&= RT(\ln C_k^i - \ln C_k^j) + z_k F(\Psi^i - \Psi^j) \\
&= RT\Delta\ln C_k + z_k F\Delta\Psi
\end{aligned}$$

by letting $\Delta \ln C_k = \ln C_k^i - \ln C_k^j$ and $\Delta\Psi = \Psi^i - \Psi^j$.

To determine the non-equilibrium thermodynamic formalism now consider a solute $S$. The flux of solute $S$ has a diffusive component which can be written as

$$J_S^{\text{diff}} = \sum_{k=1,n} L_{Sk}\Delta\mu_k \tag{3.44}$$

for $n$, the number of solutes, where

$$\Delta\mu_k = RT\Delta \ln C_k + z_k F\Delta\Psi \tag{3.45}$$

is the electrochemical potential difference of solute $k$ across the membrane (as described above), $L_{Sk}$ is a parameter that represents that flux of solute $S$ with the driving force exerted on species $k$. Note that $L_{Sk} = 0$ when $S$ and $k$ do not interact. Also note that $L_{SS}$ is related to the membrane permeability of the solute so that

$$L_{SS} = \frac{RTP_S}{\bar{C}_S} \tag{3.46}$$

where

$$\bar{C}_S = \frac{C_{S,a} - C_{S,b}}{\ln C_{S,a} - \ln C_{S,b}}$$

is the mean membrane concentration over the membrane $a, b$.

The practical use of the non-equilibrium thermodynamic formalism can be shown with the following example. The NaPi2 cotransporter in the proximal tubule has a 2:1 stoichiometry where there are 2 $Na^+$ ions cotransported with one $HPO_4{}^{2-}$ ion. Then as in the example in Layton & Edwards [75], we have that

$$\begin{pmatrix} J_{Na}^{NaPi2} \\ J_{HPO4}^{NaPi2} \end{pmatrix} = L_{NaPi2} \begin{pmatrix} +4 & +2 \\ +2 & +1 \end{pmatrix} \begin{pmatrix} \Delta\mu_{Na} \\ \Delta\mu_{HPO4} \end{pmatrix} \tag{3.47}$$

so that then the fluxes across the NaPi2 cotransporter are computed by

$$J_{Na}^{NaPi2} = L_{Na-HPO4}\left(4\Delta\mu_{Na} + 2\Delta\mu_{HPO4}\right) \tag{3.48}$$

$$J_{HPO4}^{NaPi2} = L_{Na-HPO4}\left(2\Delta\mu_{Na} + \Delta\mu_{HPO4}\right). \tag{3.49}$$

Notably, we can see that the equations given by the non-equilibrium thermodynamic formalism only require one parameter, $L_{Sk}$, the coupling coefficient. This is helpful in parameterizing the models, but we note that the limitation of this type of formalism is that

transporter expression and activity as well as translocation rates are not specified here. However, since at this time there are not data for a lot of these transporters, this formalism still has been very useful in being used in epithelial cell models to still capture solute transport along the nephron.

*Primary Active Transporters.* The $Na^+$-$K^+$-ATPase pump is located on the basolateral side of every cell along the nephron (see Fig. 2.2). $Na^+$-$K^+$-ATPase is an active transporter and moves 3 $Na^+$ ions out of the cell in exchange for 2 $K^+$ ions into the cell. Note that intracellular $K^+$ concentrations are high and intracellular $Na^+$ concentration are relatively low. The opposite is true in the extracellular $Na^+$ and $K^+$ concentrations. The $Na^+$-$K^+$-ATPase pump plays a key role in maintaining this concentration gradient. This gradient is important for regulating cell volume (since volume follows $Na^+$) as well as maintaining resting potential. Here we describe how the $Na^+$-$K^+$-ATPase pump is modeled in epithelial cell models using the approach described in Layton & Edwards [75].

The flux of $Na^+$ and $K^+$ across $Na^+$-$K^+$-ATPase can be considered as a binding of each of the ions to an enzyme independently. First, assume that the binding of one $Na^+$ ion (intracellular) to a free enzyme (denoted by $E$) form a $Na^+$-E complex (denoted by $NaE$) in a first-order, reversible reaction so that

$$\mathrm{Na^+ + E} \underset{\mathrm{k_-}}{\overset{\mathrm{k_+}}{\rightleftharpoons}} \mathrm{NaE}$$

so that the rate of formation of the complex NaE is given by

$$\frac{dC_{NaE}}{dt} = k_+ C_{Na} C_E - k_- C_{NaE} \tag{3.50}$$

where $C_{NaE}$, $C_E$, $C_{Na}$ denote the concentration of $NaE$, $E$, and intracellular $Na^+$, respectively. Let $C_E^{\text{total}} = C_E + C_{NaE}$ so that then we can rewrite (3.50) as

$$\begin{aligned} \frac{dC_{NaE}}{dt} &= k_+ C_{Na} \left( C_E^{\text{total}} - C_{NaE} \right) - k_i C_{NaE} && (3.51) \\ &= k_+ C_{Na} C_E^{\text{total}} - \left( k_+ C_{Na} + k_- \right) C_{NaE} && (3.52) \end{aligned}$$

which then we can set this to steady state to get that

$$\begin{aligned} 0 &= k_+ C_{Na} C_E^{\text{total}} - \left( k_+ C_{Na} + k_- \right) C_{NaE} \\ \iff C_{NaE} &= \frac{k_+ C_{Na} C_E^{\text{total}}}{k_+ C_{Na} + k_-} = \frac{C_{Na} C_E^{\text{total}}}{C_{Na} + \frac{k_-}{k_+}} \end{aligned}$$

and then letting $K_{Na} = k_-/k_+$ be the dissociation constant for the NaE complex we get that

$$C_{NaE} = \frac{C_E^{\text{total}} C_{Na}}{C_{Na} + K_{Na}}. \tag{3.53}$$

This means that the probability of having one $Na^+$ ion bind to one $Na^+$-$K^+$-ATPase pump is proportional to

$$\frac{C_{Na}}{C_{Na} + K_{Na}}.$$

Letting $p_{Na}$ denote this probability, if the binding of the $Na^+$ to the three $Na^+$-$K^+$-ATPase binding sites is assumed to be independent (i.e., no cooperativity), then the probability of all three sites having $Na^+$ ions bound to them is $p_{Na}^3$. In the same way, letting $p_K$ denote the probability of having an extracellular $K^+$ ion bound to a $K^+$ binding site, the probability of both $K^+$ binding sites having a $K^+$ bound to them is $p_K^2$ where $p_K$ is proportional to

$$\frac{C_K}{C_K + K_K}$$

where $C_K$ is the concentration of external $K^+$ and $K_K$ denotes the dissociation of the $K^+$ and free enzyme complex. As such, we can determine the flux of $Na^+$ ions across the $Na^+$-$K^+$-ATPase pump as

$$J_{Na}^{NaK} = J_{Na}^{NaK,max} \left[\frac{C_{Na}}{C_{Na} + K_{Na}}\right]^3 \left[\frac{C_K}{C_K + K_K}\right]^2 \tag{3.54}$$

where $J_{Na}^{NaK,max}$ is the maximum efflux of $Na^+$ ions at steady state which is a parameter. Then note that for every 3 $Na^+$ ions pumped, then there are 2 $K^+$ ions pumped across the $Na^+$-$K^+$-ATPase pump so that then we can compute flux of $K^+$ across the $Na^+$-$K^+$-ATPase pump as

$$J_K^{NaK} = -(2/3) J_{Na}^{NaK}. \tag{3.55}$$

The parameters for (3.54) and (3.55) have been determined in previous model development for each of the nephron segments [75, 80].

## 3.2 Multiple nephron model

While the superficial nephrons make up a large proportion of the kidney nephrons (about 2/3 in rats), there is another type of nephron called the juxtamedullary nephrons. The

juxtamedullary and superficial nephrons have several key differences. A major difference is that the juxtamedullary nephrons have loops of Henle that reach differing depths into the inner medulla. In contrast, the loops of superficial nephrons turn before reaching the inner medulla. Hence, in order to represent a full kidney model we should also consider the effects of the juxtamedullary nephrons.

### 3.2.1 Juxtamedullary nephrons

In the same way as the superficial nephrons, the juxtamedullary nephrons are modeled as a tubule lined by a layer of epithelial cells in which the apical and basolateral transporters vary depending on the cell type (i.e., segment, which part of the segment, intercalated and principal cells) (see Fig. 2.2). In the models, five juxtamedullary types are represented that reach into differing depths of the medulla. Specifically, we denote these nephrons JM-1, JM-2, JM-3, JM-4, and JM-5 where JM stands for juxtamedullary and the number corresponds to the differing depths of 1, 2, 3, 4, and 5 mm into the medulla. Let SF denote superficial. In the same way as in Ref. [60, 80], it is assumed that the ratios of the six nephron classes are $n_{\mathrm{SF}} = 2/3, n_{\mathrm{JM-1}} = 0.4/3, n_{\mathrm{JM-2}} = 0.3/3, n_{\mathrm{JM-3}} = 0.15/3, n_{\mathrm{JM-4}} = 0.1/3$, and $n_{\mathrm{JM-5}} = 0.05/3$. Note that the shorter juxtamedullary nephrons are the most common which turn in the upper portion of the inner medulla. These assumptions are used from Ref. [80] which are based on anatomical findings in Refs. [64, 71].

The juxtamedullary nephron models include the same segments as the superficial nephron (see Section 3.1): PCT, S3 segment, SDL, mTAL, cTAL, DCT, CNT, CCD, OMCD, and IMCD. In addition to these segments, there are longer descending limbs (LDL) and ascending thin limbs (LAL) for the juxtamedullary nephrons. The length of the LDL and LAL segments depends on the juxtamedullary nephron type and are the inner-medullary segments of the loops of Henle as illustrated in Fig. 2.2. The other major difference between juxtamedullary and superficial nephrons is the difference in SNGFR. It has been shown that the SNGFR for juxtamedullary nephrons is higher than the superficial nephron SNGFR [64, 71, 80]. We assume that the juxtamedullary SNGFR is about 40% higher than the superficial SNGFR in the NP model as done in Ref. [60] and reported in experimental studies in Refs. [54, 56, 64]. This results in a higher initial load to the juxtamedullary nephrons.

All segments in the juxtamedullary nephrons are effectively the same as the superficial nephrons except the length of the cortical thick ascending limb and the connecting tubule. Since the glomeruli of the juxtamedullary nephrons are lower down in the cortex than the superficial nephrons, these segments do not have to be as long for the nephron to pass the glomerulus at the macula densa. Hence, these segments are modeled to be shorter.

The connecting tubules of the five juxtamedullary nephrons and the superficial nephron coalesce into the cortical collecting duct. To model this, we compute the flows from the six nephrons at the start of the collecting duct. The remaining model is the collecting duct which does not have distinct nephron segments.

## 3.3 Sex-specific kidney models

As with most computational models of non-reproductive organs, the original nephron models were developed to represent kidney function in males. In recent years, experimental results have demonstrated many sex differences in kidney function [94, 103, 112]. Using these results sex-specific computational models of a rat proximal tubule [83], rat superficial nephron [59], rat multiple nephron (whole kidney) [60], and human kidney [61, 110] were developed to investigate the functional implications of sexual dimorphisms. Figure 3.2 illustrates some of the differences that have been found in transporter abundance along the nephron in female versus male rats.

Li et al. [83] developed and analyzed the first sex-specific computational epithelial transport model for the proximal convoluted tubule of the rat. Veiras et al. [112] observed experimentally that females seem to have lower fractional volume reabsorption in the proximal tubule. The modeling analysis of Li et al. [83] predicted that this difference may be attributed to the lower aquaporin (water channels) expression levels and smaller transport area due to a significantly smaller proximal tubule size in females when compared to males.

Hu et al. [59] further built on the sex-specific proximal tubule models (Ref. [83]) to represent sexual dimorphisms in morphology and transporter function along a full superficial nephron (i.e., including all segments up through the collecting ducts). Their simulations were used to analyze the functional implications of sex differences in hemodynamics, size, and renal transporters in male and female rats. Renal transporter differences used are highlighted in Fig. 3.2. Their analysis revealed that the higher transporter activity in the distal segments yield similar urinary excretion rates between males and females despite smaller transport area and fractional reabsorption in the proximal tubules of females.

Next, Hu et al. [60] developed a sex-specific multiple nephron model based on their superficial nephron model (Ref. [59]) to investigate sexual dimorphisms in how $Na^+$ transport inhibitors alter urinary solute excretion. This study was largely motivated by the sexual dimorphisms observed in blood pressure regulation, which the kidney plays a large role in via regulation of $Na^+$ reabsorption. Several pharmocological inhibitors regulate key $Na^+$ transporters so investigating the differing effects of inhibition may reveal insights into how such drugs may affect males versus females.

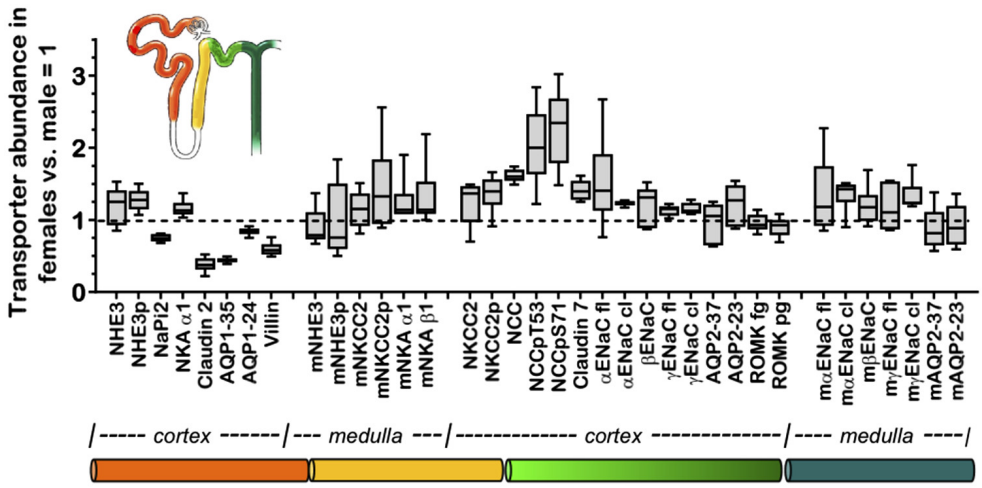


Figure 3.2: Relative differences in renal transporter abundance between males and females in a rat nephron. NHE3, $Na^+/H^+$ exchanger isoform 3; NaPi2, $Na^+$-$P_i$ cotransporter 2; NKA $\alpha$1, $Na^+$-$K^+$-ATPase $\alpha_1$ catalytic subunit; AQP, aquaporin water channel subunit; NKCC2, $Na^+$-$K^+$-$Cl^-$ cotransporter; pS71 and -pT53, phosphorylation sites associated with activation; NCC, $Na^+$-$Cl^-$ cotransporter; ENaC, epithelial $Na^+$ channel; fl, full-length form; cl, cleaved forms; ROMK, renal outer medullary $K^+$ channel. Figure used from Hu et al. [59].

Later the sex-specific epithelial transport model was further developed to represent sex-specific kidney function in humans [61]. This model was used to simulated the effect of angiotensin converting enzyme (ACE) inhibitors, a common antihypertensive drug, in the male versus female kidney. This study was motivated by the observation that ACE inhibitors tend to be less effective in women than men. Model simulations suggested that higher distal transport capacity in women lead to a blunted natriuretic and diuretic effect of ACE inhibition. Additionally, Hu et al. [61] noted that during pregnancy, the glomerular filtration rate is known to massively increase. The authors also noted that it has been shown that in females, NHE3 expression is higher in female rats compared to male rats, but NHE3 activity is lower in female rats than male rats. This leads to a reserve capacity for $Na^+$ transport via the NHE3 transporter in female rats [112]. It has been hypothesized that this apparent reserved NHE3 may be activated during pregnancy. Hu et al. [61] conducted "what-if" simulations to see the effect of activated NHE3 reserve capacity with upregulated GFR in female rats to test some implications of a few potential pregnancy-induced changes (though not comprehensive of pregnancy adaptations). Swapnasrita et al. [110] further developed the sex-specific human models (Ref. [61]) to investigate sexual

dimorphisms in kidney function in male and female patients with diabetes. This was used to test the functional implications of the effects of sodium-glucose cotransporter 2 inhibitors which are a commonly used type of diabetes medication.

These studies have revealed key insights into the differences between male and female kidney function, however a question may be asked as to why these differences occur? During pregnancy, the maternal body must have the ability to adapt significantly to be able to carry a healthy pregnancy to term. Major changes in electrolyte and volume handling have been shown to occur. Perhaps, sexual dimorphisms in the kidneys were evolved to support the female body's ability to undergo the major changes required to support a successful pregnancy. With this in mind, as well as noting the major changes that have been shown to occur during pregnancy (see Section 2.2.4), we investigate kidney function during pregnancy by extending the *female-specific* models built in Refs. [59,60,83] to capture *pregnancy-specific* kidney function.

# Chapter 4

# Adaptive changes in single-nephron GFR, tubular morphology, and transport in a pregnant rat superficial nephron: Modeling and analysis

**Abstract**

Normal pregnancy is characterized by massive increases in plasma volume and electrolyte retention. Given that the kidneys regulate homeostasis of electrolytes and volume, the organ undergoes major adaptations in morphology, hemodynamics, and transport to achieve the volume and electrolyte retention required in pregnancy. These adaptations are complex, sometimes counterintuitive, and not fully understood. In addition, the demands of the developing fetus and placenta change throughout the pregnancy. In particular, during late pregnancy, $K^+$ retention and thus enhanced renal $K^+$ reabsorption is required despite many kaliuretic factors. The goal of this study is to unravel how known adaptive changes along the nephrons contribute to the ability of the kidney to meet volume and electrolyte requirements in mid- and late pregnancy. We developed computational models of solute and water transport in the superficial nephron of the kidney of a rat in mid- and late pregnancy.

The mid-pregnant and late-pregnant models predict that morphological adaptations and increased activity of the sodium hydrogen exchanger 3 (NHE3) and epithelial sodium channel (ENaC) are essential for enhanced $Na^+$ reabsorption observed during pregnancy. Model simulations showed that for $K^+$ retention in late pregnancy, the increased activity of $H^+$-$K^+$-ATPase and decreased $K^+$ secretion along the distal segments are required. Model results also suggest that certain known sex differences in renal transporter pattern (e.g., the higher NHE3 protein abundance but lower activity in the proximal tubules of the virgin female rat compared to male) may serve to better prepare the female for the increased transport demand in pregnancy.

## 4.1 Introduction

During pregnancy, the female body must undergo major adaptations to support the solute and volume demands of a developing fetus and placenta. A large plasma volume expansion is required for a healthy pregnancy for both the mother and fetus [31, 35, 84, 129]. Remarkably, blood pressure typically decreases during pregnancy despite the large volume change [129]. Pregnancy disorders, such as gestational hypertension and preeclampsia, as well as fetal growth restriction are associated with a failure to expand plasma volume [21, 23, 26, 34, 50, 104, 129].

In a virgin or nonpregnant (NP) rat, almost all $Na^+$ intake is excreted through urine. In contrast, net $Na^+$ retention begins from early pregnancy [9, 23, 32, 53, 125, 132]. $Na^+$ retention largely drives the plasma volume expansion. Similarly, in a NP rat, about 90% of $K^+$ intake is excreted through urine, whereas the remaining 10% is excreted through feces [90]. However, during late pregnancy, there is net $K^+$ retention [23, 32, 53, 131, 132]. The majority of retained electrolytes are taken up by the fetoplacental unit [9, 32, 131].

The kidneys regulate volume and solute homeostasis [39]. Hence, to support the electrolyte and volume retention required in pregnancy, the kidneys undergo major adaptations in morphology [15, 53, 62], hemodynamics [9, 21, 23, 34, 53, 84, 132], and nephron transport [4, 19, 31, 35, 53, 63, 66, 68, 99, 125–128, 130, 131]. One of the first gestational renal adaptations observed is the large increase in the glomerular filtration rate (GFR). GFR increases by 40-50% during human pregnancy [20, 23, 34] and about 30% in rats [20, 23, 34]. This phenomenon is remarkable as there are no other nonpathological states that sustain such a high increase in GFR. That marked increase in filtration must be matched by appropriate changes in nephron transport. Otherwise, the excessive water and electrolyte loss will likely prove fatal.

Further studies found that the kidney increases in size during pregnancy [15,34,49,53]. In particular, the proximal tubule lengthens [15,49]. When taken in isolation, this should increase renal transport capacity. Along the nephron, the activity of several key transporters has been found to change during pregnancy; such adaptations are complex and sometimes counterintuitive when considered in isolation [35]. For example, Mahaney et al. [63] found that the activity of the major $Na^+$ transporter, $Na^+$-$K^+$-ATPase is downregulated during pregnancy despite the large increase in $Na^+$ reabsorption. Other $Na^+$ transporters are also downregulated [68,128], whereas others are upregulated [47,125,126,130]. Upregulation of key water channels has also been found during mid-pregnancy (MP) and late pregnancy (LP), likely facilitating increased water reabsorption [66,99]. Renal adaptations are different during MP and LP. Specifically, during LP, net $K^+$ retention occurs in addition to $Na^+$ retention, which starts from early pregnancy. West et al. [131] found significant changes in $K^+$ transport in distal nephron segments during LP. $Na^+$ and $K^+$ transporter adaptations during pregnancy in the rat have been discussed in a recent review by de Souza and West [35].

In recent years, substantial progress has been made in identifying gestational renal adaptations [23,35,129]. However, studies have generally focused on one segment or a few transporters (understandably due the difficulty and cost of conducting these complicated experiments). Therefore, how these complex adaptations come together to support the altered solute and volume demands during pregnancy is not fully understood. A comprehensive understanding of gestational kidney function is important for understanding how the female body undergoes massive adaptations required to sustain the growing fetus and placenta. Furthermore, altered renal function from normal pregnancy values has been found in gestational diseases such as preeclampsia [57], gestational hypertension [4], and gestational diabetes [65]. Hence, understanding normal renal function during pregnancy is a step toward ultimately understanding not only female physiology, but these complicated gestational diseases as well.

Computational models have been used to investigate the complex processes involved in renal function [58,73,74,76,77,79,80,119–121]. Recently, sex-specific epithelial transport models have been built for a rat proximal tubule [83], rat superficial nephron [59], rat kidney [60], and human kidney [61] based on experimental results that found sexual dimorphisms in morphology and transporter activities described in Refs. [94,103,113]. Li et al. [83] developed and analyzed the first sex-specific computational epithelial transport model for the proximal convoluted tubule (PCT) of a rat kidney. Specifically, model simulations in their study predicted that the lower fractional volume reabsorption in the female proximal tubule may be attributed to lower aquaporin (AQP) expression levels and the smaller transport area due to the significantly smaller proximal tubule size in females compared

with males. Later, Hu et al. [59] extended the model to a full superficial nephron model in the rat kidney for both males and females. Their simulations were used to analyze the functional implications of sex differences in hemodynamics, size, and renal transporters in male and female rats from experimental results described in Refs. [94, 103, 113]. The pregnancy-specific superficial nephron models presented here are based on Hu et al. [59] by incorporating pregnancy adaptations reported in the literature to represent superficial nephron function in MP and LP.

The main goal of this study was to assess the extent to which individual pregnancy adaptations, in morphology or transporter activities, contribute to the observed differences in electrolyte and volume reabsorption during pregnancy. Specifically, we identified which renal adaptations may have the largest impact on $Na^+$, $K^+$, and volume reabsorption using model simulations and sensitivity analysis. Furthermore, transporter activities in pregnant rats have not been fully characterized. We sought to predict additional renal adaptations that may occur during pregnancy. Separate analyses are conducted for MP and LP due to different renal adaptations in these stages that support evolving fetal and placental demands.

## 4.2 Methods

Hu et al. [59] developed an epithelial cell-based model of the superficial nephron of a female rat kidney (as discussed in Chapter 3). This model was used as a control in this study and is referred to as the NP model. In this study, we extended the NP model to simulate solute and volume transport along a superficial nephron of 1) a MP and 2) LP rat kidney. Note that rat gestation is approximately 21-22 days [49,129]. The MP rat model represents nephron transport at about 19-20 days of gestation (i.e., near the end of rat gestation). As previously noted, we build separate models for MP and LP because there are distinct adaptations during the different stages of pregnancy due to the growing demands of the developing fetus and placenta. Because the original model equations in the study by Hu et al. [59] were based on mass conservation that is similarly valid in pregnancy, those same equations were used here, but appropriate parameter values were changed to account for renal adaptations during MP and LP. These parameter changes are shown in Table 4.1 and are discussed in Section 4.2.1.

The model was implemented in Python 3 and can be accessed via GitHub.

In the following section we describe how the models were made to be pregnancy specific. Model equations are given in Section 3.1 of Chapter 3 so we do not repeat them here.

### 4.2.1 Pregnancy-specific models

Using the NP cell-based superficial nephron epithelial transport model developed in the study by Hu et al. [59] (described in Chapter 3), we created pregnancy-specific models (i.e., MP and LP) by increasing or decreasing relevant NP model parameter values based on experimental findings in the literature. The specific MP-to-NP and LP-to-NP parameter value ratios are listed in Table 4.1, a schematic diagram is given in Fig. 4.1, and the changes are discussed below.

The first major change in the MP and LP models is the increase in the single nephron glomerular filtration rate (SNGFR). The MP and LP SNGFR are increased by 30% and 20%, respectively, from the NP SNGFR value. These increases were based on findings in Baylis [20] where euvolemic pregnant rats were studied. We note that a previous study had shown the LP rat SNGFR was significantly higher than the MP rat SNGFR [53]; however, an important note is that study was done in hypervolemic rats, thus likely giving a differing result [20, 21]. As such, we chose to model the euvolemic rat based on the Baylis [20] result. Specifically, MP and LP SNGFR values are 31.0 and 28.8 nL/min, vs. 24 nL/min in NP [19, 29, 53]. The elevated SNGFR significantly increases the filtered load at the beginning of the nephron in both the MP and LP models. Additionally, during pregnancy, plasma osmolality is decreased, with slightly reduced plasma [$Na^+$] and [$Cl^-$], but with slightly elevated plasma [$K^+$] in LP [38, 53, 125, 131]. These changes are small compared to the SNGFR increases, still resulting in substantially increased filtered loads.

#### Morphological adapatations

During pregnancy, kidney volume increases [49, 62]. In particular, it has been shown that the proximal tubule (the first segment of the nephron) lengthens [15, 49]. Accordingly, we increased the proximal tubule length by 14% and 17% in the MP and LP models, respectively. Based on the increased kidney volume and the observed dilation in the collecting system during pregnancy [98], we assumed that the diameter in the proximal tubule increased by 7% in the proximal tubule and 5% in the distal tubule in both the pregnant rat models. (Note that we collectively refer to the loops of Henle and distal tubular segments, which include the collecting duct, as the "distal tubule".) Although tubular diameter has not been measured experimentally, without assuming this small tubular dilation, the much-elevated volume flow in pregnancy would cause an excessive drop in tubular fluid pressure.

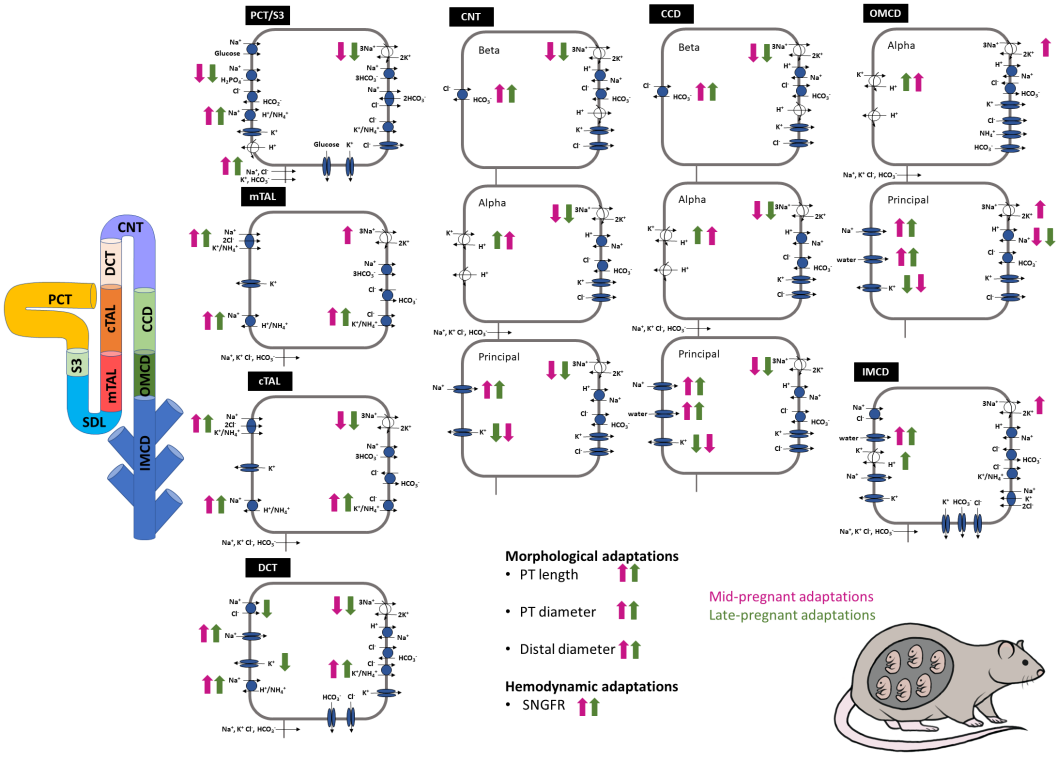


Figure 4.1: Schematic diagram of the superficial nephron cells with pregnancy adaptations indicated. The diagram displays main $Na^+$, $K^+$, and $Cl^-$ transporters as well as aquaporin water channels. MP adapatations from NP are indicated by pink arrows. LP adaptations from NP are indicated by green arrows. Upward orientation indicates increase, downward indicates decrease. No arrow indicates that the transporter is not changed in the respective model. Details are given in Table 4.1. PCT, proximal convoluted tubule; S3, proximal straight tubule; mTAL, medullary thick ascending limb; cTAL, cortical thick ascending limb; CNT, connnecting tubule; CCD, cortical collecting duct; OMCD, outer medullary collecting duct; IMCD, inner medullary collecting duct. Cell and nephron diagram adapted from Ref. [76]. Rat figure was illustrated by Karolina Suszek.

### $Na^+$ transporters

There have been a multitude of changes found in the activity and expression of $Na^+$ transporters, as recently reviewed by de Souza and West [35]. Here we explain how we implemented experimental results to determine MP and LP model parameter values for $Na^+$ transporters.

Mahaney et al. [63] found that pregnancy-induced changes in $Na^+$-$K^+$-ATPase activity and expression are region-specific: in the cortex, $Na^+$-$K^+$-ATPase activity is decreased in both MP and LP while in the medulla $Na^+$-$K^+$-ATPase activity is increased in MP, but is unchanged in LP relative to NP controls. Khraibi et al. [68] investigated the Na-Pi co-transporter 2 (NaPi2), which is located in the proximal tubule. The authors found that the protein expression of NaPi2 decreased during both MP and LP [68]. The relevant parameter value for NaPi2 ws slightly decreased in MP and LP based on this study (Table 4.1). $Na^+$-$K^+$-$2Cl^-$ cotransporter 2 (NKCC2) activity was increased significantly in LP and slightly in MP based on West et al. [126].

During pregnancy, aldosterone levels are elevated [129], which regulates the fine tuning of $Na^+$ handling in the distal segments of the nephron [25]. In a series of studies, West et al. reported that (i) epithelial $Na^+$ channel (ENaC) activity is increased significantly (about double) during both MP and LP [125], (ii) the chloride-bicarbonate exchanger, Pendrin, protein abundance is increased [130], and (iii) $Na^+$-$Cl^-$ cotransporter (NCC) activity is not changed during MP and slightly decreased during LP [128] relative to NP. These findings were implemented in the pregnancy models accordingly (Table 4.1).

$Na^+/H^+$ exchanger (NHE) activity has not been well characterized during pregnancy. During pregnancy, cortical mRNA expression of NHE isoform 3 (NHE3) was found to be increased during pregnancy [4]. However, NHE3 protein abundance was found to be slightly decreased or unchanged in MP and lP rats when compared to NP [35, 68, 125]. We note that protein abundance is not necessarily a good indicator of NHE3 activity. Specifically, it has been found that in female rats (i.e., NP), there is a higher protein expression of NHE3, but lower NHE3 activity in the proximal tubule when compared to male rats. Hence, there is reserve NHE3 in female rats that may be activated during pregnancy [59, 60, 112]. We assumed that NHE3 reserve is activated in pregnancy by increasing the NHE3 activity in the MP and LP models (Table 4.1). This is a model assumption which allows the model to avoid excess natriuresis and diuresis in pregnancy (see Section 4.4). Without this change, model predictions led to urinary excretion that was too high for sufficient $Na^+$ reabsorption in both the MP and LP models.

### $K^+$ transporters

Unlike $Na^+$ retention, which starts from early pregnancy, $K^+$ retention is not observed until LP [131]. Indeed, $K^+$-specific renal transporter changes have largely only been studied during LP to date [35,131]. West et al. [131] found that the renal outer medullary $K^+$ channnel (ROMK) and the large-conductance $K^+$ channel (BK) are significantly downregulated in the LP rat. This downregulation decreases $K^+$ secretion along the distal segments. The ROMK is located in the DCT2 (second part of the distal convoluted tubule) and the CNT where major $K^+$ secretion occurs. BK is located in the intercalated cells of the cortical collecting duct. Both channel types regulate $K^+$ secretions along these segments and are significantly downregulated during late-pregnancy [131]. This result is represented in the LP model by lowering the $K^+$ apical permeability in the appropriate segments (Table 4.1).

In addition, West et al. [131] found that $H^+$-$K^+$-ATPase type 2 activity in the connecting tubule (CNT) and collecting duct is substantially increased in the LP rat. Salhi et al. [105] reported an increase in $H^+$-$K^+$-ATPase activity in LP mice as well. Elevated progesterone levels during pregnancy activate $H^+$-$K^+$-ATPase [105]. Based on these experimental results, we significantly increased $H^+$-$K^+$-ATPase activity in the CNT and CD of the LP model (Table 4.1). Similar changes were made in the MP model to avoid excessive kaliuresis (Table 4.1, discussed in Section 4.3). We note that Abreu et al. [4] showed that mRNA expression of ROMK2 is significantly downregulated during MP, but no study has characterized $H^+$-$K^+$-ATPase activity and BK channels during MP. To avoid excessive kaliuresis and natriuresis in the MP and LP models, we also hypothesized that the $K^+$-$Cl^-$ cotransporter in the ascending limb and distal convoluted tubule (DCT) is also upregulated during pregnancy (Table 4.1; discussed in Section 4.3).

### Water channels

Collecting duct water channel, aquaporin 2 (AQP2) expression, is significantly increased during MP and LP [4, 66, 99]. It has also been hypothesized that aquaporin 1 (AQP1) in the descending limb is upregulated during LP, but largely unchanged during MP [66]. Water permeability in the appropriate segments was adjusted to reflect increased AQP1 and AQP2 based on these findings (Table 4.1).

Table 4.1: MP-to-NP and LP-to-NP ratios of parameter values used in the MP and LP models respectively. NP parameter values were used from [59] and changed by the respective ratio for the MP and LP models. Parameter values for the MP and LP models were chosen based on experimental literature and are discussed in the Materials and Methods section. PCT, proximal convoluted tubule; S3, proximal straight tubule; SDL, short descending limb; DCT, distal convoluted tubule; CNT, connecting tubule; CCD, cortical collecting duct; OMCD, outer medullary collecting duct; IMCD inner medullary collecting duct. Distal segments refer to all segments other than the PT and S3 segments (i.e., after the proximal tubule). Ratios are from the respective MP or LP model to the NP model parameter value. $P_f$: water permeability; $P_K$: $K^+$ permeability; NHE3: $Na^+/H^+$ exchanger isoform 3; ENaC: epithelial $Na^+$ channel; NKCC2: $Na^+$-$K^+$-$2Cl^-$ cotransporter isoform 2; NaPi2: $Na^+$-$H_2PO_4^-$ cotransporter; NCC: $Na^+$-$Cl^-$ cotransporter; NHE-1: $Na^+/H^+$ exchanger isoform 1; KCC: $K^+$-$Cl^-$ cotransporter

| **Parameter** | **Ratio** | |
|---|---|---|
| | **MP-to-NP** | **LP-to-NP** |
| **PCT** | | |
| $Na^+$-$K^+$-ATPase activity | 0.73 | 0.65 |
| NHE3 activity | 1.3 | 1.18 |
| NaPi2 | 0.9 | 0.85 |
| $K^+$-$Cl^-$ cotransporter | 1.35 | 1.3 |
| **S3** | | |
| $Na^+$-$K^+$-ATPase activity | 0.725 | 0.65 |
| NHE3 activity | 1.3 | 1.18 |
| NaPi2 | 0.9 | 0.85 |
| $K^+$-$Cl^-$ cotransporter | 1.35 | 1.3 |
| **SDL** | | |
| $P_f$ (transcellular) | 1.1 | 1.5 |
| **mTAL** | | |
| NKCC2 activity | 1.15 | 1.5 |
| $Na^+/H^+$ exchanger activity | 1.3 | 1.18 |
| KCC activity | 1.4 | 1.35 |
| $Na^+$-$K^+$-ATPase activity | 1.15 | 1.0 |
| **cTAL** | | |
| NKCC2 activity | 1.15 | 1.5 |
| $Na^+/H^+$ exchanger activity | 1.3 | 1.18 |

Table 4.1: MP-to-NP and LP-to-NP ratios of parameter values used in the MP and LP models respectively.

| **Parameter** | **Ratio** | |
|---|---|---|
| | **MP-to-NP** | **LP-to-NP** |
| KCC activity | 1.4 | 1.35 |
| $Na^+$-$K^+$-ATPase activity | 0.725 | 0.65 |
| **DCT** | | |
| $P_K$ (apical side, DCT2 only, ROMK) | 0.5 | 0.45 |
| $Na^+$-$K^+$-ATPase activity | 0.75 | 0.74 |
| NHE2 activity | 1.3 | 1.18 |
| KCC activity | 1.4 | 1.3 |
| NCC activity | 1.0 | 0.9 |
| ENaC activity | 1.85 | 2.15 |
| **CNT** | | |
| $P_K$ (apical side, ROMK) | 0.5 | 0.45 |
| $Na^+$-$K^+$-ATPase activity | 0.75 | 0.75 |
| $H^+$-ATPase activity | 1.0 | 1.0 |
| $H^+$-$K^+$-ATPase activity | 2.5 | 2.75 |
| Pendrin activity | 1.65 | 1.7 |
| ENaC activity | 1.85 | 2.15 |
| **CCD** | | |
| $P_f$ (transcellular, AQP2) | 1.4 | 1.4 |
| $P_K$ (apical, BK) | 0.75 | 0.7 |
| $Na^+$-$K^+$-ATPase activity | 0.75 | 0.7 |
| $H^+$-ATPase activity | 1.0 | 1.0 |
| $H^+$-$K^+$-ATPase activity | 2.5 | 2.25 |
| Pendrin activity | 1.65 | 1.7 |
| ENaC activity | 1.85 | 2.15 |
| **OMCD** | | |
| $P_f$ (transcellular, AQP2) | 1.4 | 1.4 |
| $P_K$ (apical, BK) | 0.75 | 0.7 |
| $Na^+$-$K^+$-ATPase activity | 1.13 | 1.0 |
| $H^+$-ATPase activity | 1.0 | 1.0 |
| $H^+$-$K^+$-ATPase activity | 2.5 | 2.75 |
| ENaC activity | 1.85 | 2.15 |
| NHE-1 activity | 0.9 | 0.9 |

Table 4.1: MP-to-NP and LP-to-NP ratios of parameter values used in the MP and LP models respectively.

| **Parameter** | **Ratio** | |
|---|---|---|
| | **MP-to-NP** | **LP-to-NP** |
| $Na^+$-$Cl^-$ cotransporter | 1.15 | 1.05 |
| **IMCD** | | |
| $P_f$ (trancellular, AQP2) | 1.8 | 1.8 |
| NKCC1 | 1.0 | 1.0 |
| $Na^+$-$K^+$-ATPase activity | 1.13 | 1.0 |
| $H^+$-$K^+$-ATPase activity | 2.5 | 2.75 |
| $K^+$-$Cl^-$ cotransporter | 1.4 | 1.3 |
| $Na^+$-$Cl^-$ cotransporter | 1.15 | 1.05 |
| **Morphology** | | |
| **PCT, S3** | | |
| Length | 1.14 | 1.17 |
| Diameter | 1.07 | 1.07 |
| **Distal segments** | | |
| Length | 1.0 | 1.0 |
| Diameter | 1.05 | 1.05 |
| **Hemodynamics** | | |
| SNGFR | 1.30 | 1.20 |
| **Plasma concentration** | | |
| Plasma $Na^+$ concentrations | 0.95 | 0.95 |
| Plasma $K^+$ concentrations | 1.0 | 1.15 |
| Plasma $Cl^-$ concentrations | 0.95 | 0.95 |

## 4.3 Results

### 4.3.1 Baseline results: electrolyte and fluid handling during pregnancy

Model simulations were conducted for the NP, MP, and LP models to determine how pregnancy-induced changes in renal hemodynamics, morphology, and transporter activity together modify tubular transport in the superficial nephrons of the rat kidney. Delivery of

key solutes and volume to each segment is shown in Fig. 4.2 and Fig. 4.3 with transport for each segment and accumulated along the nephron shown in Figs. 4.4 and 4.5, respectively.

In the NP model, 58% of the filtered $Na^+$ is reabsorbed along the proximal tubule, primarily via the coordinated transport of the apical NHE3 and basolateral $Na^+$-$K^+$-ATPase. In MP and LP, because of pregnancy-induced hyperfiltation and enhanced tubular transport capacity, net $Na^+$ reabsorption along the proximal tubule increased by 27% and 18%, respectively (Fig. 4.4A). Interestingly, those net increases in reabsorption correspond to only minor increases in fractional reabsoprtion, to about 60% in both the MP and LP models (Fig. 4.2A; Fig. 4.3A), due to increased filtered $Na^+$ load. (Recall that SNGFR increases in MP and LP by 30% and 20%, respectively, or to 31 and 28.8 nL/min, vs. 24 nL/min in NP.) The relative stability of the fractional reabsorption is reminiscent of the glomerulotubular balance observed in the proximal tubules. The marked increase in net $Na^+$ proximal tubule transport in pregnancy can be attributed to tubular hypertrophy and elevated NHE3 activity in the proximal tubule, despite reduction in $Na^+$-$K^+$-ATPase activity (Table 4.1).

Most of the remaining $Na^+$ is reabsorbed downstream along the thick ascending limbs (Fig. 4.4A). Compared to the NP model, $Na^+$ transport along the thick ascending limb is predicted to be about 18% and 8% higher in the MP and LP models, respectively (Fig. 4.4A). This enhanced transport is facilitated by increased NKCC2 and NHE activity. Downstream of the thick ascending limb, (i.e., segments after the macula densa or the distal segments), $Na^+$ reabsorption is predicted to be about the same in each of the NP, MP, and LP models (Fig. 4.4A). Urine $Na^+$ excretions are 32, 34, and 35 pmol/min for the NP, MP, and LP models, respectively. Urinary $Na^+$ excretion is the highest in LP, at 10% above the NP model (Fig. 4.2A). The predicted natriuresis is consistent with reported ranges [14, 32, 125].

Like $Na^+$, about 55% of the filtered $Cl^-$ is reabsorbed along the proximal tubule in the NP, MP, and LP models with most of the remaining $Cl^-$ reabsorbed along the thick ascending limbs (Fig. 4.4C). Along the thick ascending limb, $Cl^-$ reabsorption is increased by 19% and 9% in the MP and LP models, respectively (Fig. 4.4C). In both pregnant models, increased transport in the thick ascending limb is due to the increased NKCC2 activity. Additionally, $K^+$-$Cl^-$ cotransporter activity is increased resulting in increased $Cl^-$ reabsorption. Urinary $Cl^-$ excretions for the NP, MP, and LP models are 7.4, 8.0, and 7.4 pmol/min, respectively. We note that urinary $Cl^-$ excretion is slightly increased during pregnancy and the increase in predicted urinary $Cl^-$ excretion in the MP and LP models from NP is within reported ranges [14, 53].

The model predicted that 54% of filtered $K^+$ is reabsorbed along the proximal tubule

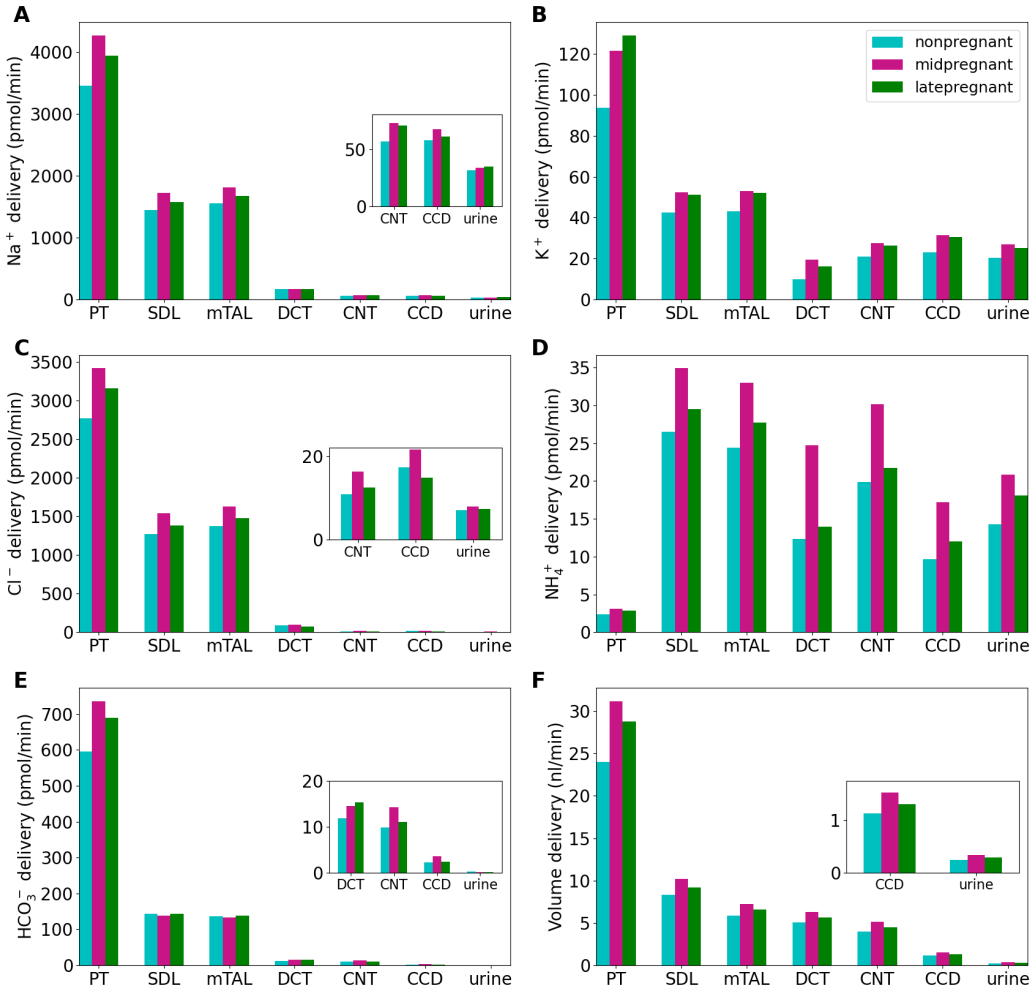


Figure 4.2: Delivery of key solutes (*A*-*E*) and volume (*F*) to the beginning of the individual nephron segments in the NP, MP, and LP models. PT, proximal tubule; SDL, short descending limb; mTAL, medullary thick ascending limb; DCT, distal convoluted tubule, CNT; connecting tubule; CCD, cortical collecting duct. *Insets:* reproduction of distal segment values.

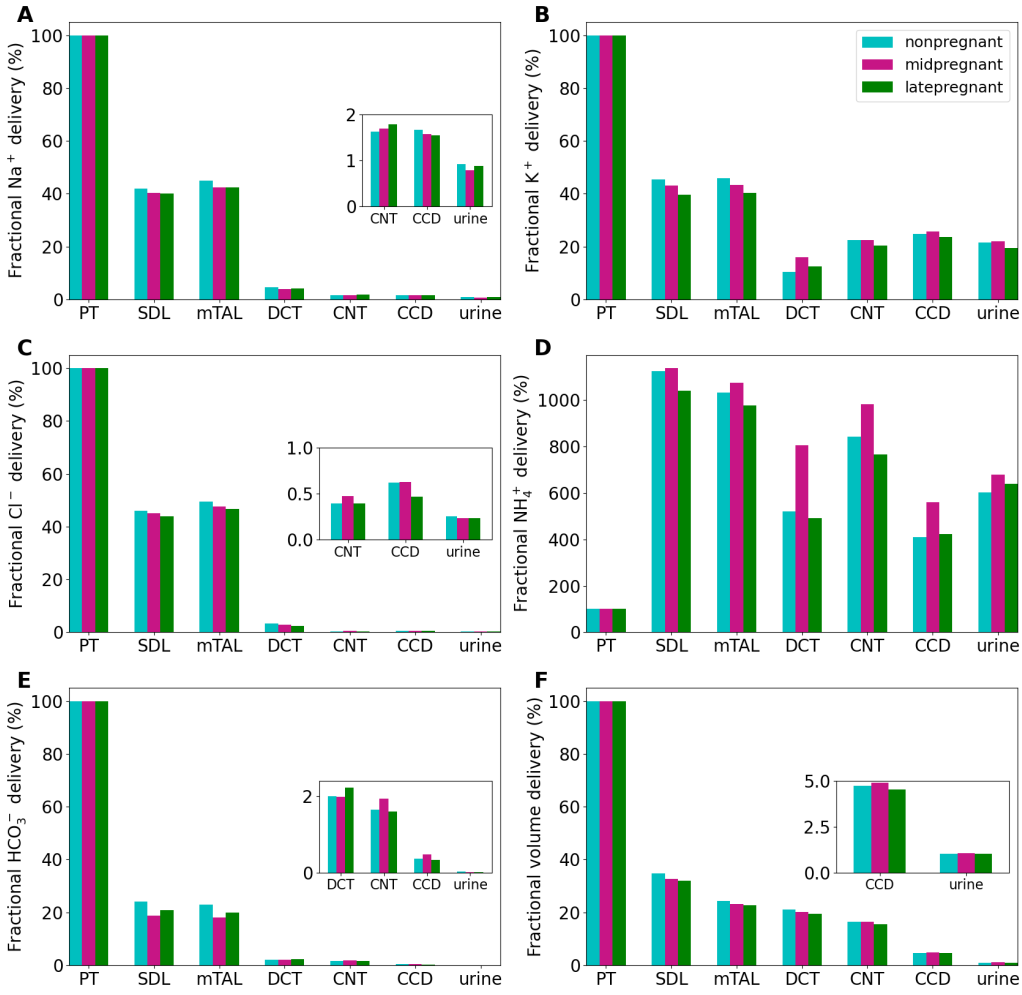


Figure 4.3: Fractional delivery of key solutes ($A$-$E$) and volume ($F$) to the beginning of the individual nephron segments in the NP, MP, and LP rat models. PT, proximal tubule; SDL, short descending limb; mTAL, medullary thick ascending limb; DCT, distal convoluted tubule, CNT; connecting tubule; CCD, cortical collecting duct. *Insets:* reproduction of distal segment values.

in the NP model (Fig. 4.2B; Fig. 4.3B). Net $K^+$ reabsorption along the proximal tubule increases by 36% in MP and 52% in LP (Fig. 4.4B). Together with the increases in filtered $K^+$ load, due to increased SNGFR and, in LP, increased $K^+$ plasma concentration, the net increases in $K^+$ reabsoprtion yield increases in fractional reabsorption, at 57% in MP and 60% in LP, along the proximal tubule (Fig. 4.3B). Like $Na^+$ and $Cl^-$, most of the remaining $K^+$ is also reabsorbed along the thick ascending limb. Downstream of the loop of Henle, the distal convoluted tubules and connecting tubules vigorously secrete $K^+$ (Fig. 4.4B). Consequently, 22% of the filtered load of $K^+$, or 21 pmol/min per (superficial) nephron is excreted in urine in the NP model (Fig. 4.2B; Fig. 4.3B). Interestingly, $K^+$ transport along the distal segments differs significantly in pregnancy; $H^+$-$K^+$-ATPase activity is increased and $K^+$ secretion in the distal segment $K^+$ secretory channels is reduced. As a result, in MP, $K^+$ secretion along the distal convoluted tubule and connecting tubule is decreased by 10% despite increased ENaC activity that would, in isolation, increase $K^+$ secretion. In addition, reabsorption in the collecting duct is increased by 54% compared to the NP model (Fig. 4.4B). Similar changes occur in LP. These changes lead to 29% and 42% more accumulated $K^+$ reabsorption along the full nephron during MP and LP, respectively (Fig. 4.5B).

Renal $NH_4^+$ handling is predicted to be qualitatively similar in NP and pregnancy. In all three cases considered, the proximal tubule is a major site of $NH_4^+$ secretion via substitution of $H^+$ in the NHE3 transporter, whereas a substantial fraction of $NH_4^+$ is reabsorbed along the thick ascending limbs by substituting for $K^+$ in the NKCC2 (Fig. 4.4D). The proximal tubule also serves as a major site for $HCO_3^-$ reabsorption, with the remainder reabsorbed along the thick ascending limbs (Fig. 4.4E).

The majority (65%) of the filtered volume is reabsorbed along the proximal tubule in the NP model (Fig. 4.2F; Fig. 4.4F). Net water reabsorption along the proximal tubule increased by 34% and 25% in MP and LP, respectively (Fig. 4.4F). This yields similar fractional reabsorption of about 68% in both MP and LP models along the proximal tubule. Enhanced water reabsorption is primarily due to increased proximal tubule length. More water is reabsorbed downstream, albeit at a slower rate. The models, which represent a superficial nephron of the kidney in an antidiuretic state, predict a urine output of 0.25 nl/min per nephron (superficial) in the NP model and about 0.30 nl/min per nephron (superficial) in both the MP and LP models. The increase in volume excretion during pregnancy is within reported ranges [14, 53, 125].

Taken together, baseline results suggest that the adaptations represented in the MP and LP models yield an appropriate response to the marked elevation in filtered loads of solutes and volume during normal pregnancy.

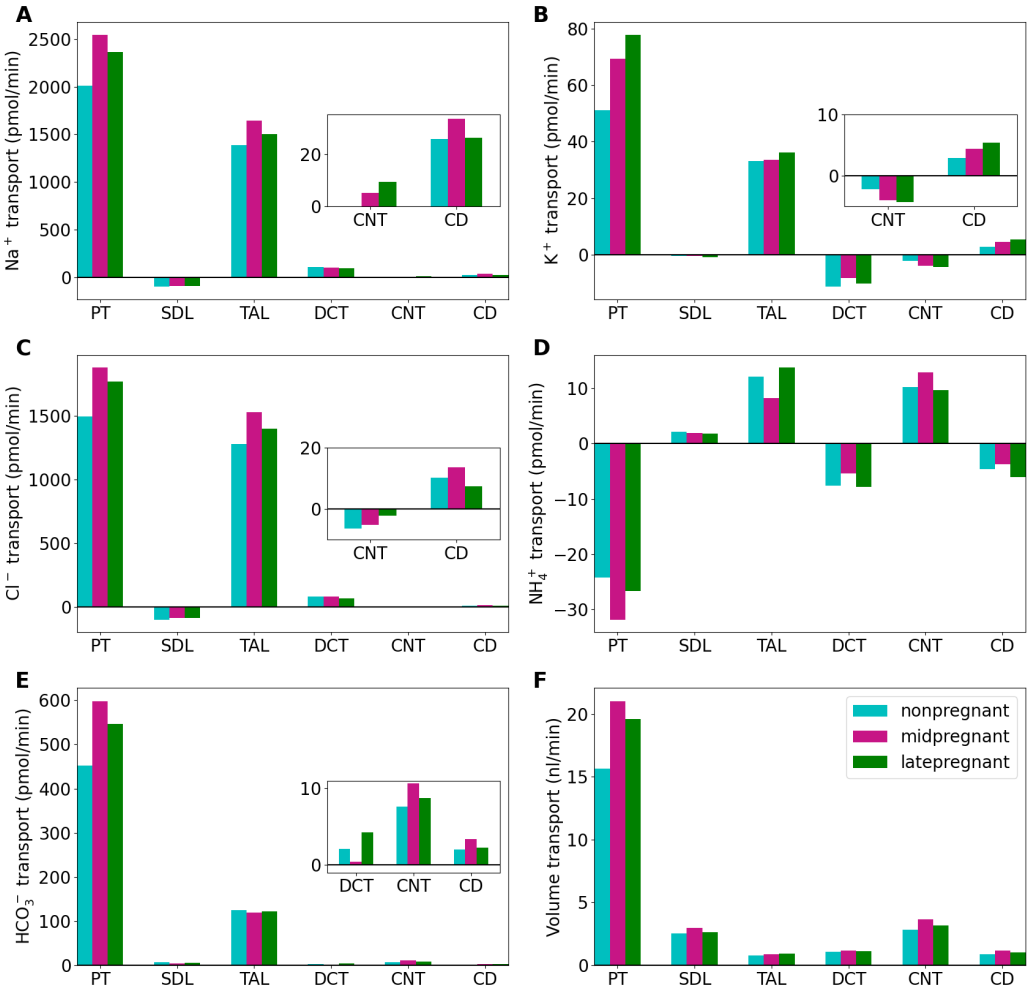


Figure 4.4: Net segmental transport of key solutes (*A*-*E*) and volume (*F*) along the individual nephron segments in the NP, MP, and LP models. Transport is taken to be positive out of the nephron segment, i.e., positive transport shows ret reabsorption and negative shows net secretion along the respective segment. PT, proximal tubule; SDL, short descending limb; DCT, distal convoluted tubule; CNT, connecting tubule; CD, collecting duct. *Insets.* reproduction of the distal segment values

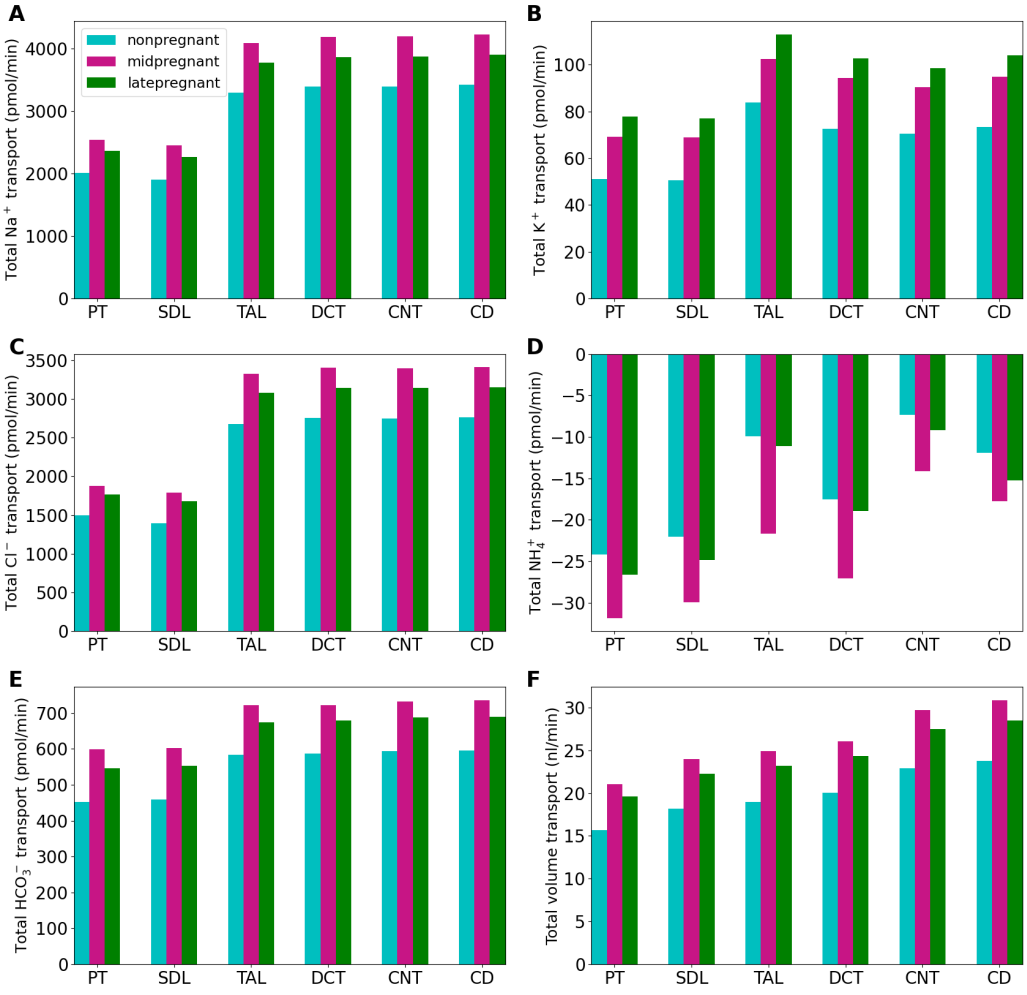


Figure 4.5: Accumulated transport of key solutes ($A$-$E$) and volume ($F$) along the individual nephron segments in the NP, MP, and LP models. Transport convention and segment labels are the same as in Fig. 4.4.

### 4.3.2 Sensitivity analysis: impact of morphological adaptations

We first assess the effects of the increases in model proximal and distal tubule dimensions. To assess the impact of individual morphological changes, we set each of the individual MP or LP parameter changes (proximal tubule length, proximal tubule diameter, and distal tubule diameter) to the NP value, while keeping all other model parameters at the respective MP or LP values. The respective $Na^+$, $K^+$, or volume urinary excretion was computed by running the full nephron model with the one parameter change. Fractional change in excretion (denoted $\Delta$s excretion) for $s = Na^+$, $K^+$, or volume is then computed as follows:

$$\Delta s \text{ excretion } (\%) = \frac{U_{s,p}^{\text{new}} - U_{s,p}^{\text{baseline}}}{U_{s,p}^{\text{baseline}}} \times 100\% \tag{4.1}$$

where $p$ = MP or LP denotes which pregnancy-specific model is being analyzed, $U_{s,p}^{\text{new}}$ denotes the new urinary excretion of $Na^+$, $K^+$, or volume computed, and $U_{s,p}^{\text{baseline}}$ denotes the original baseline model urinary excretion. Urine output and $Na^+$ excretion are key measures due to the importance of water and $Na^+$ retention in maintaining plasma volume expansion during pregnancy [35, 129]. $K^+$ excretion is another important measure, given the dangers of hypokalemia and hyperkalemia, and because of $K^+$ retention observed during LP [35, 131]. Results are shown in Fig. 4.6.

As previously noted, the proximal tubule reabsorbs just over half of the filtered $Na^+$, $K^+$, and volume in each of the models. Without the respective increased proximal tubule length in the MP model, the proximal tubule reabsorbs 12% less of the filtered $Na^+$ load. The downstream segments make up for some of the $Na^+$ transport; nonetheless, urinary excretion is predicted to increase by 50%. Analogous results are obtained for $K^+$ and fluid, and for LP (see Fig. 4.6).

The distal tubular segments absorb only about half of what the proximal tubule does. Without the increase in distal tubular diameter, urinary $Na^+$ excretion would increase by about 4% in MP and LP (Fig. 4.6A). Similar increases are predicted for urine output (Fig. 4.6C). Although there is significant $K^+$ reabsorption along the thick ascending limb, the distal convoluted tubule and connecting tubule secrete $K^+$, resulting in net $K^+$ secretion along these distal segments. As such, taken in isolation, a reduction in distal tubule diameter and transport area would reduced $K^+$ secretion. However, $Na^+$ flow is also increased, which created a favorable electrical potential gradient to facilitate increased $K^+$ secretion as shown in Fig. 4.6B.

In summary, pregnancy-induced changes in tubular morphology markedly increase net $Na^+$, $K^+$, and volume reabsorption. Increased proximal tubule length is likely the most

important morphological factor in avoiding excessive diuresis, natriuresis, and kaliuresis in pregnancy.

### 4.3.3 Sensitivity analysis: impact of transporter adaptations

The MP and LP models represent a multitude of changes in transporter activity, based largely on experimental findings that have characterized transporter activity and expression during pregnancy (see Table 4.1; graphical summary of the changes in Fig. 4.1). Following the approach aforementioned, we assessed the effect of individual transporter adaptations by setting the transporter activity or permeability value in the MP or LP model to the NP value, while keeping all other model parameters at the respective MP or LP values. We then computed changes in urinary excretion rates of $Na^+$, $K^+$, and volume that result from that local change. Results are shown in Fig. 4.7.

#### $Na^+$ transporters.

Without increased NHE activity, urinary $Na^+$ excretion increased by 21% and 10% in the MP and LP models, respectively. This change had one of the largest impact on urinary $Na^+$ excretion for any of the $Na^+$ transporter pregnancy changes for the MP and LP models (see Fig. 4.7A). In addition, the NHE activity has the second largest impact on the urinary volume excretion in both the MP and LP models, with an increase of 9% and 7%, respectively (see Fig. 4.7C). These results indicate that upregulation of NHE activity may play a key role in $Na^+$ and fluid retention in pregnancy.

Mahaney et al. [63] observed that changes in $Na^+$-$K^+$-ATPase activity during pregnancy are region-dependent. Specifically, cortical $Na^+$-$K^+$-ATPase activity is decreased in both MP and LP, wherease medullary $Na^+$-$K^+$-ATPase activity is increased during MP and unchanged during LP [63]. In the LP model, resetting $Na^+$-$K^+$-ATPase activity to the higher NP value leads to a 17% increase in $Na^+$ reabsorption along the proximal tubule and ascending limb, resulting in lower $Na^+$ delivery to segments after the macula densa so that the urinary $Na^+$ excretion is decreased by 19%. In the MP model, the opposite changes in cortical and medullary $Na^+$-$K^+$-ATPase activity results in a smaller decrease of 12% in urinary $Na^+$ excretion (Fig. 4.7A). Because water transport is largely driven by $Na^+$ reabsorption, volume excretion is decreased by about 7% in both the MP and LP models (see Fig. 4.7C). And because distal $K^+$ secretion is driven by $Na^+$ reabsorption, the reduced luminal $Na^+$ flow and $Na^+$ transport decreased urinary $K^+$ excretion by 6% and 3% in the MP and LP models, respectively (see Fig. 4.7B).

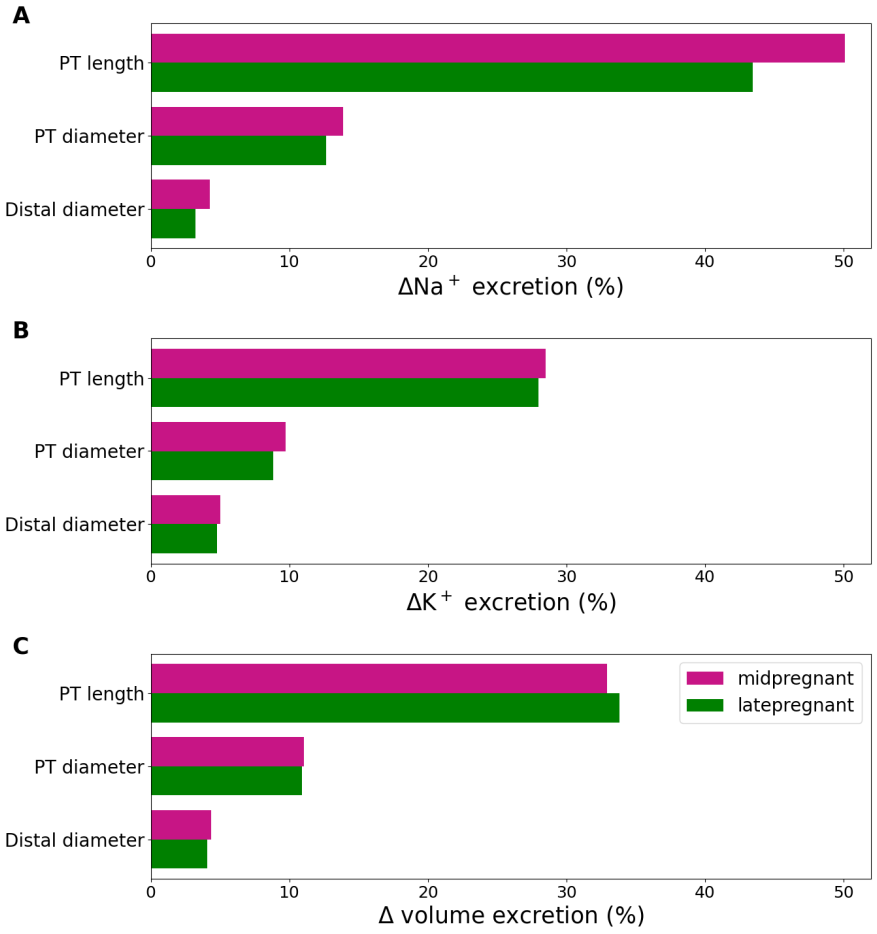


Figure 4.6: Sensitivity of $Na^+$ ($A$), $K^+$ ($B$), and volume ($C$) excretion to pregnancy-induced changes in morphology parameters. Individual model parameters in the mid-pregnant (MP) and late-pregnant (LP) models were set to non-pregnant (NP) values and excretion of $Na^+$, $K^+$, or volume was computed. The fractional change in excretion from the original MP or LP model result (as labeled) is shown. Distal segments refer to all segments other than the PCT and S3 segments (i.e., after the proximal tuble). PT denotes the proximal tubule. MP and LP parameter details are listed in Table 4.1.

NKCC2 activity in the thick ascending limb was increased by 15% and 50% in the MP and LP models, respectively (Table 4.1). However, NKCC2 activity does not seem to have a large effect on the MP and LP models. Without NKCC2 upregulation, net $Na^+$ transporter along the thick ascending limb decreased by about 1% in both the MP and LP models. This results in a change of <1% in urinary $Na^+$ excretion in both the MP and LP models (Fig. 4.7A.).

ENaC activity in the distal segment was increased by 85% and 115% in the MP and LP models, respectively, based on experimental data in Refs. [125–127]. Our analysis indicates that increased ENaC activity has the largest impact on predicted urinary excretion in both MP and LP (Fig. 4.7A). ENaC plays a role in fine-tuning $Na^+$ transport in the distal segments, so without the increase during pregnancy, our model predicts about a 5% decrease in reabsorption in the distal segments (downstream of the macula densa) in both the MP and LP models. This, in turn, resulted in urinary $Na^+$ excretion increasing by about 21% (Fig. 4.7A), together with about 3% increase in urine output (Fig. 4.7C) in both the MP and LP models. We also noted that since ENaC is a known potent kaliuretic factor, $K^+$ excretion is significantly decreased without its upregulation (Fig. 4.7B).

Other $Na^+$ transporters including NaPi2, NCC, and NHE1 are all downregulated during pregnancy (Table 4.1). An analysis of these changes impact on $Na^+$, $K^+$, and volume excretion reveal a <2% change for each of these transporters in both the MP and LP models (Fig. 4.7).

In summary, our analysis shows that the likely increased activities of NHE3 and ENaC play key roles in the increased $Na^+$ reabsorption of the kidneys and subsequent $Na^+$ retention observed during pregnancy. These transporters also have a significant impact on volume retention, and thus pregnancy-induced plasma volume expansion.

### Water channels

The collecting duct water channel aquaporin 2 (AQP2) is upregulated during MP and LP (see Table 4.1) [4, 99]. Without this adaptation, volume excretion increased by 8% and 5% in the MP and LP models, respectively due to decreased (about 2% in both MP and LP) collecting duct water reabsorption (Fig. 4.7C). It has also been hypothesized that the water channel aquaporin 1 (AQP1) is upregulated in the descending limb during LP [66]. We found that this change did not have as significant of an impact on urinary excretion as AQP2; downregulating AQP1 to the NP value only increased the volume excretion by <1% (Fig. 4.7C). Therefore, our analysis suggests that the upregulation of AQP2 may play a key role in volume reabsorption during pregnancy.

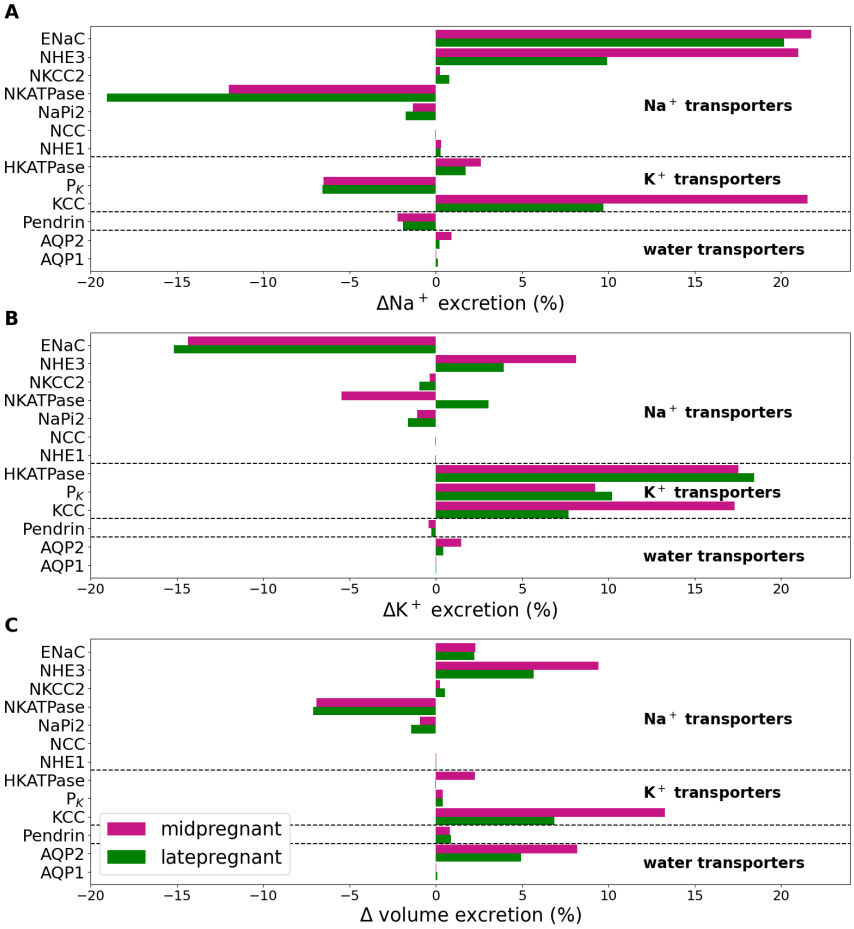


Figure 4.7: Sensitivity of $Na^+$ ($A$), $K^+$ ($B$), and volume ($C$) excretion to pregnancy-induced changes in transporter parameters. Individual model parameters in the mid-pregnant (MP) and late-pregnant (LP) models were set to non-pregnant (NP) values and excretion of $Na^+$, $K^+$, or volume was computed. The fractional change in excretion from the original MP or LP model result is shown. NHE: $Na^+/H^+$ exchanger, ENaC: epithelial $Na^+$ channel, NKCC2: $Na^+$-$K^+$-ATPase, NaPi2: $Na^+$-$H_2PO_4^-$ cotransporter, NCC: $Na^+$-$Cl^-$ cotransporter, NHE1: $Na^+/H^+$ exhanger isoform 1, KCC: $K^+$-$Cl^-$ cotransporter, $P_K$: apical $K^+$ permeability, HKATPase: $H^+$-$K^+$-ATPase activity, AQP1: transcellular water permeability in PT, AQP2: transcellular water permeability in distal segments. Parameter details are listed in Table 4.1.

### $K^+$ transporters

Apical $K^+$ permeability in the distal segments was signficantly lowered to account for downregulated major $K^+$ secretory channels (ROMK and BK) in the distal tubule during pregnancy (Table 4.1). In the LP model, without this downregulation, $K^+$ secretion along the distal convoluted tubule and connecting tubule is increased by 21%, resulting in a 10% increase in urinary $K^+$ excretion (Fig. 4.7B). In the MP model, without downregulated secretion in the distal segments, $K^+$ secretion along the distal convoluted tubule and connecting tubule increased by 25%, resulting in $K^+$ excretion prediction increasing by 9% (Fig. 4.7B). We also noted that when the apical $K^+$ permeability was increased to NP levels, $Na^+$ excretion greatly decreases due to the natriuretic effect of lower $K^+$ secretion (Fig. 4.7A).

$H^+$-$K^+$-ATPase type 2 activity in the connecting tubule and collecting duct is substantially increased pregnancy [105,131]. Without the increase in $H^+$-$K^+$-ATPase activity, urinary $K^+$ excretion increased by about 18% in both the MP and LP models (Fig. 4.7B), due to a 40% and 26% decrease in $K^+$ reabsorption along the collecting duct in the MP and LP models, respectively. Similarly, without increased $H^+$-$K^+$-ATPase activity in the MP model, there is a 13% increase in $K^+$ excretion (Fig. 4.7B). This result shows that increased $H^+$-$K^+$-ATPase activity during pregnancy is essential to prevent excess kaliuresis in both MP and LP.

Activity of the $K^+$-$Cl^-$ cotransporters (KCC) has yet to be characterized in the pregnant rat. We estimated that KCC activity should be increased by 40% in MP and 35% in LP to avoid excessive water and electrolyte loss (Table 4.1). In the absence of KCC upregulation, predicted $K^+$ excretion increases by 17% and 8% (Fig. 4.7B), $Na^+$ excretion increases by 22% and 10% (Fig. 4.7A), and volume excretion increases by 13% and 7% (Fig. 4.7C) in the MP and LP models, respectively. This result suggests that the KCC may play a role in electrolyte and water retention during pregnancy.

In summary, model analysis supports the hypothesis by West et al. [131] that $K^+$ retention in LP is driven by decreased secretion due to decreased ROMK and BK channel expression in conjunction with significantly increased $H^+$-$K^+$-ATPase activity. Model analysis also suggests that similar adaptations are made during MP to prevent excessive kaliuresis. In addition, simulation results suggest that the upregulation of KCC may be necessary to prevent excessive diuresis, natriuresis, and kaliuresis in pregnancy.

### 4.3.4 Sensitivity analysis: model parameter sensitivity

To assess model sensitivity to variations in key parameters, we conducted a sensitivity analysis for each of the parameters that were changes in the MP and LP models. To that end, we computed model solutions by increasing the respective parameter by 10% and decreasing by 10%, and then evaluated the changes in $Na^+$, $K^+$, and volume excretions. Letting $U_{s,t,p}^{+10\%}$ and $U_{s,tp}^{-10\%}$ denote the urinary excretion for $Na^+$, $K^+$, or volume (denoted by the subscript '$s$') for some adaptation $t$ (e.g., '$t$' may denote NHE3 activity), where the parameter value for $t$ is increased or decreased by 10%. The subscript '$p$' denotes the pregnancy status described by the model, i.e., $p$= MP or LP. We then computed the fractional change in excretion rates as follows:

$$\frac{U_{s,t,p}^{+10\%} - U_{s,t,p}^{-10\%}}{U_{s,p}} \tag{4.2}$$

where $U_{s,p}$ denotes the baseline model urinary excretion, to measure the sensitivity of the model to parameter $t$. Note that (4.2) measures sensitivity to changes in a given parameter at its MP or LP value, and is independent of the NP value, i.e., how much that parameter is changed due to pregnancy. This is the key difference from the earlier sensitivity analysis (Figs. 4.6 and 4.7).

Sensitivity results are shown in Fig. 4.8. The results are similar for MP and LP, indicating that both models are most sensitive to morphological adaptations, especially proximal tubule length. This is consistent with the analysis above (Fig. 4.6). In terms of transporters, the predicted $Na^+$ excretion is notably more sensitive to changes in $Na^+$-$K^+$-ATPase activity, whereas $K^+$ excretion is more sensitive to the distal KCC and $H^+$-$K^+$-ATPase.

## 4.4 Discussion

Pregnancy induces major changes in the structure and function of the kidney, resulting in kidney growth as well as elevated blood flow, in a process that changes continually throughout pregnancy [35, 49, 53, 129]. A particular drastic change is the 30% increase in GFR in pregnant rats [19, 21]. While osmolality of the plasma is slightly decreased, this massive increase in GFR results in an increased filtered load to the nephrons during pregnancy. How do the kidneys of a pregnant rat handle the increased filtered load? Pregnancy-induced renal adaptations, as recently reviewed by de Souza and West [35], are complex and extensive. How might those coordinated changes not only meet that increased

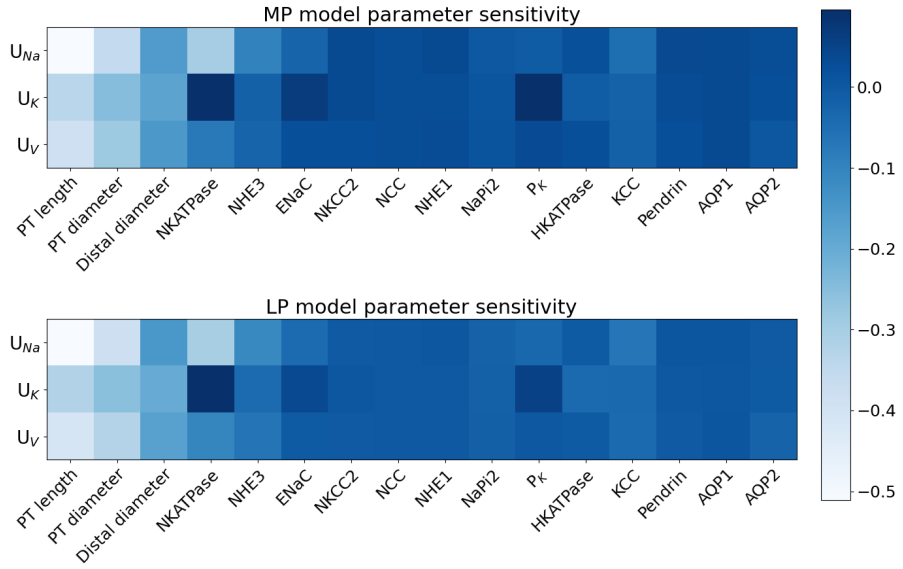


Figure 4.8: Sensitivity of $Na^+$, $K^+$, and volume excretion (denoted by $U_{Na}$, $U_K$, and $U_V$ respectively) to parameters involved in pregnancy adaptations. Sensitivity was assess for the mid-pregnant (MP) and late-pregnant (LP) models using (4.2). MP and LP parameter changes from NP are listed in Table 4.1. Notations are analogous to those in Fig. 4.6 and Fig. 4.7.

demand but retain electrolytes? These are the questions that the present study seeks to answer.

The increase in plasma volume required to supply the developing fetus and placenta is largely driven by $Na^+$ retention [125,128,129]. During pregnancy, aldosterone, angiotensin II, estrogen, and insulin are elevated; all these hormones are known to stimulate renal $Na^+$ retention [35,48,95]. However, progesterone, nitric oxide, and GFR are also elevated; these are factors known to promote $Na^+$ excretion [15,35,36,48,63,95,129]. Thus, $Na^+$ retention in pregnancy is a result of several competing factors.

Located on the apical side of the proximal tubular cells, NHE3 drives most renal $Na^+$ transport along the proximal tubule. The protein abundance of NHE3 has been reported to decrease in MP and LP rats [68], or remain unchanged in whole kidney homogenates [125]. That said, the difference between transporter protein abundance and activity must be appreciated, and it is the latter, i.e., activity that ultimately determines the transport

capacity of the cell. For example, the proximal tubules in female rats exhibit a higher protein expression of NHE3 compared to males, but a lower NHE3 activity due to a higher level of phosphorylation in male rat nephrons [59, 112]. These two competing effects result in lower $Na^+$ transport along the female rat proximal tubules [59, 112]. The mystery of "untapped" NHE3 in the female rat kidney has led to the hypothesis that it gives females the reserved capacity to handle the increased transport demand in pregnancy and lactation [59,60]. No known study to date has determined NHE3 activity during pregnancy. We have postulated that NHE3 is elevated in MP and LP (Table 4.1), making it possible for pregnant females to reabsorb the enhanced filtered $Na^+$ load [60]. In the absence of this adaptation, model analysis suggests that the water and electrolyte retention required in pregnancy would not have been possible (Fig. 4.7).

Although the proximal tubules reabsorb most of the filtered $Na^+$ and fluid, the distal tubular segments are responsible for fine-tuning the remaining filtrate so that urinary excretion approximately equals intake. West et al. [125] reported an increase in the renal $\alpha$-ENaC activity during MP and LP. In addition, Fu et al. [47] found a significant increase in ENaC protein expression during pregnancy, and hypothesized this was driven by activation of the intrarenal renin-angiotensin-aldosterone system via the prorenin receptor. West et al. [127] found that chronic ENaC blockade in a pregnant rat resulted in reduced $Na^+$ retention and plasma volume expansion, and pups with lower birthweight. Our sensitivity analysis indicated that without the ENaC activity increase, excess natriuresis occurs (Fig. 4.7A). Together, model analysis and previous experimental reports demonstrate the importance of massively increased ENaC activity during pregnancy.

Despite $Na^+$ retention occurring in pregnancy, some renal transporters are downregulated. Mahaney et al. [63] showed that $Na^+$-$K^+$-ATPase activity is decreased in the renal cortex during both MP and LP. In the medulla, the $Na^+$-$K^+$-ATPase activity is slightly increased during MP and then largely remained unchanged during LP [63]. It is likely that the increased progestrone and nitric oxide during pregnancy decrease the activity of cortical $Na^+$-$K^+$-ATPase [63, 93]. These findings are initially surprising as an increase in $Na^+$-$K^+$-ATPase activity would likely be expected to facilitate $Na^+$ retention. Also notable is the finding that renal NCC is essentially unchanged during MP and decreased during LP [127]. That observation appears to be counterintuitive to the upregulation of aldosterone during pregnancy, which normally activates NCC [35, 128]. Nonetheless, model simulations indicate that, with other renal adaptations, the kidney can meet the $Na^+$ transport demand in pregnancy via $Na^+$ reabsorption through other transporters and increased nephron size (Fig. 4.2A).

The kidney is larger in both MP and LP rats [49,62]. In particular, the proximal tubule significantly increases in length [15,53]; its diameter likely increases as well. Together, these

imply a significantly larger transport area. For example, in the LP model, the 17% and 7% increases in proximal length and diameter imply a 25% increase in transport area, which has a major impact on electrolyte and water transport. The effect of larger transport area has been previously assessed in a modeling study that focused on sex differences (not pregnancy). Li et al. [83] suggests that the larger transport area of the proximal tubules of the male rat compared to female (about 50%) led to a corresponding 50% higher $Na^+$ reabsorption. In the case of the pregnant rat, its larger proximal tubule may be what drives overall increased $Na^+$ retention despite downregulated key $Na^+$ transporters. It is also noteworthy that to allow for the pregnancy-induced renal hypertrophy, the cortex of a virgin female kidney may have developed to be smaller, which may explain the observation that much of the difference in size between female and male rat kidneys can be attributed to the cortex [100].

Pregnancy is marked by increased water reabsorption and water retention. Joyner et al. [66] found that AQP1, expressed along the descending thin limb, is unchanged during MP but significantly upregulated during LP. Ohara et al. [99] found that in the collecting duct, AQP2 was significantly upregulated during both MP and LP. As noted previously, the distal tubular segments are responsible for fine-tuning electrolyte and water transport. Our sensitivity analysis indicates that the marked increase in water transport along the proximal tubules alone is not enough to achieve the water retention required in pregnancy; the additional upregulation of AQP2 is necessary to avoid excessive water loss (Fig. 4.7C).

Unlike $Na^+$ retention which begins at early gestation, $K^+$ retention is only observed in LP [14, 35, 131]. $K^+$ is retained despite known kaliuretic factors, including elevated levels of circulating aldosterone [48], increased plasma $K^+$ concentration [14, 53, 131], decreased NCC activity [128], and increased ENaC activity [125] that, when taken in isolation, tend to increase $K^+$ secretion. In contrast, $K^+$ secretion along much of the distal nephron segments is mediated by the apical renal outer medullary $K^+$ channels, which are significantly downregulated in LP, likely promoting $K^+$ retention [131]. In addition, West et al. [131] found that $H^+$-$K^+$-ATPase expression is highly upregulated during LP. Salhi et al. [105] showed that in LP mice, elevated progesterone levels activated $H^+$-$K^+$-ATPase and attenuate collecting duct $K^+$ secretion. Taken together, these competing changes reduce $K^+$ excretion leading to $K^+$ retention in LP. Our sensitivity analysis indicated that upregulation of $H^+$-$K^+$-ATPase activity and significantly decreased $K^+$ secretion along the distal nephron is needed for $K^+$ retention (Fig. 4.7B), consistent with the hypothesis by West et al. [131].

Abreu et al. [4] showed major decreased ROMK2 mRNA expression in MP rats, but no other study to date has investigated $K^+$ transporter activity or expression during MP specifically. However, kaliuretic factors have been found during MP, including increased al-

dosterone and ENaC activity [35,125]. In addition, there are high progesterone levels which is known to increase $H^+$-$K^+$-ATPase activity [53,105]. Our model analysis found that without decreased $K^+$ secretion along the distal segments and collecting duct, with increased $H^+$-$K^+$-ATPase activity, excessive kaliuresis is predicted in MP (Fig. 4.7B). Therefore, we hypothesize that the $K^+$ transport adaptations that occur during LP also occur in MP (likely to a lesser extent) despite $K^+$ retention occurring only in LP.

This study sought to answer this question: What is the physiological implication of the differences in renal transporter distribution between female and male rat nephrons: lower $Na^+$ and water trasnporters and lower fractional reabsorption in the proximal nephron of female versus male rats, coupled with more abundant transporters in renal tubule segments downstream of the macula densa [112]? Our findings suggest this answer: To better prepare females for the electrolyte and fluid retention adaptations required in pregnancy. More specifically, a key finding is that the relatively large fraction of inactivated NHE3 in the proximal tubule of the female rat [112] makes it possible for increased $Na^+$ transport capacity to meet the higher demands in pregnancy, by activating reserved NHE3 without increasing the overall abundance of NHE3 proteins. Moreover, compared to males, females exhibit more abundant transporters along the distal nephron segments, which are responsible for the fine control of electrolyte excretion [52]. Indeed, simulation results indicated that $Na^+$ and $K^+$ retention in pregnancy is accomplished, in large part, by the changes in transporters along the distal nephron (Fig. 4.7). Taken together, model simulations indicated that the pregnancy-induced morphological and molecular changes allow the kidneys of a pregnant rat to meet the marked increase in filtered load, and to retain $Na^+$ and $K^+$ necessary for supporting rapid fetal growth.

### Model limitations and future extensions

Computational models of renal tubular function developed in the past two decades [58–61, 73, 74, 76, 77, 79, 80, 83, 119–121] have provided an accurate accounting of solute and water transport, and yielded insights into transport pathways, driving forces, and coupling mechanisms. As discussed in Refs. [75, 118], limitations of these models primarily include some that stem from the paucity of experimental data, and others that are inherent to the model structure (e.g., not considering spatial inhomogeneity within a compartment or intracellular signaling pathways). Given the present study's focus on pregnancy, we will discuss limitations of computational models of kidney function in pregnancy.

A notable limitation is that some of the adaptations represented in the MP and LP models are not well characterized by experimental studies or are model assumptions (e.g.,

upregulation of the $K^+$-$Cl^-$ co-transporter). Also, the present models represent a superficial nephron only. The juxtamedullary nephrons, which are not included in the models presented here, have loops of Henle that reach into the inner medulla and generally have a higher SNGFR than the superficial nephrons. More comprehensive models that include both superficial and juxtamedullary nephrons (such as in Ref. [60, 76, 80, 121]), would be able to predict more accurate urine output for MP and LP, thus giving a more comprehensive picture of kidney function during pregnancy.

This study focused on renal adaptations in a normal pregnancy, which is characterized by avid plasma volume expansion as well as $Na^+$ and $K^+$ retention. In a NP state, hypertension is generally associated with water and $Na^+$ retention [5]. Interestingly, that association appears to be broken during pregnancy. Remarkably, pregnancy tends to have an anti-hypertensive effect on spontaneously hypertensive rats [10, 85]. Hypertension during pregnancy is highly complicated and not fully understood. Additionally, hypertensive disorders of pregnancy (meaning onset of high blood pressure after start of gestation), such as gestational hypertension or pre-eclampsia, are associated with a lower plasma volume than normal pregnancy [26, 129]. Further complicating the picture is the observation that hypertension alters renal transport differently in virgin and pregnant rats. Abreu et al. [4] showed that in a virgin hypertensive rat NHE3 and NCC are upregulated signficantly and NKCC2 is slightly doesnregulated leading to increased $Na^+$ reabsorption compared to the normotensive virgin control. However, in a MP hypertensive rat $Na^+$ transporter NHE3 mRNA expression was significantly downregulated compared to normotensive MP rat control [4]. How do these hypertension-induced renal transport changes affect kidney function differently in NP and pregnancy? A combination of experimental, clinical, and theoretical efforts may be required to fully understand the pathogenesis of hypertension in pregnancy, including preeclampsia. Theoretical efforts may leverage the sex-specific computational models that have been developed for blood pressure regulation [6–8, 82].

## 4.5 Perspectives and Significance

A healthy pregnancy requires a myriad of physiological adaptations. Due to an essential increase in plasma volume and electrolyte retention, major adaptations in the kidney are required. Experimental studies have shown several major adaptations specifically in kidney morphology and renal transporter activities. To investigate the functional implications of these changes, we have developed the first computational models of nephron function during MP and LP in the rat. Model simulations quantify which adaptations play major roles in electrolyte and volume homeostasis during pregnancy, analyze the synergy of these

changes, and predicts additional adaptations necessary for homeostasis. The insights provided by the present study into renal physiology during normal pregnancy is a step towards understanding pregnancy disorders that may alter renal transport.

# Chapter 5

# Multi-nephron model of kidney function during pregnancy and hypertension

**Abstract**

During pregnancy, major adaptations in renal morphology, hemodynamics, and transport occur to achieve the volume and electrolyte retention required in pregnancy. These changes are complex, and in isolation are sometimes counterintuitive. During chronic hypertension altered renal function occurs. When a female with chronic hypertension becomes pregnant it is likely that renal function will be different than normal pregnancy renal function due the underlying pathology. The goal of this study is to analyze how altered renal function during chronic hypertension impacts renal function during pregnancy. We hypothesize that hypertension-induced changes in renal transport pattern shifts $Na^+$ transport to downstream segments, while retaining sufficient $K^+$ for pregnancy needs. To test this hypothesis, we first developed epithelial cell-based computational models of solute and water transport in the superficial and juxtamedullary nephrons of the kidney for a pregnant rat. Using this models we analyzed the full kidney impact of key pregnancy-induced renal adaptations found in our previous study. Then we developed the models to capture changes made during chronic hypertension. Reductions in proximal tubule and medullary loop transporters are represented in the models. The models predict

a shift of $Na^+$ transport load to distal segments, where transporters are up-regulated; that partially counteract natriuresis and diuresis. Our results also suggest that differential regulation of medullary (decrease) and cortical (increase) thick ascending limb transporters is important to preserve $K^+$ while minimizing $Na^+$ retention during hypertension.

## 5.1 Introduction

Normal pregnancy is characterized by complicated, multifactorical adaptations in the maternal body in almost all physiological systems [95]. These changes are dynamic, often competing, and are sometimes counterintuitive, when considered in isolation. Remarkably, in a healthy pregnancy, the maternal body can sufficiently adapt to sustain the rapidly developing fetus and placenta, and later return to normal pre-pregnancy levels post-parturition. However, when the maternal body does not sufficiently adapt, dangerous gestational disorders or fetal growth restriction may occur.

Hypertensive disorders of pregnancy are the most common gestational complication worldwide. About 10-15% of pregnancies are complicated by a hypertensive disorder, which includes chronic hypertension (hypertension before the start of gestation), gestational hypertension (onset of hypertension after 20-week gestation), preeclampsia (often diagnosed by gestational hypertension and proteinuria, severe risk of eclampsia), and chronic hypertension with superimposed preeclampsia (chronic hypertension with symptoms of preeclampsia such as proteinuria) [27,46,96,111]. Each of these disorders are highly complex and are known to have both short and long term health effects for both mother and fetus [86,88,96,111].

The kidneys play an essential role in regulating body homeostasis, namely water, electrolyte, and acid-base balance [40]. During pregnancy, the plasma volume of the mother must expand significantly to support the rapidly developing fetus and placenta [129]. In a virgin or non-pregnant (NP) rat, almost all $Na^+$ intake is excreted through urine, but in pregnancy this is not the case, there is a net $Na^+$ retention [35]. In late pregnancy, net $K^+$ retention occurs [35,127]. Since the kidneys are regulators in volume and electrolyte homeostasis, major adaptations are made in renal hemodynamics [9,15,19,21,53,84], morphology [15,53,62], and nephron transport [4,31,35,63,66,68,99,125–127,130] to support these changes.

The kidneys also play an essential role in long-term blood pressure control by maintaining $Na^+$ homeostasis. Altered renal function in a NP rat occurs during hyperten-

sion [41,97,113]. Indeed, during a pregnancy complicated by hypertension, altered expression of renal transporters has been observed [4]. There is still much to be learned about hypertensive pregnancy. In this paper we seek to investigate how hypertension impacts renal function in a female (i.e., NP) rat and pregnant rat through computational modeling. Specifically, since there are multiple hypertensive disorders of pregnancy, we investigate what may happen in the kidneys of a hypertensive female rat becomes pregnant. More details are discussed in Section 5.2.

In our previous study, we investigated the effect of pregnancy-induced renal adaptations in mid- and late pregnancy on transport in a rat superficial nephrons using computational modeling [109]. That study suggested that increased proximal tubule length, increased $Na^+/H^+$ exchanger activity, and increased epithelial $Na^+$ channel activity are likely the key players in retaining $Na^+$ during pregnancy. Additionally, the significantly downregulated $K^+$ channels in the distal segments with increased $H^+$-$K^+$-ATPase activity ensure that excess kaliuresis does not occur through pregnancy and for retention of $K^+$ in late pregnancy [109]. In this study, we expand the models developed for the superficial nephron into a model of a full kidney of a mid- and late pregnant rat. Additionally, we extend the models to investigate how hypertension may affect kidney function in pregnancy.

## 5.2 Method Details

In our previous work (Ref. [109]; Chapter 4), we developed epithelial cell-based models of a superficial nephron in the kidney of a NP, mid-pregnant (MP), and late pregnant (LP) rat. While the superficial nephrons do make up about 2/3 of the total nephron population, to capture full kidney function, we consider various types of nephrons. More specifically, both superficial and juxtamedullary nephrons. This type of model can be described as a multiple nephron model and has been developed extensively for non-pregnant rats (both male and female) [60, 80] (also see Chapter 3 Section 3.2). In this study, we developed *pregnancy-specific* multiple nephron models for MP and LP rats. Additionally, we developed models of hypertensive NP and investigated what may happen in the kidneys when a hypertensive (NP) female becomes pregnant by adding pregnancy changes to the model.

Note that the original model equations (see Ref. [60]; Chapter 3) are based on mass conservation which are also valid in pregnancy and hypertension. Hence, those same equations are used in the MP, LP, and hypertensive models, but appropriate parameter values are changed to account for the appropriate renal adaptations. The parameter changes for the MP and LP models versus NP are summarized in Table 5.1. The hypertensive NP and MP model parameter changes are summarized in Table 5.2.

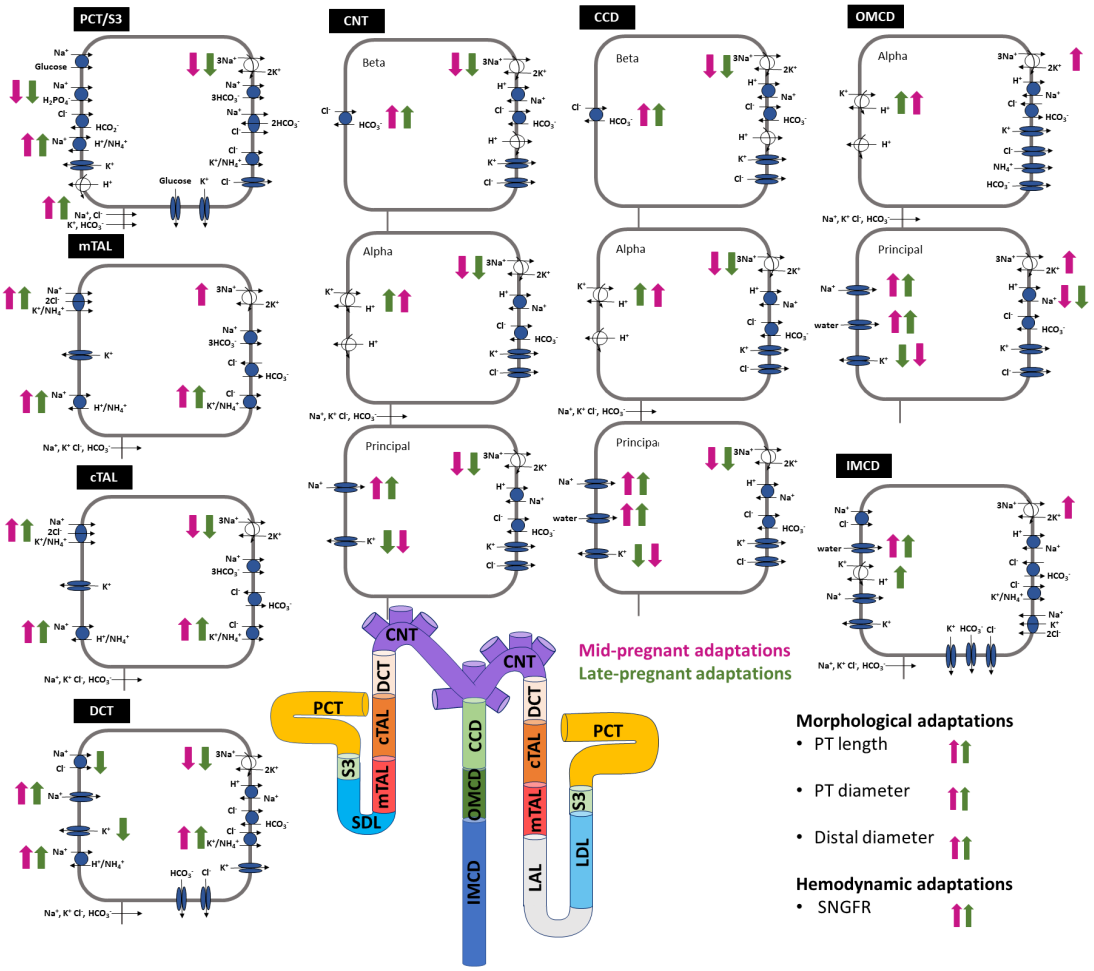


Figure 5.1: Schematic diagram of the nephrons represented in the models. The model includes a superficial and five representative juxtamedullary nephrons scaled by the appropriate population ratio. Here only one superficial and one juxtamedullary nephron are illustrated. The juxtamedullary nephron is the nephron including the LAL and LDL segments. The diagram displays main $Na^+$, $K^+$, and $Cl^-$ transporters as well as aquaporin water channels. Mid-pregnant adaptations from non-pregnancy are indicated by pink arrows. Late pregnant adaptations from non-pregnancy are indicated by green arrows. Upward orientation indicates and increase; downward orientation indicates a decrease. No arrow indicates that the transporter is not changed in the respective model. Details are shown in Table 5.1. SNGFR, single-nephron glomerular filtration rate. Other abbreviations are as listed in Fig.4.1. Cell and nephron diagram adapted from Refs. [80, 109].

### 5.2.1 Multi-nephron epithelial transport model

Each nephron segment is modeled as a tubule lined by a layer of epithelial cells in which the apical and basolateral transporters vary depending on the cell type (i.e., segment, which part of segment, intercalated and principal cells). The model accounts for the following 15 solutes: $Na^+$, $K^+$, $Cl^-$, $HCO_3^-$, $H_2CO_3$, $CO_2$, $NH_3$, $NH_4^+$, $HPO_4^{2-}$, $H_2PO_4^-$, $H^+$, $HCO_2^-$, $H_2CO_2$, urea, and glucose. The model consists of a large system of coupled ordinary differential and algebraic equations, solved for steady state, and predicts luminal fluid flow, hydrostatic pressure, membrane potential, luminal and cytosolic solute concentrations, and tancellular and paracellular fluxes through transporters and channels. A schematic diagram of the various cell types, with MP and LP changes highlighted, is given in Fig. 5.1.

*Superficial vs.juxtamedullary nephrons.* Kidneys have multiple types of nephrons; superficial and juxtamedullary nephrons make up most of them [54, 56, 64]. In a rat, about two-thirds of the nephron population are superficial nephrons: the remaining third are called juxtamedullary nephrons. These two nephron types have several key differences. The first major difference is that the juxtamedullary nephrons have loops of Henle that reach differing depths into the inner medulla. In contrast, the loops of superficial nephrons turn before reaching the inner medulla. To capture this, in the model there are six classes of nephrons: a superficial nephron (denoted by "SF") and five juxtamedullary nephrons that are assumed to reach depths of 1,2,3,4, and 5 mm (denoted by "JM-1", "JM-2", "JM-3", "JM-4", and "JM-5", respectively) into the inner medulla. In the same was as in Ref. [80], the ratios for the six nephron classes are $n_{\text{sf}} = 2/3$, $n_{\text{JM}-1} = 0.4/3$, $n_{\text{JM}-2} = 0.3/3$, $n_{\text{JM}-3} = 0.15/3$, $n_{\text{JM}-4} = 0.1/3$, and $n_{\text{JM}-5} = 0.05/3$ so that 2/3 of the nephrons are superficial and juxtamedullary nephrons make up the remaining 1/3 of the nephrons. Note that shorter juxtamedullary nephrons are the most common, thus turning in the upper portion of the inner medulla. These assumptions are used from Ref. [80] which were based on anatomical findings in Ref. [71].

The previously developed superficial nephron NP, MP, and LP models (see Ref. [109]; Chapter 4) include the proximal tubule, short descending limb, thick ascending limb, distal convoluted tubule, connecting tubule, and the collecting duct segments. The juxtamedullary nephron models include all the same segments of the superficial nephrons with the addition of the long descending limbs and ascending thin limbs; these are the segments of the loops of Henle that extend into the inner medulla (see Fig. 5.1). The length of the long descending limbs and ascending limbs are determined by which type of juxtamedullary nephron is being modeled.

It has been shown that the SNGFR for juxtamedullary nephrons is higher than the superficial nephron SNGFR [64, 80]. We assume that the juxtamedullary SNGFR is about

40% higher than the superficial SNGFR in the NP model as done in Ref. [60] and is reported in experimental studies in Refs. [54, 56, 64].

All other segments in the juxtamedullary nephrons are the same as the superficial nephrons except the length of the cortical thick ascending limb and the connecting tubule. Since the glomeruli of the juxtamedullary nephrons are lower down in the cortex than the superficial nephrons these segments do not have to be as long for the nephron to pass the glomerulus in the macula densa. Hence, these segments are modeled with a shorter length.

The connecting tubules of the five juxtamedullary nephrons and the superficial nephron coalesce into the cortical collecting duct. To model this, we compute the flows from the six nephrons at the start of the collecting duct. The remaining model is the collecting duct which does not have distinct nephron segments.

### 5.2.2 Pregnancy-specific models

We created pregnancy-specific models to simulate kidney function in MP and LP by using the NP (female-specific) multiple nephron epithelial transport model developed in Ref. [60] (discussed in Chapter 3; Section 3.3) and increasing or decreasing relevant NP model parameter values based on experimental findings in the literature. The specific MP-to-NP and LP-to-NP parameter value ratios are listed in Table 5.1.

During pregnancy, there is a significant increase in GFR compared to the NP values [13, 20–22, 29, 45, 53, 129]. Specifically, in rats, the GFR increase is by about 30% in MP and drops in LP to about 20% above pre-gestational (NP) GFR [20, 22, 53, 129]. The GFR is the total filtration by a kidney, hence is a total combination of the SNGFR of the superficial and juxtamedullary nephrons (denoted by $\text{SNGFR}_{\text{sup}}$ and $\text{SNGFR}_{\text{jux}}$, respectively) so that

$$\text{GFR} = n_{\text{sup}}\text{SNGFR}_{\text{sup}} + n_{\text{jux}}\text{SNGFR}_{\text{jux}} \tag{5.1}$$

where $n_{\text{sup}}$ and $n_{\text{jux}}$ denote the total number of superficial and juxtamedullary nephrons in a rat kidney (i.e., $n_{\text{sup}} = 2/3 \times 36,000$ and $n_{\text{jux}} = 1/3 \times 36,000$).

In our pregnancy-specific superficial nephron models (see Ref. [109]; Chapter 4), $\text{SNGFR}_{\text{sup}}$ was increased by 30% in MP and 20% in LP based on Ref. [20]. Note that by using (5.1) we can note that to have a 30% and 20% increase in the MP and LP GFR, respectively, that $\text{SNGFR}_{\text{jux}}$ must be increased by 30% and 20% in the MP and LP models, respectively (see Table 5.1). We note that it has been shown that increased GFR in pregnancy has been attributed to increased renal blood flow [22], so then a similar increase in filtration in both the superficial and juxtamedullary nephrons would be supported by this hypothesis.

We changed parameters in the same way as the pregnancy-specific superficial nephron models developed by Stadt & Layton [109] (Chapter 4. See Table 5.1 for the full list of MP and LP model changes from NP. It is assumed that the activity levels of the transporters in the superficial nephrons are changed in the same way as in the juxtamedullary nephrons.

Table 5.1: MP-to-NP and LP-to-NP ratios of parameter values used in the MP and LP models, respectively. NP parameter values were used from [60] and changed by the respective ratio for the MP and LP models. Parameter values for the MP and LP models were chosen based on experimental literature and are discussed in the Materials and Methods section. PCT, proximal convoluted tubule; S3, proximal straight tubule; LDL, thin descending limb; LAL, thin ascending limb; mTAL, medulalry thick ascending limb; cTAL, cortical thick ascending limb; DCT, distal convoluted tubule; CNT, connecting tubule; CCD, cortical collecting duct; OMCD, outer medullary collecting duct; IMCD inner medullary collecting duct; $P_f$, water permeability; $P_K$, $K^+$ permeability; NHE3, $Na^+/H^+$ exchanger isoform 3; ENaC, epithelial $Na^+$ channel; NKCC2, $Na^+$-$K^+$-$2Cl^-$ cotransporter 2; NaPi2, $Na^+$-$H_2PO_4^-$ cotransporter 2; NCC, $Na^+$-$Cl^-$ cotransporter; KCC, $K^+$-$Cl^-$ cotransporter; PT, proximal tubule. Distal segments refer to all segments other than the PT and S3 segments (i.e., after the proximal tubule). Ratios are from the respective MP or LP model to the NP model parameter value. The same ratios are used for both the superficial and juxtamedullary nephrons. $P_f$: water permeability; $P_K$: $K^+$ permeability; NHE3: $Na^+/H^+$ exchanger isoform 3; ENaC: epithelial $Na^+$ channel; NKCC2: $Na^+$-$K^+$-$2Cl^-$ cotransporter isoform 2; NaPi2: $Na^+$-$H_2PO_4^-$ cotransporter; NCC: $Na^+$-$Cl^-$ cotransporter; NHE-1: $Na^+/H^+$ exchanger isoform 1; KCC: $K^+$-$Cl^-$ cotransporter

| **Parameter** | **Ratio** | |
|---|---|---|
| | **MP-to-NP** | **LP-to-NP** |
| **PCT** | | |
| NHE3 activity | 1.40 | 1.20 |
| $Na^+$-$K^+$-ATPase activity | 0.75 | 0.65 |
| $P_f$ (transcellular) | 1.00 | 1.00 |
| $K^+$-$Cl^-$ cotransporter | 1.35 | 1.30 |
| NaPi2 | 0.90 | 0.85 |
| **S3** | | |
| NHE3 activity | 1.40 | 1.20 |
| $Na^+$-$K^+$-ATPase activity | 0.73 | 0.65 |
| $P_f$ (transcellular) | 1.00 | 1.00 |
| $K^+$-$Cl^-$ cotransporter | 1.35 | 1.3 |

Table 5.1: MP-to-NP and LP-to-NP ratios of parameter values used in the MP and LP models, respectively.

| **Parameter** | **Ratio** | |
|---|---|---|
| | **MP-to-NP** | **LP-to-NP** |
| NaPi2 | 0.90 | 0.85 |
| **SDL** | | |
| $P_f$ (transcellular) | 1.10 | 1.50 |
| **LDL** | | |
| $P_f$ (transcellular) | 1.10 | 1.50 |
| **LAL** | | |
| | | |
| **mTAL** | | |
| NKCC2 activity | 1.15 | 1.50 |
| NHE3 activity | 1.20 | 1.18 |
| KCC4 activity | 1.40 | 1.30 |
| $Na^+$-$K^+$-ATPase activity | 1.15 | 1.00 |
| **cTAL** | | |
| NKCC2 activity | 1.15 | 1.50 |
| $Na^+/H^+$ exchanger activity | 1.20 | 1.18 |
| KCC activity | 1.35 | 1.30 |
| $Na^+$-$K^+$-ATPase activity | 0.73 | 0.65 |
| **DCT** | | |
| $P_K$ (apical side, DCT2 only, ROMK) | 0.65 | 0.55 |
| $Na^+$-$K^+$-ATPase activity | 0.75 | 0.74 |
| NHE2 activity | 1.20 | 1.18 |
| KCC activity | 1.40 | 1.30 |
| NCC activity | 1.00 | 0.45 |
| ENaC activity | 2.08 | 2.15 |
| **CNT** | | |
| $P_K$ (apical side, ROMK) | 0.65 | 0.55 |
| $Na^+$-$K^+$-ATPase activity | 0.75 | 0.75 |
| $H^+$-$K^+$-ATPase activity | 2.5 | 2.75 |
| $H^+$-ATPase activity | 1.00 | 1.00 |
| Pendrin activity | 1.65 | 1.70 |
| ENaC activity | 2.08 | 2.15 |
| **CCD** | | |

Table 5.1: MP-to-NP and LP-to-NP ratios of parameter values used in the MP and LP models, respectively.

| **Parameter** | **Ratio** | |
|---|---|---|
| | **MP-to-NP** | **LP-to-NP** |
| $P_f$ (transcellular, AQP2) | 1.40 | 1.40 |
| $P_K$ (apical, BK) | 0.75 | 0.75 |
| $Na^+$-$K^+$-ATPase activity | 0.80 | 0.75 |
| $H^+$-ATPase activity | 1.00 | 1.00 |
| $H^+$-$K^+$-ATPase activity | 2.25 | 2.75 |
| ENaC activity | 1.85 | 2.15 |
| Pendrin activity | 1.65 | 1.70 |
| **OMCD** | | |
| $P_f$ (transcellular, AQP2) | 1.40 | 1.4 |
| $P_K$ (apical, BK) | 0.88 | 0.85 |
| $Na^+$-$K^+$-ATPase activity | 1.20 | 1.08 |
| $H^+$-ATPase activity | 1.00 | 1.00 |
| $H^+$-$K^+$-ATPase activity | 2.25 | 2.75 |
| ENaC activity | 2.08 | 2.15 |
| $Na^+$-$Cl^-$ cotransporter | 1.15 | 1.00 |
| NHE1 activity | 0.90 | 0.90 |
| **IMCD** | | |
| $P_f$ (trancellular, AQP2) | 1.80 | 1.80 |
| NKCC1 activity | 1.00 | 1.00 |
| $Na^+$-$K^+$-ATPase activity | 1.20 | 1.08 |
| $K^+$-$Cl^-$ cotransporter | 1.40 | 1.30 |
| $Na^+$-$Cl^-$ cotransporter | 1.15 | 1.00 |
| $H^+$-$K^+$-ATPase activity | 2.25 | 2.75 |
| **Morphology** | | |
| **PCT, S3** | | |
| Length | 1.15 | 1.17 |
| Diameter | 1.07 | 1.07 |
| **Distal segments** | | |
| Length | 1.00 | 1.00 |
| Diameter | 1.05 | 1.05 |
| **Hemodynamics** | | |
| SNGFR | 1.30 | 1.20 |

Table 5.1: MP-to-NP and LP-to-NP ratios of parameter values used in the MP and LP models, respectively.

| **Parameter** | **Ratio** | |
|---|---|---|
| | **MP-to-NP** | **LP-to-NP** |
| **Plasma concentration** | | |
| Plasma $Na^+$ concentrations | 0.95 | 0.95 |
| Plasma $K^+$ concentrations | 1.0 | 1.15 |
| Plasma $Cl^-$ concentrations | 0.95 | 0.95 |

### 5.2.3 Simulating hypertension in females and pregnancy

To study the impact of hypertension in a NP female as well as during pregnancy, we developed models that captured renal changes during hypertension in an approach similar to Edwards and McDonough [41]. We note that during pregnancy there are multiple types of hypertensive disorders of pregnancy. In this study, we simulate what happens when a female rat that is hypertensive (pre-gestation) gets pregnant. Therefore, we simulate the hypertensive mid-pregnant rat as the hypertensive NP rat model with the mid-pregnancy changes in order to test what may happen if a female rat with hypertension became pregnant. We note that this is different than gestational hypertension which is hypertension that occurs after the start of pregnancy.

The parameter changes made to simulate hypertension were based largely on the hypertensive NP (female) rat study by Veiras et al. [113], which investigated the effect of hypertension on female and male rats. Additionally, we make parameter changes using the results from Abreu et al. [4], who investigated the effects of hypertensive non-pregnancy and hypertensive mid-pregnancy on renal $Na^+$ and aquaporin (AQP) transporters. The exact parameter changes made are listed in Table 5.2 and are described here.

Table 5.2: Parameter changes made in the hypertensive non-pregnant and hypertensive mid-pregnant models given as ratios from the hypertensive (HT) model parameter to the normotensive (NT) model parameter. Parameter change ratios for hypertension are the same in both the hypertensive non-pregnant and hypertensive mid-pregnant models. Abbreviations are the same as listed in Table 5.1.

| **Parameter** | **Ratio: HT-to-NT** |
|---|---|
| **PCT** | |
| NHE3 activity | 0.82 |
| NaPi2 | 0.85 |
| $Na^+$-$K^+$-ATPase activity | 1.00 |
| **S3** | |
| NHE3 activity | 0.82 |
| NaPi2 | 0.85 |
| $Na^+$-$K^+$-ATPase activity | 1.00 |
| **mTAL** | |
| NKCC2 activity | 0.70 |
| NHE3 activity | 0.82 |
| $Na^+$-$K^+$-ATPase activity | 0.70 |
| **cTAL** | |
| NKCC2 activity | 1.74 |
| NHE3 activity | 1.00 |
| $Na^+$-$K^+$-ATPase activity | 1.00 |
| **DCT** | |
| $P_K$ (apical side, DCT2 only, ROMK) | 0.30 |
| $Na^+$-$K^+$-ATPase activity | 1.00 |
| NCC activity | 1.95 |
| ENaC activity | 1.45 |
| **CNT** | |
| $P_K$ (apical side, ROMK) | 0.30 |
| $Na^+$-$K^+$-ATPase activity | 1.00 |
| ENaC activity | 1.45 |
| **CCD** | |
| $P_f$ (transcellular, AQP2) | 1.30 |
| $Na^+$-$K^+$-ATPase activity | 1.00 |
| ENaC activity | 1.45 |
| **OMCD** | |

Table 5.2: Hypertensive to normotensive ratios of parameter values used in the hypertensive models.

| **Parameter** | **Ratio: HT-to-NT** |
|---|---|
| $P_f$ (transcellular, AQP2) | 1.30 |
| $Na^+$-$K^+$-ATPase activity | 1.00 |
| ENaC activity | 1.45 |
| **IMCD** | |
| $P_f$ (trancellular, AQP2) | 1.30 |
| $Na^+$-$K^+$-ATPase activity | 1.00 |
| ENaC activity | 1.45 |
| **Hemodynamics** | |
| SNGFR | 1.00 |

### Proximal segment changes

The fluid inflow at the start of the proximal tubule is assumed to be the same as the normotensive NP and MP models in the hypertensive NP (NP-HTN) and hypertensive MP (MP-HTN) models in the same way as Edwards and McDonough [41].

Located on the basolateral side of every cell type in every segment along the nephron, the $Na^+$-$K^+$-ATPase pump is a key driver of $Na^+$ transport. $Na^+$-$K^+$-ATPase abundance has been shown to be decreased in the medullary thick ascending limb during hypertension [97, 113]. $Na^+$-$K^+$-ATPase abundance in the proximal and distal tubules, as well as the cortical part of the ascending limb was largely unchanged [97, 113]. To incorporate this into the model, we decreased $Na^+$-$K^+$-ATPase activity in the medullary thick ascending limb and left the activity unchanged in the other segments in the hypertensive models (see Table 5.2).

The $Na^+/H^+$ exchanger isoform 3 (NHE3) is located along the apical side of the epithelial cells in the proximal tuble and thick ascending limb. This transporter plays a major role in $Na^+$ reabsorption along these early segments of the nephrons. During hypertension, there is blunted pressure-natriuresis which often is attributed to lower NHE3 activity. Abreu et al. [4] showed that in MP rats, there was decreased expression of NHE3. Veiras et al. [113] found that along the proximal tubule and the medullary thick ascending limb, NHE3 activity in hypertensive rats was decreased from normotensive NHE3 activity. We chose a value slightly higher for the NP (female) rats from the parameter change chosen in

Edwards and McDonouugh [41] since hypertensive females seemed to have slightly higher relative NHE3 activity than hypertensive males [113]. In the cortical segment of the thick ascending limb, it has been shown that the NHE3 activity is largely unchanged in a hypertensive rat, hence we did not change the NHE3 activity in that segment in the hypertensive models [97]. See Table 5.2 for exact changes made in the NP-HTN and MP-HTN models.

The $Na^+/P_i$ cotransporter 2 (NaPi2) is in the proximal tubule. Veiras et al. [113] found in hypertensive rats that NaPi2 expression was decreased compared to normotensive rats. As such, we decreased NaPi2 activity in the hypertensive models (Table 5.2).

The $Na^+$-$K^+$-$2Cl^-$ cotransporter (NKCC2) is located on the apical membrane along the thick ascending limb. During hypertesnion, NKCC2 activity is different in the medullary and cortical segments [41,97,113]. Specifically, in the cortex, NKCC2 activity is increased, while in the medulla, NKCC2 is significantly decreased [41, 97, 113]. We altered NKCC2 activity in the hypertensive models accordingly (Table 5.2).

### Distal segment changes

The $Na^+$-$Cl^-$ cotransporter (NCC) is located along the first part of the distal convoluted tubule. During hypertension, NCC abundance and phosphorylation has been found to increase significantly [41,97,113]. Parameter changes in NCC activity in the hypertensive models is listed in Table 5.2.

Abreu et al. [4] found a major decrease in the expression of the renal outer medullary $K^+$ channel (ROMK) during hypertension for both NP and MP. To capture this, we significantly decreased $K^+$ permeability in the late distal convoluted tubule (DCT2) and connecting tubule (see Table 5.2).

The epithelial $Na^+$ channel (ENaC) is one of the major $Na^+$ channels in the distal segments. The ENaC plays an important role in fine-tuning the remaining $Na^+$ in the nephron in the distal segments before what is left is excreted through urine. During hypertension, ENaC activity is increased [41, 97, 113]. Since the female ENaC relative increase appears to be slightly higher than males as shown by Veiras et al. [113], we chose to increase the ENaC activity more than done in the previous hypertensive male model by Edwards & McDonough [41]. The hypertensive modell parameter change is given in Table 5.2.

Abreu et al. [4] showed major changes in aquaporin 2 (AQP2) expression in the collecting duct. Specifically, in the hypertensive NP results, the AQP2 expression increased from normotensive NP levels. We changed the water permeability in the collecting duct segments based on this result (see Table 5.2).

We chose to only simulate hypertension in the MP model because no study to date has studied transporter function during hypertension in LP.

## 5.3 Results

### Differences in segmental transporter during mid- and late pregnancy

Solute and fluid reabsorption along specific nephron segments depend on activity of membrane transporters, permeability of the apical and basolateral membrane, as well as tubular morphology. There are many changes in almost all nephron segments during pregnancy. To investigate this, we developed baseline models to represent kidney function in a NP, MP, and LP rat. The models are based on our previous work (see Ref. [109]; Chapter 4) and are described in Section 5.2. Delivery of key solutes ($Na^+$, $K^+$, $Cl^-$, $NH_4{}^+$, $HCO_3{}^-$) and fluid volume to each segment is shown in Fig. 5.2 and transport predictions for each segment given in Fig. 5.3.

There are two classes of nephrons captured in the models: superficial and juxtamedullary. Note that, the single nephron glomerular filtration rate (SNGFR) for juxtamedullary nephrons is higher than the superficial nephron SNGFR. However, the ratio of the number of superficial nephrons to juxtamedullary nephrons is 2:1 so juxtamedullary nephrons have a smaller contribution to total filtration when compared to the superficial nephrons (Fig. 5.2).

In the NP model, the superficial SNGFR is 24 nL/min and the juxtamedullary SNGFR is 33.6 nL/min. A similar ratio between juxtamedullary and superficial SNGFR parameter values is assumed to hold for the MP and LP models (i.e., juxtamedullary SNGFR to superficial SNGFR is about 1.4). The superficial and juxtamedullary SNGFR is assumed to be 30% higher in the MP model, when compared to the respective NP model values (Table 5.1). In the LP model, the superficial and juxtamedullary nephron SNGFR is 20% higher compared to the respective NP models values (Table 5.1). For both the MP and LP models, this yields a proportional increase in total fluid and solute delivery at the start of the proximal tubule in the MP and LP model predictions (see Fig. 5.2).

Model predictions indicated that $Na^+$ and $Cl^-$ reabsorption in the proximal tubule of the MP and LP models is significantly larger than in NP (Fig. 5.2A; Fig. 5.2C). Specifically, MP and LP models predicted a 27% and 16% increase in net $Na^+$ reabsorption along the proximal tubule when compared to NP. However, note that due to the large increase in filtration in MP and LP, fractional reabsorption of $Na^+$ is about 60% for each of the NP,

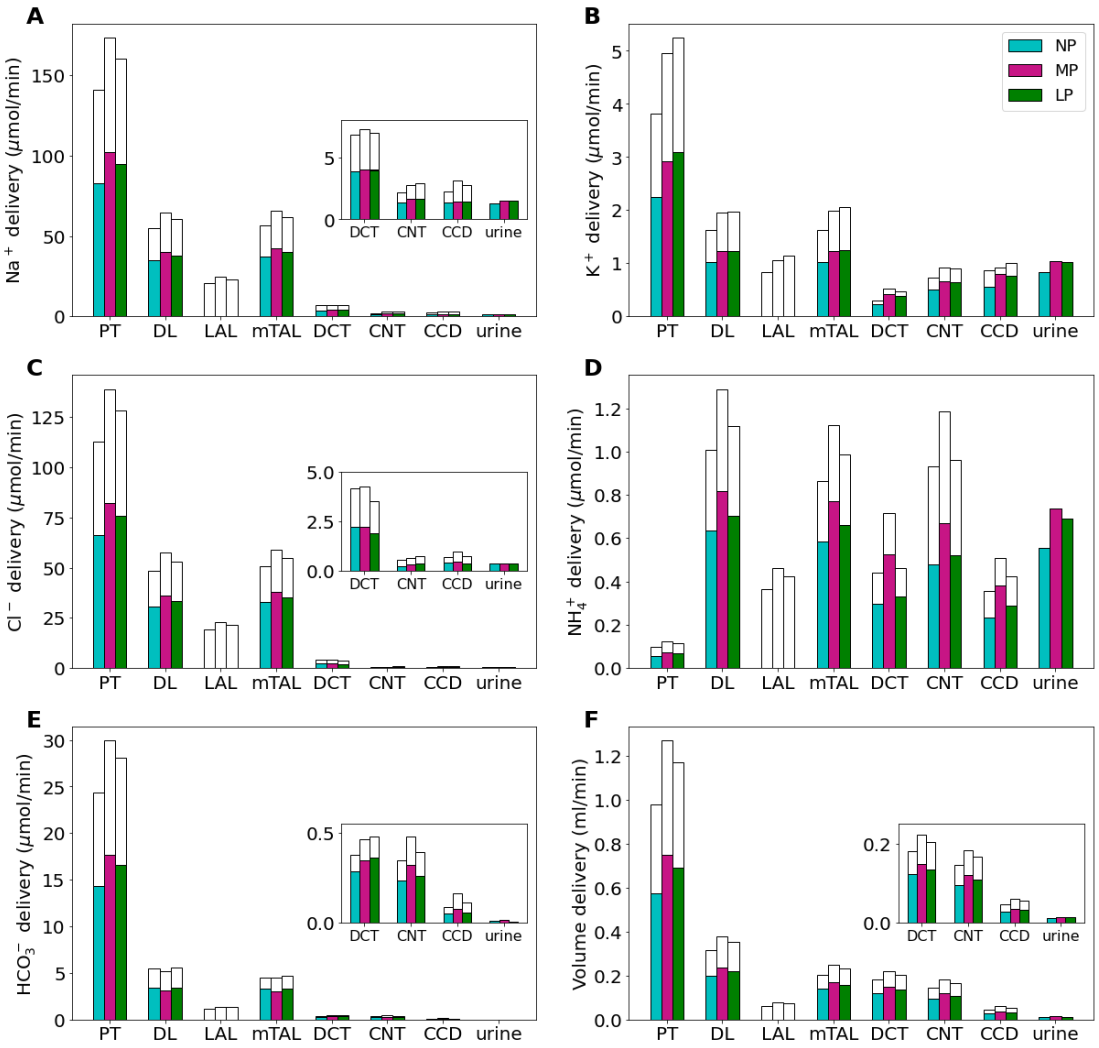


Figure 5.2: Delivery of key solutes (*A*-*E*) of fluid volume (*F*) to the beginning of individual nephron segments in the non-pregnant (NP), mid-pregnant (MP), and late pregnant (LP) rat models. The colored bars denote the superficial nephron values, and the white bars denote the weighted totals of the juxtamedullary nephrons (five representative model nephrons). Note that since the model assumes the the superficial-to-juxtamedullary nephron ratio is 2:1, the superficial delivery values are generally higher. Additionally, the juxtemedullary and superficial nephrons merge at the collecting duct so that the urine output value is combined. PT, proximal tubule, DL, descending limb; mTAL, medullary thick ascending limb; DCT, distal convoluted tubule; CNT, connecting tubule; CCD, cortical collecting duct. *Insets:* reproduction of distal segment values.

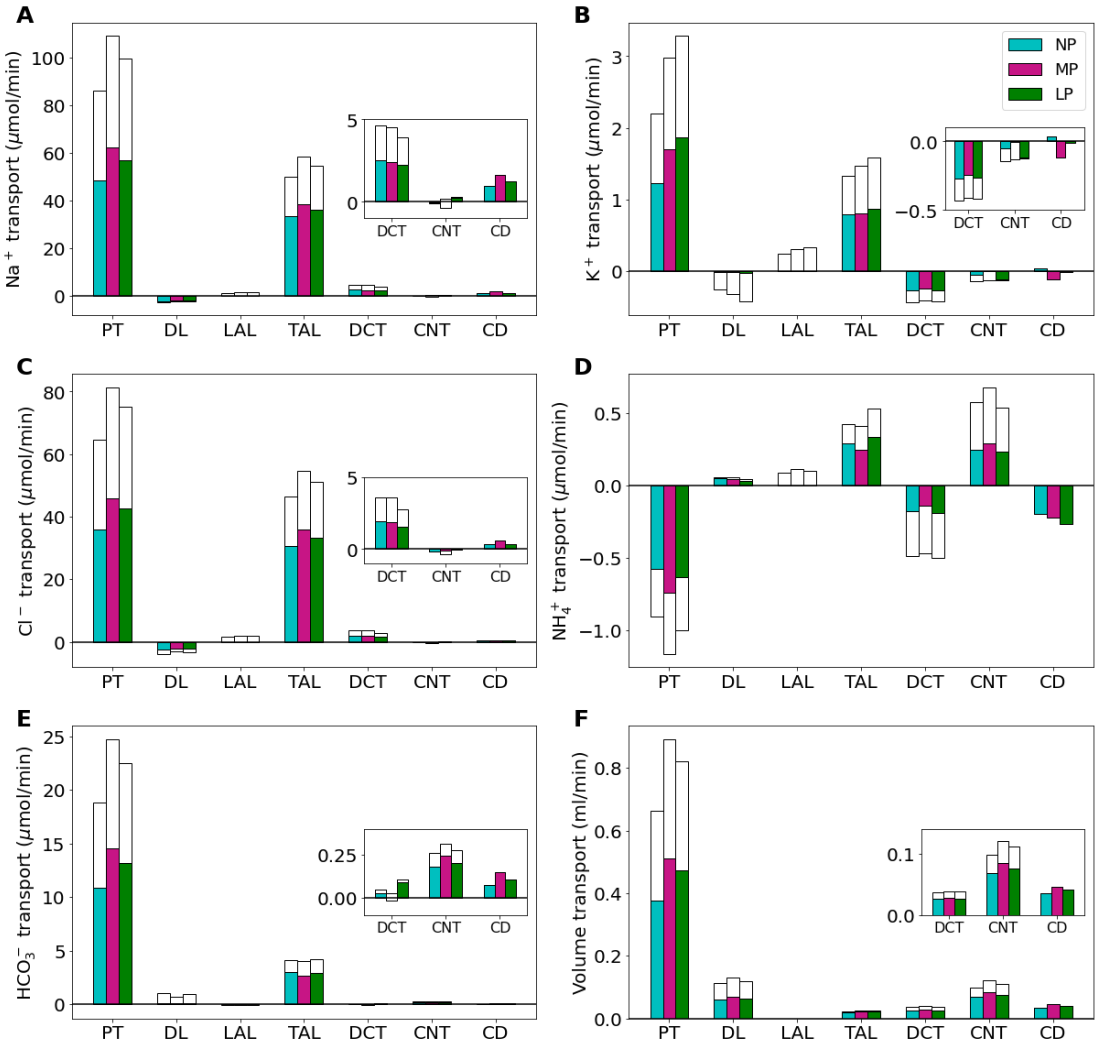


Figure 5.3: Net segmental transport of key solutes (*A*-*E*) and volume (*F*) along the individual nephron segments in the NP, MP, and LP models. Transport is positive out of the nephron segment, i.e., positive transport indicates net reabsorption and negative indicates net secretion along that segment. Colored bars denote the superficial nephron values and white bars denote juxtamedullary values computed as a weighted sum of the five representative juxtamedullary nephrons. PT, proximal tubule, DL, descending limb; LAL, thin ascending limb; mTAL, medullary thick ascending limb; DCT, distal convoluted tubule; CNT, connecting tubule; CD, collecting duct. *Insets:* reproduction of distal segment values.

MP, and LP models along the proximal tubule. Analogous results are obtained for $Cl^-$ and fluid volume along the proximal tubule (see Fig. 5.2). Downstream of the proximal tubule, the thick ascending limb reabsorbs much of the remaining $Na^+$ and $Cl^-$. In the MP model, $Na^+$ delivery to the thick ascending limb is 16% higher than NP values (Fig. 5.2A). Reabsorption along the thick ascending limb increased by about 16% in MP (Fig. 5.3A). Analogous results are obtained for $Cl^-$. In the end, urinary $Na^+$ excretion for both MP and LP is about 16% higher than NP values and urinary $Cl^-$ excretion is increased by 4% and 6% in the MP and LP models, respectively. The increase in natriuresis and $Cl^-$ excretion in the pregnancy models versus the NP model are within reported ranges [14, 125].

Fluid volume reabsorption follows in a similar way to $Na^+$ reabsorption. In the proximal tubule, the increased tubular transport area from the increased length and diameter of the tubule, as well as increased $Na^+$ reabsorption, increase water reabsorption along the proximal tubule by 34% and 24% in the MP and LP models, respectively, when compared to NP values (Fig. 5.3F). In the segments after the macula densa and the collecting duct, water reabsorption is also increased by 22% and 12% in the MP and LP models, respectively when compared to NP values (Fig. 5.3F). This is likely driven by increased AQP2 expression, increased nephron diameter and length, as well as increased fluid volume delivery to these segments.

Along the proximal tubule, about 58% of the filtered $K^+$ is reabsorbed in the NP model. During LP, the fractional reabosrption of $K^+$ in the proximal tubule increases to about 63% (Fig. 5.3B). This is due to the massive increase in delivery of $K^+$ from increased plasma $[K^+]$ and total filtered load at the beginning of the proximal tubule with increased $K^+$ transport capacity (Fig. 5.2B). Distal segment $K^+$ secretion along the distal convoluted tubule and connecting tubules is decreased by about 8% in the MP and LP models from NP values despite known kaliuretic factors such as increased $Na^+$ delivery (Fig. 5.3B). This is due to the decreased $K^+$ channel permeability in these segments (see Table 5.1). In all, $K^+$ urinary excretion is predicted to be about 2.4, 3.0, and 2.9 mmol/day in the NP, MP, and LP models, respectively. The increase in kaliuresis from NP values in the MP and LP models is within reported ranges [14, 127].

In summary, similar to our previously developed superficial nephron model (see Ref. [109]), the pregnancy-induced adaptations captured in the multiple nephron MP and LP models yield functional changes that predict sufficient reabsorption of the enhanced filtered loac induced by increased GFR during normal pregnancy.

### Impact of key pregnancy-induced renal adaptations in LP

In our previous study we investigated the functional implications of pregnancy-induced hemodynamic, morphological, and transporter renal adaptations on a superficial nephron [109]. We predicted which adaptations may have the largest impact on $Na^+$ and $K^+$ reabsorption in pregnancy. The adaptations in the proximal segment that had the largest impact on $Na^+$ and $K^+$ urinary excretion was PT length, $Na^+/H^+$ exchanger isoform 3 (NHE3) activity, and $Na^+$-$K^+$-ATPase activity. In the distal segments, epithelial $Na^+$ channel activity, $H^+$-$K^+$-ATPase activity, and $K^+$ channel permeability had the most significant impact on $Na^+$ and $K^+$ reabsorption. Here we use the full-kidney pregnancy-specific computational models to predict how some of the major changes may affect renal function during LP. To do this we considered the renal adaptations that were indicated to have a major impact on nephron transport and conducted simulations of LP kidney function without such adaptation (i.e., respective parameter value at the NP model value). Transport of $Na^+$ and $K^+$ for adaptations that effect the proximal segments of the nephron (i.e., proximal tubule length, NHE3 activity, and $Na^+$-$K^+$-ATPase activity) are given in Fig. 5.4.

Most reabsorption in the kidneys occurs in the proximal segments, which include the proximal tubule and the loop of Henle. During LP, the proximal tubule length is increased by about 17% from the baseline NP length (Table 5.1; Refs. [15, 53, 109]), which increases transport capacity along the proximal tubule of the nephrons. Without this change, we predict that the PT reabsorbs 11% less $Na^+$ than the baseline LP model (Fig. 5.4A). While the TAL and distal segments increase reabsorption, it is not enough to make up for the loss of proximal tubule $Na^+$ reabsorption, resulting in an increase of about 77% in urine excretion of $Na^+$ (Fig. 5.4A). Similarly, without the PT length increase, $K^+$ reabsorption is signficantly decreased in the PT segment, ultimately resulting in a 46% increase in urinary $K^+$ excretion.

NHE3 is a major driver of $Na^+$ reabsorption in the proximal tubule. In our previous study ( [109]; Chapter 4), we predicted that NHE3 activity was likely increased during pregnancy to prevent excessive natriuresis and kaliuresis. For LP, we assume about a 20% increase in activity (Table 5.1). Decreasing NHE3 activity to the NP values results in a 2% decrease in PT reabsorption. This change is not made up for in the late segments and results in a 17% increase in urinary $Na^+$ excretion. Additionally, since $K^+$ and $Na^+$ reabsorption is mutually dependent due to the electrochemical gradient and exchange through the $Na^+$-$K^+$-ATPase pump, this change in NHE3 activity alters $K^+$ handling. $K^+$ secretion along the CNT is increased by about 62%. In the end, urinary $K^+$ excretion is predicted to increase by 8%.

The effect of pregnancy on $Na^+$-$K^+$-ATPase activity in the kidneys is region-specific

[63]. Specifically, Mahaney et al. [63] found that in LP, cortical $Na^+$-$K^+$-ATPase activity is decreased from NP values, while medullary $Na^+$-$K^+$-ATPase activity is largely unchanged ( [63]; Table 5.1). Setting the $Na^+$-$K^+$-ATPase activity in each segment to the NP value resulted in a 16% decrease in urinary excretion of $Na^+$ and a 5% decrease in $K^+$ excretion (see Fig. 5.4).

The distal segments account for much of the fine tuning of fluid concentration in the kidney nephrons before excreting what is remaining inside the nephron. In our analysis of a superficial nephron, we predicted that key distal segment adaptations seem to play a significant role in gestational nephron function [109]. The epithelial $Na^+$ channel (ENaC) has been found to be increased in abundance during pregnancy [125,127], likely contributing to increased ENaC activity. Additionally, key $K^+$ transporters are altered, namely the activity of key distal segment $K^+$ channels, the renal outer medullary $K^+$ channel (ROMK) and big $K^+$ channel (BK), are significantly decreased [131]. (Note that this is represented by $P_K$ in Table 1.) These channels are secretory in that they secrete $K^+$ along the distal segments. Additionally, the $H^+$-$K^+$-ATPase transporter has been found to have significantly increased activity [105, 131]. We conducted simulations of the LP model without such changes and present the results for $Na^+$ and $K^+$ transport as well as urinary excretion in Fig. 5.5.

The ENaC plays a key role in reabsorbing $Na^+$ along the late distal convoluted tubule, connecting tubule, and collecting duct. Without a large increase in ENaC activity in the LP model, $Na^+$ reabsorption in the distal convoluted tubule and connecting tubule decreased by 13%. This yielded a 22% increase in urinary $Na^+$ excretion (Fig. 5.5A). Notably, increased ENaC activity is a known kaliuretic factor. Without a pregnancy-induced increase in ENaC activity, we predict a 15% decrease in urinary $K^+$ excretion (Fig. 5.5B).

$K^+$ secretory channels are significantly decreased during LP. Without this change, in the LP model, $K^+$ secretion along the DCT increased by 26%. CNT $K^+$ secretion does decrease to make up for this extra $K^+$ loss, but excess kaliuresis does occur with an increase in $K^+$ excretion by about 8%. The other $K^+$ transporter altered during LP is $H^+$-$K^+$-ATPase activity, which is significantly increased (Table 5.1). Without this change, both the CNT and CD $K^+$ secretion more than doubles (Fig. 5.5B). This results in urinary $K^+$ increase by 19%.

In summary, our model predictions indicated that the proximal tubule lengthening during pregnancy has the largest impact on urinary $Na^+$ and $K^+$ excretion. This major morphological change along with altered transporter activity is essential for preventing excess natriuresis and kaliuresis during pregnancy.

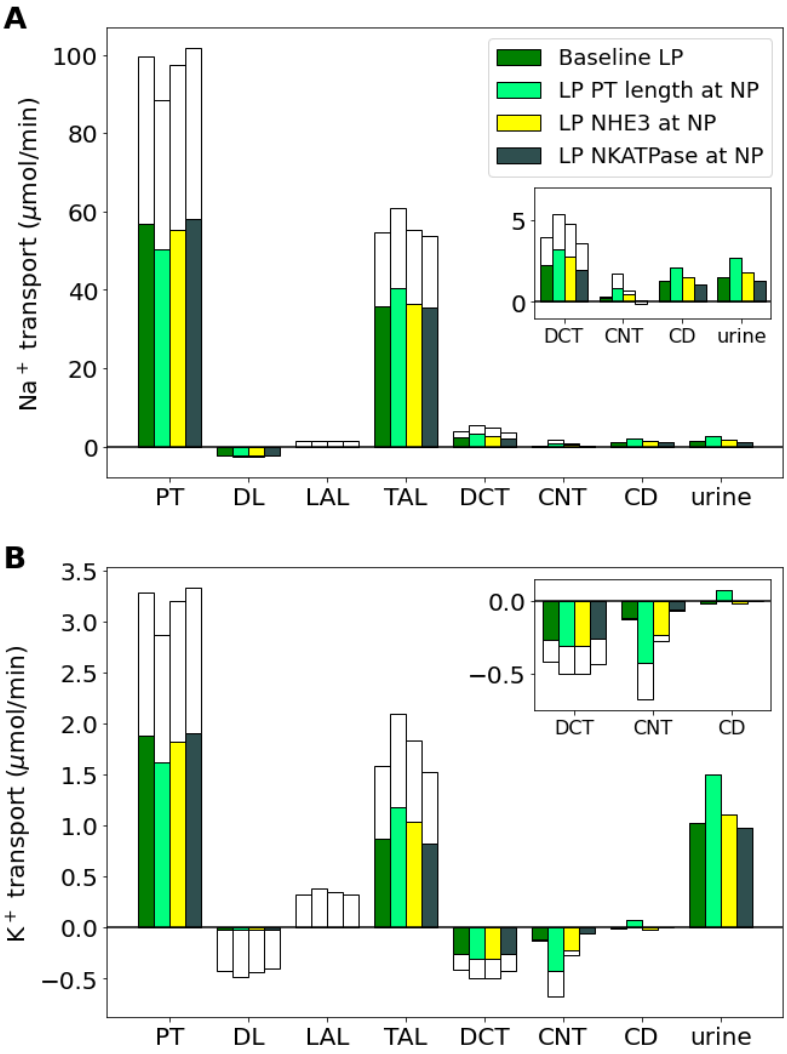


Figure 5.4: Impact of key pregnancy-induced proximal segment renal adaptations on net segmental transport and urine excretion of $Na^+$ (*A*) and $K^+$ (*B*) along individual nephron segments in the baseline LP model and LP model with one pregnancy-induced change as labeled: NHE3 activity, PT length, and $Na^+$-$K^+$-ATPase activity. Transport orientation and abbreviations for the PT, DL, LAL, TAL, DCT, CNT, and CD are the same as in Fig. 5.3. Delivery of urine is the same convention as in Fig. 5.2. NHE3, $Na^+$-$H^+$ exchanger isoform 3; NKATPase, $Na^+$-$K^+$-ATPase.

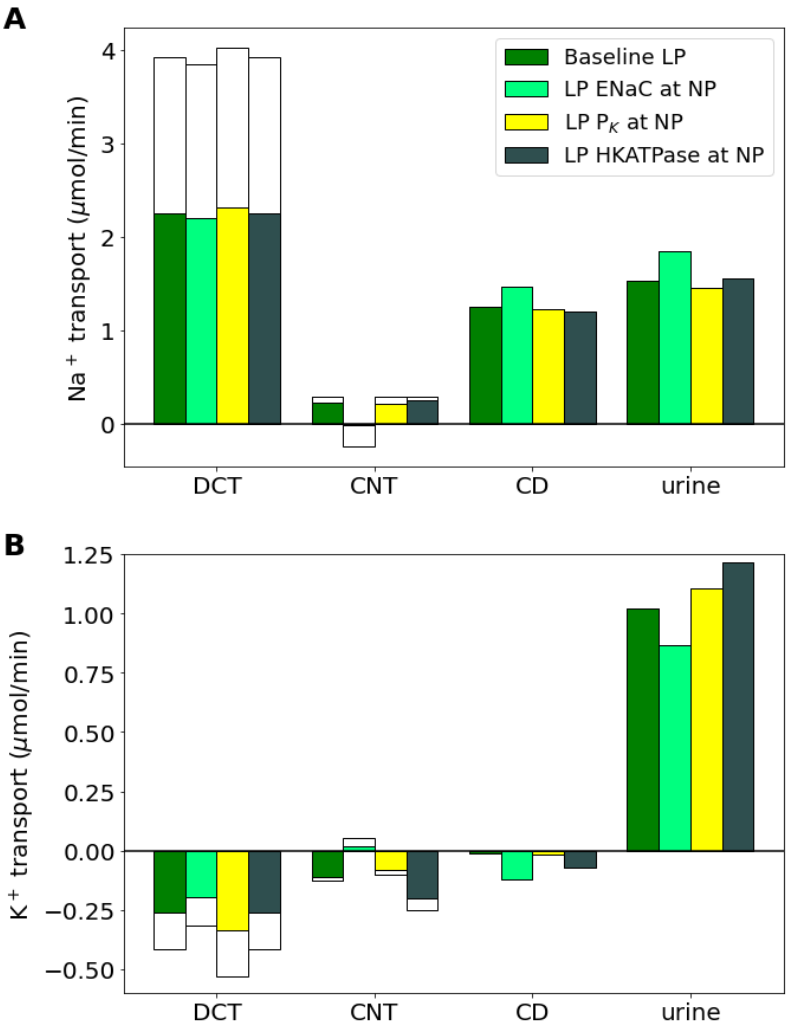


Figure 5.5: Impact of key pregnancy-induced proximal segment renal adaptations on net segmental transport and urine excretion of $Na^+$ ($A$) and $K^+$ ($B$) along individual nephron segments in the baseline LP model and LP model with one pregnancy-induced change: ENaC activity, $P_K$, and $H^+$-$K^+$ATPase activity. Transport orientation and abbreviations for the DCT, CNT, and CD are the same as in Fig. 5.3. Delivery of urine is the same convention as in Fig. 5.2. Only the distal segment results are shown because these changes only affect distal segments. HKATPase, $H^+$-$K^+$-ATPase; ENaC, epithelial $Na^+$ channel; $P_K$, permeability of $K^+$.

### Hypertension: effect on NP and MP kidney function

We developed hypertensive NP and MP models using changes listed in Table 5.2 and as described in Section 5.2. We denote the hypertensive NP model by NP-HTN and the hypertensive MP model by MP-HTN. Delivery of $Na^+$, $K^+$, and fluid volume to each segment for the baseline NP, NP-HTN, baseline MP, and MP-HTN models are shown in Fig. 5.6. Net segmental transport predictions for each of the normotensive and hypertensive NP and MP models is in Fig. 5.7.

*$Na^+$ transport.* $Na^+$ handling in the proximal segments of the NP-HTN and MP-HTN models are predicted to have similar changes when compared to the respective normotensive NP and MP models. Specifically, due to pressure natriuresis, proximal tubule $Na^+$ reabsorption is decreased by about 4% in the NP-HTN and MP-HTN models from the respective normotensive model predictions (Fig. 5.7A).

Region-specific changes in the $Na^+$-$K^+$-$2Cl^-$ cotransporter (NKCC2), NHE3, and $Na^+$-$K^+$-ATase activity (Table 5.2) lead to altered effects on transport in the medullary and cortical segments of the thick ascending limb. In the medullary thick ascending limb (mTAL), parameter values for NKCC2, NHE3, and $Na^+$-$K^+$-ATPase activity are decreased from normotensive values in both the hypertensive models (Table 5.2). This decrease in $Na^+$ transporter activity results in decreased in $Na^+$ reabsorption along the mTAL by 12% in the NP-HTN model and 8% in the MP-HTN model relative to the respective normotensive models (Fig. 5.7A). Along the cortical thick ascending limb (cTAL), NKCC2 activity is increased from normotensive values in the hyertensive models, while NHE3 and $Na^+$-$K^+$-ATPase activity is unchanged from normotensive values (Table 5.2). This results in a bout a 27% increase in $Na^+$ reabsorption along this segment in both the hypertensive models, when compared to the normotensive NP and MP model predictions (Fig. 5.7A). The increased NKCC2 activity as well as increased $Na^+$ load to the cTAL from the reduced $Na^+$ reabsorption in previous segments contributes to this increase.

Along the distal convoluted tubule and connecting tubule there is a signficant increase in $Na^+$-$Cl^-$ cotransporter (NCC) and epithelial $Na^+$ channel activity in the hypertensive models when compared to the respective normotensive models (Table 5.2). In the NP-HTN model, the $Na^+$ reabsorption along these segments is 69% greater than the normotensive NP model prediction. The MP-HTN model has an increase of 42% in $Na^+$ reabsorption along these segments when compared to the normotensive MP model prediction.

Together, $Na^+$ transport in the hypertensive models is decreased in the proximal segments which then requires the distal segments to increase $Na^+$ transport via increased $Na^+$ transporter abundance. Similar changes in $Na^+$ transport is found in both the NP-HTN and MP-HTN models.

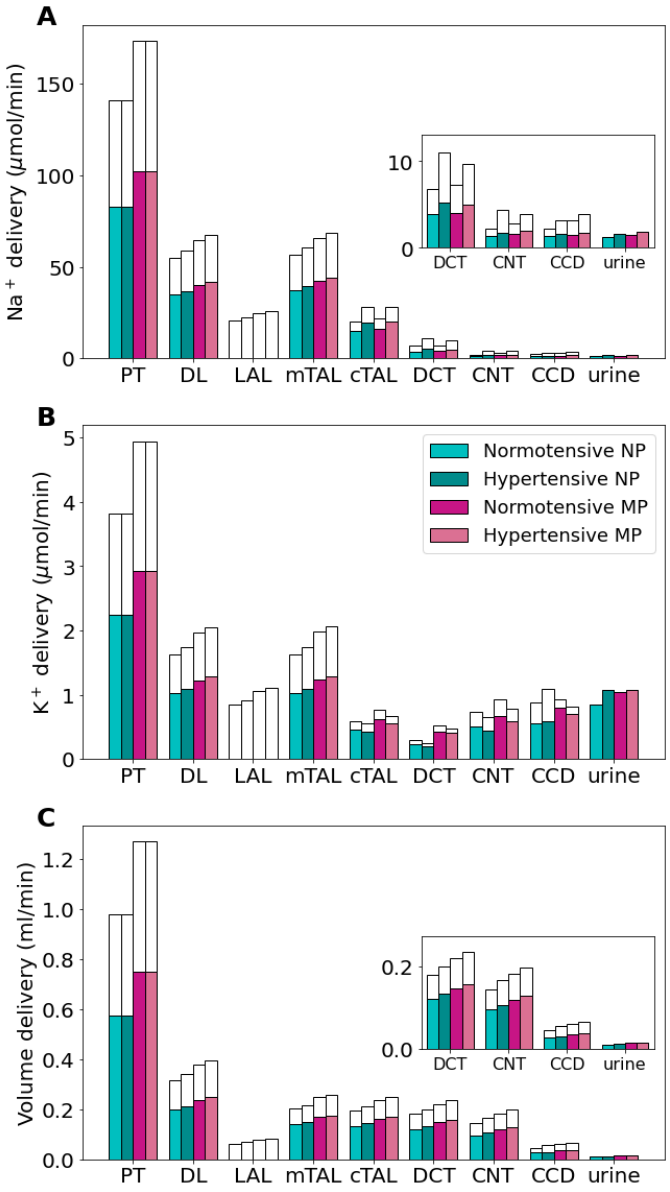


Figure 5.6: Delivery of key solutes (*A*-*E*) and fluid volume (*F*) in the normotensive and hypertensive non-pregnant (NP) and mid-pregnant (MP) models. The colored bars denote the superficial nephron values, and the white bars denote the weighted totals of the juxtamedullary nephrons (five representative model nephrons). PT, proximal tubule; DL, descending limb; LAL, thin ascending limb; mTAL, medullary thick ascending limb; cTAL, cortical thick ascending limb; DCT, distal convoluted tubule; CNT, connecting tubule; CCD, cortical collecting duct. *Insets:* reproduction of distal segment values.

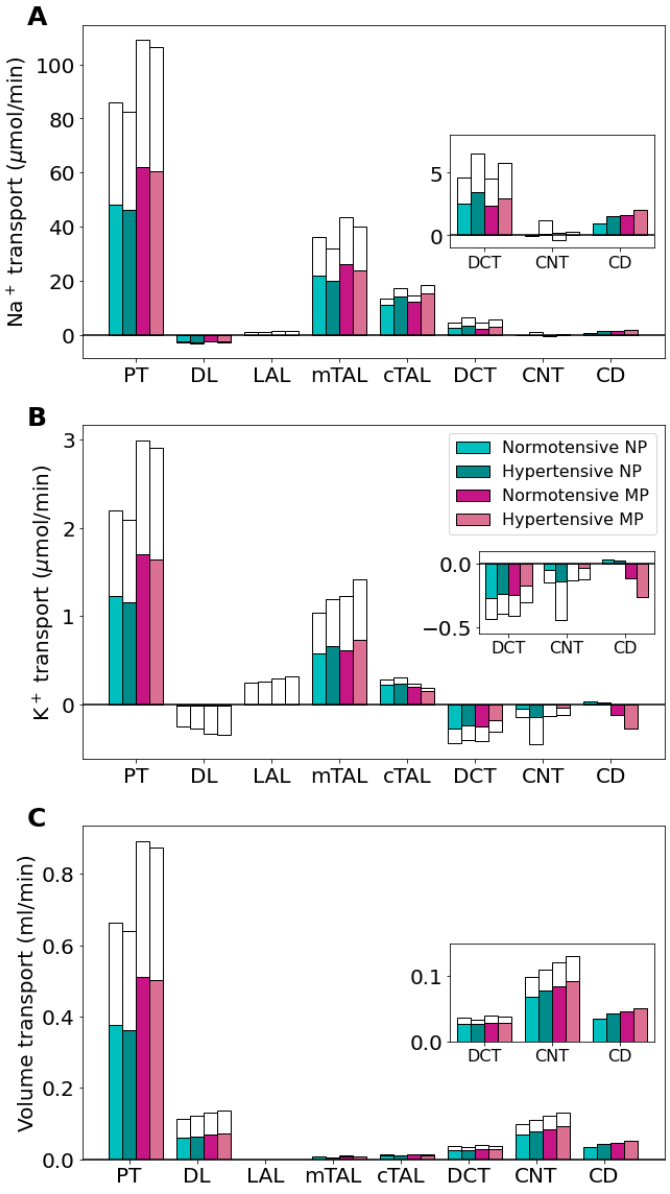


Figure 5.7: Net segmental transport of key solutes (*A*-*E*) and volume (*F*) along the individual nephron segments in the normotensive and hypertensive non-pregnant (NP) and mid-pregnant (MP) models. Transport is positive out of the nephron segment, i.e., positive transport shows net reabsorption and negative transport shows net secretion along that segment. Colored bars denote the superficial nephron values and white bars denote juxtamedullary values computed as a weighted sum of the five representative juxtamedullary nephrons. Segment labels as listed in Fig. 5.6. *Insets:* reproduction of distal segment values.

*$K^+$ transport.* Along the proximal tubule, about 60% of the filtered $K^+$ load is reabsorbed in the NP and MP baseline models. The NP-HTN and MP-HTN models predict a 5% and 3% decrease in proximal tubule $K^+$ reabsorption when compared to the respective normotensive models (Fig. 5.7B). Since $K^+$ reabsorption is related to $Na^+$ reabsorption, this is likely driven by the decreased $Na^+$ reabsorption due to decreased NHE3 and NaPi2 activity in the hypertensive models (see Table 5.2).

The reduced proximal tubule $K^+$ reabsorption leads to a 7% increase in $K^+$ delivery to the thick ascending limb in the NP-HTN model when compared to the baseline NP model (Fig. 5.6B). MP-HTN model $K^+$ delivery to the thick ascending limb is 5% higher than the baseline MP model prediction (Fig. 5.6B). Along the mTAL, $K^+$ transport is increased by about 15% in the hypertensive models compared to the respective normotensive models (Fig. 5.7B). This increased transport in the mTAL results in decreased cTAL $K^+$ delivery in the hypertensive models compared to the respective normotensive models for both the NP-HTN and MP-HTN models.

Major $K^+$ secretion occurs along the distal convoluted tubule and connecting tubule. During hypertension, the expression of $K^+$ secretory channel ROMK is significantly decreased (Table 5.2). In the late distal convoluted tubule, the reduced $K^+$ secretion from the ROMK leads to 8% and 25% lower $K^+$ secretion in the distal convoluted tubule for the NP-HTN and MP-HTN models, respectively when compared to the normotensive NP and MP models. This is where the NP-HTN and MP-HTN models seem to differ. Connecting tubule $K^+$ secretion is increased in the NP-HTN model when compared to NP so that in total the $K^+$ secretion along the distal convoluted tubule and connecting tubule is 45% higher than NP distal tubule $K^+$ secretion. This increase is likely driven by the effect of increased $Na^+$ flow in the CNT and increased ENaC activity (a known kaliuretic factor). The increased $Na^+$ in the CNT creates a favorable electrical otential gradient which in turn increases $K^+$ secretion. $K^+$ secretion in the MP-HTN model along the DCT and CNT is predicted to be about the same as MP distal tubule $K^+$ secretion. This is likely due to the already significantly decreased ROMK channel permeability in the normotensive MP model (Table 5.1).

In summary, altered $Na^+$ transort effects the early $K^+$ reabsorption which leads to higher flow to the distal segments. Later $K^+$ secretory channels are reduced to lower $K^+$ secretion despite high $Na^+$ flow and kaliuretic factors such as increased ENaC activity.

*Volume transport.* Fluid volume follows in a similar way with $Na^+$ transport due to the dependence on the osmolality gradient. Along the proximal tubule, about 68% of the volume load is reabsorbed in the NP model. In NP-HTN, net fluid volume reabsorption decreased by 3% resulting in a fractional volume reabsorption of 65%. Along the MP

proximal tubule, 70% of the volume load is reabsorbed. Like NP-HTN, the MP-HTN model also decreases net fluid reabsorption by about 3% resulting in a fractional reabsorption of 68%. The lower fluid volume reabsorption results in increased volume delivery to each of the segments along the nephron. This is essentially the same for NP-HTN and MP-HTN when compared to the respective normotensive NP and MP models.

## 5.4 Discussion

What are the physiological implications of the renal adaptations that occur during pregnancy? How does altered expression and activity of renal transporter impact kidney function in a female with hypertension? How does pregnancy alter transport along the nephrons during pregnancy in a hypertensive female rat? To try to answer these questions, we developed computational models of full kidney function including the superficial and juxtamedullary nephrons during mid- and late pregnancy. Additionally, we developed a female-specific hypertension model as well as a model that captures proposed kidney function during mid-pregnancy for a rat with chronic hypertension. We did not model late pregnant hypertension since there have not been any studies to date that investigated nephron function in late pregnant hypertensive rats.

### Kidney function during pregnancy

The kidneys play a key role in maintaining body homeostasis, especially for $Na^+$, $K^+$, and volume. Pregnancy is unique in that plasma volume expansion and electrolyte retention is required to sufficiently supply the rapidly developing fetus and placenta. Without this, it is likely that fetal growth restriction will occur [21, 23, 26, 31, 50, 84, 104, 129]. Gestational disorders such as gestational hypertension and preeclampsia are also associated with low plasma volume expansion [26,50,104,129]. Indeed, renal adaptations must occur to be able to support such a significant change in the maternal body.

Pregnancy-induced renal adaptations are both complex and dynamic. Starting from early pregnancy, filtration to the nephrons is massively increased due to increased plasma flow [19, 21, 22]. This requires major adaptations in the nephron segments to reabsorb this increased load [35, 109]. The proximal tubule is the first segment of the nephron and reabsorbs a majority of the filtered load. During pregnancy, the tubule length is increased which leads to more transport capacity [15,49,109]. Without this change, excess natriuresis and kaliuresis will likely occur (Fig. 5.4), due to the inadequate $Na^+$ reabsorption by the proximal tubule. The $Na^+$ reabsorption in the TAL and distal segments does increase, but

even with that compensation, $Na^+$ excretion is massively increased. This result is similar to our previous study where we studied the effect of individual pregnancy-induced adaptations on urinary excretion of a single superficial nephron [109]. Similarly, we hypothesize that NHE3 activity increases during pregnancy [109]. This has not been reported experimentally, but our simulation results indicate that some increase in NHE3 activity must occur to reabsorb the excess filtered $Na^+$ load to the nephrons (see Fig. 5.4). Without NHE3 upregulation, proximal tubule $Na^+$ reabsorption is insufficient, resulting in excess natriuresis.

Distal segment transporters also seem to play a key role in maintaining sufficient $Na^+$ retention during pregnancy [109, 125, 127, 130, 131]. West et al. [127] showed that with chronic ENaC blockade, pregnant rats were unable to sustain sufficient $Na^+$ and water retention and were poor reproducers (i.e., pup weight was significantly lower than control). This result together with modeling simulations presented here and in our previous study (see Ref. [109]) emphasize the importance of this transporter in pregnancy.

Several kaliuretic factors act on the kidneys of a pregnant female: elevated aldosterone levels [48], decreased NCC activity [128], and increased ENaC activity [125,127]. However, through pregnancy the maternal body is able to maintain $K^+$ homeostasis and even retain $K^+$ in late pregnancy [35, 131]. It has been found that the $K^+$ secretory channels in the distal segments, which in a NP rat vigorously secrete $K^+$, are downregulated. In addition, the $K^+$ transporter, $H^+$-$K^+$-ATPase has been shown to be significantly upregulated during pregnancy [105, 131]. Together these transport changes prevent excess $K^+$ loss.

Female rats, pregnant or not, express more $Na^+$ transporters along the distal nephron segments compared to males [59, 60, 112]. While the proximal tubules transport the bulk of the volume and electrolytes, the distal segments are responsible for "fine-tuning" tubule transport, to yield the target urinary excretion. Placing a larger transport load on the distal segments enables the females to adapt to the changing electrolyte and volume homeostasis more easily in pregnancy and lactation. In pregnancy, GFR and filtered $Na^+$ load is increase as is their respective transport; these two competing factors yield urinary excretion that approximately, but only approximately, equals intake. Overall, there is a net whole-body $Na^+$ retention, and in late pregnancy, net $K^+$ retention; nevertheless, plasma $Na^+$ concentration decreases. Given the large amount of fluid and solutes handled by the kidneys, minute adjustments in transport are sufficient to yield the almost imperceptible difference in intake and urinary excretion, to attain net volume and electrolyte retention seen in pregnancy. That kind of fine-tuning can best be achieved via signalling to the distal segments.

As previously noted, the marked increase in renal hemodynamics is remarkable. Studies

have suggested roles for nitric oxide syntase, prostaglandins, endothelin, and relaxin. This area of research is exciting, as unraveling why glomerular filtration rate and renal plasma flow increase in pregnancy may eventually benefit patients with acute and chronic renal function loss.

### Hypertension in females and pregnancy

Hypertension is a highly complex disease with many underlying pathophysiological mechanisms, some of which remain to be fully understood. Hypertension affects over 30% of the global adult population and is the leading cause of cardiovascular disease [92]. It is likely that the prevalence of hypertension will continue to rise due to ageing populations, increases in the exposure to high $Na^+$ and low $K^+$ diets, and a lack of physical activity [92]. It has been estimated that about 10% of women of reproductive age have chronic hypertension [18].

Motivated by the kidney's role in maintaining blood pressure through control of $Na^+$ balance and the pressure natriuresis mechanism [40], we developed a female-specific model of kidney function in angiotensin II-induced hypertension. The model was formulated based on experimental results that studied the effect of hypertension on kidney function in female rats [4,113]. Significant sexual dimorphisms have been reported in nephron function [78, 112]. Specifically, when compared to males in female rat nephrons, the fractional reabsorption of $Na^+$ in the proximal tubule is lower so that a larger proportion of $Na^+$ reabosorption is handled by the distal segments [59, 83, 112]. Veiras et al. [113] found that in hypertension, male and female rats have similar proportional changes in transporter activation as are the resulting changes in renal function as discussed below. In addition, we investigated the effect of pregnancy on a hypertensive (NP) female rat by using the same changes to renal function as in the hypertensive female (NP) model and then adding the changes that occur in the nephrons during MP.

During hypertension, pressure natriuresis reduces NHE3 activity and proximal tubular $Na^+$ reabsorption, which leads to a higher $Na^+$ load to the distal segments. In a modeling study of angiotensin II-induced hypertension in the male rat, Edwards & McDonough [41] hypothesized that the differential regulation of NKCC2 in the medullary and cortical segments of the thick ascending limb during hypertension occur to minimize $Na^+$ retention while preserving $K^+$. They suggest that angiotensin II stimulates NKCC2 in the cortex but not in the medulla. In our study we found that similar results occur in both the hypertensive female (NP-HTN) and the hypertensive MP rat (MP-HTN) models.

Along the distal segments, the $Na^+$ transporters the $Na^+$-$Cl^-$ cotransporter (NCC) and

the epithelial $Na^+$ channel (ENaC) are both upregulated in hypertension (see Table 5.2). In both the hypertensive NP and hypertensive MP models, this change led to increased $Na^+$ reabsorption in the distal segments.

In hypertension, both with or without pregnancy, there is a shift in $Na^+$ transport from the proximal tubules to the distal tubules (see Fig. 5.7). Given that the proximal tubules are more efficient than distal tubules in transporting $Na^+$ [70], in that less oxygen is consumed to reabsorb a given amount of $Na^+$, the downstream shift implied an increase in overall oxygen demand. The elevated metabolic demand, if accompanied by maternal endothelial dysfunction that negatively impact renal oxygen supply, may lead to renal hypoxia and eventually chronic kidney disease.

### Future work

Studying hypertensive disorders of pregnancy is complicated in that there are multiple types: chronic hypertension (hypertension before 20-weeks gestation or pre-gestation), gestational hypertension (onset of hypertension after 20-weeks gestation), and pre-eclampsia (generally diagnosed by gestational hypertension and proteinuria, severe risk of eclampsia) [96, 107]. In this study we chose to investigate chronic hypertension due to little experimental data on nephron function in gestational hypertension and pre-eclampsia. Abreu et al. [4] investigated only mRNA data on a few transporters in hypertensive and normotensive pregnant rats. Hu et al. [57] investigated altered expression of renal $Na^+$ transporters using urinary vesicles in pregnant women with pre-eclampsia. In a similar way to Refs. [61, 110], human-specific models of kidney function during pregnancy may be developed to study the functional implications of this altered renal function.

Another common complication of pregnancy that may affect the kidneys is gestational diabetes [91]. Gestational diabetes is diagnosed by hyperglycemia that develops in the third trimester (of human pregnancy) and resolves post-parturition. Jiang et al. [65] investigated the impact of high-fat diet induced gestational diabetes on the SGLT2 and GLUT2 transporters in mice nephrons. The present model may be modified to simulate gestational diseases and its functional implications on kidney function.

As average maternal age increases and the rates of comorbities such as hypertension and diabetes increase in the population of women of childbearing age, rates of pregnancies complicated by a disorder will increase [17, 18, 91, 106, 111]. However, our understanding of pregnancy physiology and especially gestational disorders is limited. The study of pregnancy and its related pathologies has been historically limited by the fetal risks and ethical implications of running clinical trials on pregnant women, as well as in general fewer stud-

ies done on understanding female physiology [2, 74]. This limitation may be overcome, in part, by using computational models to test hypotheses, unravel complicated mechanisms, and potentially test the efficacy for therapies for gestational diseases *in silico* with the use of pregnancy-specific models as developed in this study. Indeed, there is much more work to be done in understanding pregnancy physiology as well as gestational diseases as we recently reviewed in much more detail in Ref. [2].

### Limitations of the study

Epithelial transport models have been extensively developed to provide an accurate accounting of solute and water transport to yield insights along with experimental evidence for the complicated transport pathways, driving forces, and coupling mechanisms that are involved in kidney function. These models have been used to study the functional implications of sexual dimorphisms [59–61, 83, 110], diabetes [58, 110], hypertension [41], and hyperkalemia [122] among others. However, as discussed in Layton & Edwards [75] and Weinstein [118], there are limitations that often stem from the paucity of experimental data as well as model structure.

One key limitation is that in the models presented in this study it is assumed that the interstitial fluid composition is known a priori. There are changes in these models that may affected interstitial fluid composition, but since there is not evidence that has measured these changes, we did not include those changes in our model assumptions. This has the potential to change some of the electrolyte transport in the models due to a differing electrochemical potential gradient with the interstitial fluid.

Similar to the limitations in our previous study [109], gestational kidney physiology has not been fully studied as there are some parameters that had to be assumed rather than directly based on experimental evidence. A similar limitation is in the hypertension models. We used experimental evidence from Veiras et al. [113] to inform our model parameter choices, however this study only investigated $Na^+$ transporters. It is likely that there are other renal alterations that are impacted by hypertension. As more experimental evidence on renal transporter function during pregnancy and hypertension becomes available these models can be further improved.

# Chapter 6

# Conclusions

Globally the rate of pregnancies complicated with a comorbidity is increasing. This is likely driven by increased average maternal age along with increased rates of comorbidities such as hypertension and diabetes in the population of women of child-bearing age [18, 106]. Indeed, it is more important than ever to fully understand pregnancy physiology and the unique complexities of gestational disorders.

The study of pregnancy and its related pathologies has historically been limited due to fetal risks and the ethical implications of running clinical trials on pregnant women along with the significant lack of female-specific physiology studies due to sexist practices that have ignored women's health. However, this limitation may be overcome, in part, by using computational modeling to test hypotheses, unravel complicated mechanisms, and test the efficacy of potential therapies for gestational diseases *in silico* with the use of pregnancy-specific models. We recently wrote a review on current sex-specific models that could be expanded on to investigate pregnancy physiology [2]. This thesis work on developing and analyzing models of kidney function during pregnancy as well as the pathology of chronic hypertension is a step in unravelling the complexities of pregnancy physiology and its unique disorders. Since pregnancy requires a myriad of physiological adaptations, there is much more work that can and should be done to have a full understanding of not only gestational renal physiology, but a comprehensive understanding of pregnancy physiology as a whole.

In summary, in this thesis we have presented cell-based epithelial transport models of kidney function during pregnancy and hypertension. We first developed models of a superficial nephron in a mid- and late pregnant rat kidney. Model analysis was conducted to study how individual pregnancy-induced renal adaptations impact single nephron uri-

nary excretion of $Na^+$, $K^+$, and fluid volume. This in turn gives insight into what renal adaptations made during pregnancy may be most important for maternal plasma volume expansion as well as electrolyte retention by quantifying such impacts. Model results predicted that morphological adaptations such as the increased proximal tubule length had the largest impact on electrolyte and volume handling in the kidneys. Additionally, increased activity of the $Na^+$ transporters, the $Na^+/H^+$ exchanger in the early nephron segments and the epithelial $Na^+$ channel in the distal segments are essential to prevent excess urinary $Na^+$ excretion during pregnancy, and even sustain $Na^+$ retention. The other key electrolyte studied, $K^+$, required that the distal tubule $K^+$ secretory channels are significantly downregulated and the $H^+$-$K^+$-ATPase pump should be significantly upregulated in order to prevent excess loss of $K^+$ during pregnancy and retain $K^+$ in late pregnancy.

Using the superficial nephron mid- and late pregnant models, we developed computational models of kidney function that captured heterogeneity in the nephron populations. Based on our superficial nephron models results we developed multiple nephron models that captured both superficial nephron and several juxtamedullary nephron types. This type of model gives a more accurate accounting of solute and water handling in a full kidney. Model simulations were conducted to show the functional differences in kidney function for a non-pregnant, mid-pregnant, and late pregnant rat. Further simulations were conducted to investigate the functional implications of key pregnancy-induced renal changes that were identified in the superficial nephron study (i.e., Ref. [109]). Specifically, we investigated the impact of setting individual parameter values to their respective non-pregnant value in the late pregnant model. We investigated the impact of the proximal tubule length, $Na^+/H^+$ exchanger isoform 3 activity, and $Na^+$-$K^+$-ATPase activity in the proximal segments. Additionally, we conducted simulations to investigate key distal segment transporters: the epithelial $Na^+$ channel, the $K^+$ secretory channels, and the $H^+$-$K^+$-ATPase pump. Together we showed how these gestational renal adaptations impact the kidneys of a mid- and late pregnant rat.

We then developed a female-specific model of the impact of hypertension in the kidneys. The kidney plays a key role in regulating blood pressure through its regulation of $Na^+$ and volume homeostasis. As such, studying the effect of hypertension on kidney function can help to understand this highly complicated multi-factorial disorder. Despite differential transporter abundance between male and female kidneys, it appears that the changes that occur in hypertension are similar. However, we further investigated the impact of pregnancy on a female with chronic hypertension. This is a disorder that can have a severe effect on both the mother and fetus. The prominence of pregnancies complicated by chronic hypertension is increasing as rates of chronic hypertension increase in the general population, and more specifically in women of child-bearing age. Model results indicated

that the decreased $Na^+$ reabsorption in the proximal tubules of the nephrons leads to a higher $Na^+$ load to the distal segments where there is upregulated $Na^+$ transporter activity.

The models presented in this thesis are the first *pregnancy-specific* models of kidney function. It has been shown many times that the kidneys play essential roles in regulating body homeostasis, blood pressure, excreting waste, and more. This role is just as crucial in pregnancy and can be harmful when is altered. The demands on a pregnant female are significant, but the ability of the maternal body to adapt is remarkable.

*Future work.* Here we presented the first models of kidney function during pregnancy to combine multiple experimental studies on the effects of pregnancy on renal function. With these models we were able to unravel the functional implications of these adaptations as well as predict adaptations that have not been investigated. Kidneys are highly complex and involve many competing processes, hence studying gestational renal adaptations through computational modelling enables us to unravel individual effects which cannot easily be done experimentally. We do note that these models can continually be improved upon as more experiments are conducted and results are published.

Another potential area of study is the post-partum period, specifically in lactating females. During the lactation period there is differential needs on the maternal body which likely affects kidney function [11, 12]. At this time there has not been significant research in the effects of lactation on renal function, though as more experimental research emerges, a similar computational study may be conducted. Additionally, in this thesis work we developed models of kidney function in a rat with chronic hypertension during pregnancy. Other hypertensive disorders of pregnancy likely effect the kidneys. Again, at this time there is not sufficient experimental evidence to develop models of these disorders, though a similar study may be conducted to unravel individual effects on renal function.

Applied mathematics has been used to provide insights into many systems from the social sciences to physics and more. Mathematical physiology has proven to be powerful in unravelling the complex systems involved in biological and physiological phenomenon [67]. Computational modelling (as with most physiological research) has only recently considered sex as a biological variable [74]. Even fewer models have been built to be *pregnancy-specific* [2]. Indeed, almost all organs and tissues in the maternal body are significantly impacted by pregnancy. Similar studies may be conducted on many organ systems to reveal insights and unravel how pregnancy-induced changes impact the maternal body.

# References


[1] Maaz Ahmed Abbasi, Glenn M Chertow, and Yoshio N Hall. End-stage renal disease. *BMJ Clinical Evidence*, 2010:2002, July 2010.

[2] Stéphanie Abo, Delaney Smith, Melissa Stadt, and Anita Layton. Modelling female physiology from head to Toe: Impact of sex hormones, menstrual cycle, and pregnancy. *Journal of Theoretical Biology*, 540:111074, May 2022.

[3] Stéphanie M. C. Abo and Anita T. Layton. Modeling the circadian regulation of the immune system: Sexually dimorphic effects of shift work. *PLoS computational biology*, 17(3):e1008514–e1008514, 2021. Place: United States Publisher: Public Library of Science.

[4] NP Abreu, Joisse Caria Barboza Monerat Tardin, Mirian Aparecida Boim, Ruy R. Campos, Cassia T. Bergamaschi, and Nestor Schor. Hemodynamic Parameters During Normal and Hypertensive Pregnancy in Rats: Evaluation of Renal Salt and Water Transporters. *Hypertension in pregnancy*, 27(1):49–63, 2008. Place: England Publisher: Informa UK Ltd.

[5] Horacio J. Adrogué and Nicolaos E. Madias. Sodium and Potassium in the Pathogenesis of Hypertension. *New England Journal of Medicine*, 356(19):1966–1978, May 2007. Publisher: Massachusetts Medical Society _eprint: https://doi.org/10.1056/NEJMra064486.

[6] Sameed Ahmed, Rui Hu, Jessica Leete, and Anita T. Layton. Understanding sex differences in long-term blood pressure regulation: insights from experimental studies and computational modeling. *American journal of physiology. Heart and circulatory physiology*, 316(5):H1113–H1123, 2019. Place: United States Publisher: American Physiological Society.

[7] Sameed Ahmed and Anita T. Layton. Sex-specific computational models for blood pressure regulation in the rat. *American journal of physiology. Renal physiology*, 318(4):F888–F900, 2020. Place: United States Publisher: American Physiological Society.

[8] Sameed Ahmed, Jennifer C. Sullivan, and Anita T. Layton. Impact of sex and pathophysiology on optimal drug choice in hypertensive rats: Quantitative insights for precision medicine. *iScience*, 24(4):102341–102341, 2021. Place: United States Publisher: Elsevier Inc.

[9] Edward A. Alexander, Susanne Churchill, and Howard H. Bengele. Renal hemodynamics and volume homeostasis during pregnancy in the rat. *Kidney international*, 18(2):173–178, 1980. Place: United States Publisher: Elsevier Inc.

[10] W. Aoi, D. Gable, R. E. Cleary, P. C. M. Young, and M. H. Weinberger. The Antihypertensive Effect of Pregnancy in Spontaneously Hypertensive Rats. *Proceedings of the Society for Experimental Biology and Medicine*, 153(1):13–15, 1976. Place: London, England Publisher: SAGE Publications.

[11] S K Arthur and R Green. Renal function during lactation in the rat. *The Journal of Physiology*, 334(1):379–393, 1983.

[12] S K Arthur and R Green. Fluid reabsorption by the proximal convoluted tubule of the kidney in lactating rats. *The Journal of Physiology*, 371(1):267–275, 1986.

[13] J. C. Atherton. Glomerular filtration rate and salt and water reabsorption during pregnancy in the conscious rat. *The Journal of physiology*, 334(1):493–504, 1983. Place: England Publisher: The Physiological Society.

[14] J. C. Atherton, J. M. Dark, H. O. Garland, M. R. Morgan, J. Pidgeon, and S. Soni. Changes in water and electrolyte balance, plasma volume and composition during pregnancy in the rat. *The Journal of Physiology*, 330(1):81–93, September 1982. Publisher: John Wiley & Sons, Ltd.

[15] J.C. Atherton and Susan C. Pirie. The effect of pregnancy on glomerular filtration rate and salt and water reabsorption in the rat. *Journal of Physiology*, 319:153–164, January 1981.

[16] Steven A. Atlas. The Renin-Angiotensin Aldosterone System: Pathophysiological Role and Pharmacologic Inhibition. *Journal of Managed Care Pharmacy*, 13(8 Supp B):9–20, October 2007.

[17] Brian T. Bateman, Pooja Bansil, Sonia Hernandez-Diaz, Jill M. Mhyre, William M. Callaghan, and Elena V. Kuklina. Prevalence, trends, and outcomes of chronic hypertension: a nationwide sample of delivery admissions. *American Journal of Obstetrics and Gynecology*, 206(2):134.e1–134.e8, February 2012.

[18] Ashley N. Battarbee, Rachel G. Sinkey, Lorie M. Harper, Suzanne Oparil, and Alan T. N. Tita. Chronic hypertension in pregnancy. *American Journal of Obstetrics and Gynecology*, 222(6):532–541, June 2020.

[19] C. Baylis. The mechanism of the increase in glomerular filtration rate in the twelve-day pregnant rat. *The Journal of physiology*, 305(1):405–414, 1980. Place: England Publisher: The Physiological Society.

[20] C. Baylis. Renal effects of cyclooxygenase inhibition in the pregnant rat. *American Journal of Physiology-Renal Physiology*, 253(1):F158–F163, July 1987.

[21] Christine Baylis. Renal hemodynamics and volume control during pregnancy in the rat. *Seminars in Nephrology*, 4(3):208–220, September 1984. Publisher: Elsevier.

[22] Christine Baylis. The determinants of renal hemodynamics in pregnancy. *American Journal of Kidney Diseases*, 9(4):260–264, April 1987.

[23] Kelly Beers and Niralee Patel. Kidney Physiology in Pregnancy. *Advances in Chronic Kidney Disease*, 27(6):449–454, November 2020.

[24] Annaliese K Beery and Irving Zucker. Sex bias in neuroscience and biomedical research. *Neuroscience & Biobehavioral Reviews*, 35(3):565–572, 2011.

[25] Marie Briet and Ernesto L. Schiffrin. Aldosterone: effects on the kidney and cardiovascular system. *Nature Reviews Nephrology*, 6(5), May 2010.

[26] M. A. Brown and E. D. Gallery. Volume homeostasis in normal pregnancy and pre-eclampsia: physiology and clinical implications. *Baillière's clinical obstetrics and gynaecology*, 8(2):287–310, 1994. Place: England.

[27] Mark A. Brown, Laura A. Magee, Louise C. Kenny, S. Ananth Karumanchi, Fergus P McCarthy, Shigeru Saito, David R. Hall, Charlotte E. Warren, Gloria Adoyi, and Salisu Ishaku. The hypertensive disorders of pregnancy: ISSHP classification, diagnosis & management recommendations for international practice. *Pregnancy Hypertension*, 13:291–310, July 2018.

[28] Graham J. Burton and Eric Jauniaux. What is the placenta? *American Journal of Obstetrics and Gynecology*, 213(4):S6.e1–S6.e4, October 2015.

[29] Antonio Dal Canton, Giuseppe Conte, Ciro Esposito, Giorgio Fuiano, Raffaele Guasco, Domenico Russo, Massimo Sabbatini, Francesco Uccello, and Vittorio E. Andreucci. Effects of pregnancy on glomerular dynamics: Micropuncture study in the rat. *Kidney international*, 22(6):608–612, 1982. Place: United States Publisher: Elsevier Inc.

[30] Ying Chen, Jennifer C. Sullivan, Aurélie Edwards, and Anita T. Layton. Sex-specific computational models of the spontaneously hypertensive rat kidneys: factors affecting nitric oxide bioavailability. *American Journal of Physiology-Renal Physiology*, 313(2):F174–F183, August 2017. Publisher: American Physiological Society.

[31] Katharine L. Cheung and Richard A. Lafayette. Renal Physiology of Pregnancy. *Advances in Chronic Kidney Disease*, 20(3):209–214, 2013. Publisher: Elsevier.

[32] S. E. Churchill, H. H. Bengele, and E. A. Alexander. Sodium balance during pregnancy in the rat. *American Journal of Physiology - Regulatory, Integrative and Comparative Physiology*, 239(1):143–148, 1980. Place: United States Publisher: American Physiological Society.

[33] Tanja Cvitanović Tomaš, Žiga Urlep, Miha Moškon, Miha Mraz, and Damjana Rozman. LiverSex Computational Model: Sexual Aspects in Hepatic Metabolism and Abnormalities. *Frontiers in physiology*, 9:360–360, 2018. Place: Switzerland Publisher: Frontiers Research Foundation.

[34] J.M. Davison and W. Dunlop. Changes in renal hemodynamics and tubular function induced by normal human pregnancy. *Seminars in Nephrology*, 4(3):198–207, September 1984. Publisher: Elsevier.

[35] Aline M. A. de Souza and Crystal A. West. Adaptive remodeling of renal Na+ and K+ transport during pregnancy. *Current Opinion in Nephrology and Hypertension*, 27(5):379–383, September 2018.

[36] A. Deng, K. Engels, and C. Baylis. Impact of nitric oxide deficiency on blood pressure and glomerular hemodynamic adaptations to pregnancy in the rat. *Kidney International*, 50(4):1132–1138, October 1996.

[37] Zhaopeng Du, Yi Duan, QingShang Yan, Alan M. Weinstein, Sheldon Weinbaum, and Tong Wang. Mechanosensory function of microvilli of the kidney proximal tubule. *Proceedings of the National Academy of Sciences*, 101(35):13068–13073, August 2004.

[38] J. A. Durr, B. Stamoutsos, and M. D. Lindheimer. Osmoregulation during pregnancy in the rat. Evidence for resetting of the threshold for vasopressin secretion during gestation. *The Journal of clinical investigation*, 68(2):337–346, 1981. Place: United States.

[39] Douglas C. Eaton. *Vander's renal physiology.* McGraw-Hill Medical, New York, 8th ed. edition, 2013.

[40] Douglas C Eaton, John Pooler, and Arthur J Vander. *Vander's renal physiology.* McGraw-Hill Medical, New York, 7th edition, 2009.

[41] Aurélie Edwards and Alicia A. McDonough. Impact of angiotensin II-mediated stimulation of sodium transporters in the nephron assessed by computational modeling. *American Journal of Physiology-Renal Physiology*, 317(6):F1656–F1668, December 2019.

[42] David H. Ellison, Andrew S. Terker, and Gerardo Gamba. Potassium and Its Discontents: New Insight, New Treatments. *Journal of the American Society of Nephrology*, 27(4):981–989, April 2016.

[43] Murray Epstein and Meyer D. Lifschitz. The Unappreciated Role of Extrarenal and Gut Sensors in Modulating Renal Potassium Handling: Implications for Diagnosis of Dyskalemias and Interpreting Clinical Trials. *Kidney International Reports*, 1(1):43–56, May 2016.

[44] A. Essig and S. R. Caplan. The use of linear nonequilibrium thermodynamics in the study of renal physiology. *American Journal of Physiology-Renal Physiology*, 236(3):F211–F219, March 1979.

[45] M. M. Faas, G. A. Schuiling, P. A. Klok, N. Valkhof, and W. W. Bakker. The Glomerular Filtration Rate during Pregnancy: Saline Infusion Enhances the Glomerular Filtration Rate in the Pregnant Rat. *Kidney & blood pressure research*, 19(2):121–127, 1996. Place: Basel, Switzerland.

[46] Diane M. Folk. Hypertensive Disorders of Pregnancy: Overview and Current Recommendations. *Journal of Midwifery & Women's Health*, 63(3):289–300, 2018.

[47] Ziwei Fu, Jiajia Hu, Li Zhou, Yanting Chen, Mokan Deng, Xiyang Liu, Jiahui Su, Aihua Lu, Xiaodong Fu, and Tianxin Yang. (Pro)renin receptor contributes to pregnancy-induced sodium-water retention in rats via activation of intrarenal RAAS and $\alpha$-ENaC. *American Journal of Physiology-Renal Physiology*, 316(3):F530–F538, March 2019.

[48] H. O. Garland, J. C. Atherton, C. Baylis, M. R. Morgan, and C. M. Milne. Hormone profiles for progesterone, oestradiol, prolactin, plasma renin activity, aldosterone and corticosterone during pregnancy and pseudopregnancy in two strains of rat: correlation with renal studies. *The Journal of Endocrinology*, 113(3):435–444, June 1987.

[49] H. O. Garland, R. Green, and R. J. Moriarty. Changes in Body Weight, Kidney Weight and Proximal Tubule Length during Pregnancy in the Rat. *Kidney & blood pressure research*, 1(1):42–47, 1978. Place: Basel, Switzerland.

[50] Helen M. Gibson. Plasma volume and glomerular filtration rate in pregnancy and their relation to differences in fetal growth. *BJOG : an international journal of obstetrics and gynaecology*, 80(12):1067–1074, 1973. Place: Oxford, UK Publisher: Blackwell Publishing Ltd.

[51] Megan Greenlee, Charles S. Wingo, Alicia A. McDonough, Jang-Hyun Youn, and Bruce C. Kone. Narrative Review: Evolving Concepts in Potassium Homeostasis and Hypokalemia. *Annals of Internal Medicine*, 150(9):619–625, May 2009. Publisher: American College of Physicians.

[52] R. Greger. Physiology of Renal Sodium Transport. *The American journal of the medical sciences*, 319(1):51–62, 2000. Place: Hagerstown, MD Publisher: Elsevier Inc.

[53] H O Garland and R Green. Micropuncture study of changes in glomerular filtration and ion and water handling by the rat kidney during pregnancy. *The Journal of physiology*, 329(1):389–409, 1982. Place: England Publisher: The Physiological Society.

[54] J. A. Haas, J. P. Granger, and F. G. Knox. Effect of renal perfusion pressure on sodium reabsorption from proximal tubules of superficial and deep nephrons. *American Journal of Physiology - Renal Physiology*, 250(3):425–429, 1986. Publisher: American Physiological Society.

[55] Ewout J. Hoorn, Martin Gritter, Catherina A. Cuevas, and Robert A. Fenton. Regulation of the Renal NaCl Cotransporter and Its Role in Potassium Homeostasis. *Physiological Reviews*, 100(1):321–356, January 2020.

[56] M. Horster and K. Thurau. Micropuncture studies on the filtration rate of single superficial and juxtamedullary glomeruli in the rat kidney. *Pflügers Archiv für die gesamte Physiologie des Menschen und der Tiere*, 301(2):162–181, 1968. Place: Germany.

[57] Chih-Chiang Hu, Marina Katerelos, Suet-Wan Choy, Amy Crossthwaite, Susan P. Walker, Gabrielle Pell, Mardiana Lee, Natasha Cook, Peter F. Mount, Kathy Paizis, and David A. Power. Pre-eclampsia is associated with altered expression of the renal sodium transporters NKCC2, NCC and ENaC in urinary extracellular vesicles. *PLOS ONE*, 13(9):e0204514, September 2018.

[58] Rui Hu and Anita Layton. A Computational Model of Kidney Function in a Patient with Diabetes. *International Journal of Molecular Sciences*, 22(11):5819, January 2021. Number: 11 Publisher: Multidisciplinary Digital Publishing Institute.

[59] Rui Hu, Alicia A. McDonough, and Anita T. Layton. Functional implications of the sex differences in transporter abundance along the rat nephron: modeling and analysis. *American journal of physiology. Renal physiology*, 317(6):F1462–F1474, 2019. Place: United States Publisher: American Physiological Society.

[60] Rui Hu, Alicia A. McDonough, and Anita T. Layton. Sex differences in solute transport along the nephrons: effects of Na+ transport inhibition. *American journal of physiology. Renal physiology*, 319(3):F487–F505, 2020.

[61] Rui Hu, Alicia A. McDonough, and Anita T. Layton. Sex differences in solute and water handling in the human kidney: Modeling and functional implications. *iScience*, 24(6):102667, June 2021.

[62] J M Davison and M D Lindheimer. Changes in renal haemodynamics and kidney weight during pregnancy in the unanaesthetized rat. *The Journal of physiology*, 301(1):129–136, 1980. Place: England Publisher: The Physiological Society.

[63] J Mahaney, C Felton, D Taylor, W Fleming, J Q Kong, and C Baylis. Renal cortical Na+-K+-ATPase activity and abundance is decreased in normal pregnant rats. *American Journal of Physiology - Renal Physiology*, 275(5):812–817, 1998. Place: United States Publisher: American Physiological Society.

[64] Rex L. Jamison. Intrarenal heterogeneity: The case for two functionally dissimilar populations of nephrons in the mammalian kidney. *The American Journal of Medicine*, 54(3):281–289, March 1973.

[65] Yong-Kuan Jiang, Kai-Yue Xin, Hong-Wei Ge, Fei-Juan Kong, and Gang Zhao. Upregulation Of Renal GLUT2 And SGLT2 Is Involved In High-Fat Diet-Induced Gestational Diabetes In Mice. *Diabetes, Metabolic Syndrome and Obesity: Targets and Therapy*, 12:2095–2105, October 2019.

[66] J. Joyner, L. A. A. Neves, K. Stovall, C. M. Ferrario, and K. B. Brosnihan. Angiotensin-(1-7) serves as an aquaretic by increasing water intake and diuresis in association with downregulation of aquaporin-1 during pregnancy in rats. *American Journal of Physiology - Regulatory, Integrative and Comparative Physiology*, 294(3):1073–1080, 2008. Place: United States Publisher: American Physiological Society.

[67] James P. Keener. *Mathematical physiology*. Interdisciplinary Applied Mathematics ; Volume 8. Springer, New York, 1st ed. 1998. edition, 1998.

[68] Ali A. Khraibi, Anca D. Dobrian, Tianzheng Yu, Michael J. Solhaug, and Reinhart B. Billiar. Role of RIHP and Renal Tubular Sodium Transporters in Volume Retention of Pregnant Rats. *American journal of hypertension*, 18(10):1375–1383, 2005. Place: New York, NY Publisher: Elsevier Inc.

[69] Jin Kim, Young-Hee Kim, Jung-Ho Cha, C. Craig Tisher, and Kirsten M. Madsen. Intercalated Cell Subtypes in Connecting Tubule and Cortical Collecting Duct of Rat and Mouse. *Journal of the American Society of Nephrology*, 10(1):1–12, January 1999.

[70] Saulo Klahr, L. Lee Hamm, Marc R. Hammerman, and Lazaro J. Mandel. Renal Metabolism: Integrated Responses. In *Comprehensive Physiology*. John Wiley & Sons, Ltd, 2011.

[71] Mark A. Knepper, Robert A. Danielson, Gerald M. Saidel, and Robert S. Post. Quantitative analysis of renal medullary anatomy in rats and rabbits. *Kidney International*, 12(5):313–323, November 1977.

[72] Pratap Kumar and Navneet Magon. Hormones in pregnancy. *Nigerian Medical Journal : Journal of the Nigeria Medical Association*, 53(4):179–183, 2012.

[73] Anita T. Layton. Mathematical modeling of kidney transport. *WIREs Systems Biology and Medicine*, 5(5):557–573, 2013.

[74] Anita T. Layton. His and her mathematical models of physiological systems. *Mathematical Biosciences*, page 108642, June 2021.

[75] Anita T. Layton and Aurelie Edwards. *Mathematical Modeling in Renal Physiology*. Lecture Notes on Mathematical Modelling in the Life Sciences. Springer Berlin Heidelberg, Berlin, Heidelberg, 1st ed. 2014. edition, 2014.

[76] Anita T. Layton, Kamel Laghmani, Volker Vallon, and Aurélie Edwards. Solute transport and oxygen consumption along the nephrons: effects of Na+ transport inhibitors. *American journal of physiology. Renal physiology*, 311(6):F1217–F1229, 2016. Place: United States Publisher: American Physiological Society.

[77] Anita T. Layton and Harold E. Layton. A computational model of epithelial solute and water transport along a human nephron. *PLoS computational biology*, 15(2):e1006108–e1006108, 2019. Place: United States Publisher: Public Library of Science.

[78] Anita T. Layton and Jennifer C. Sullivan. Recent advances in sex differences in kidney function. *American Journal of Physiology-Renal Physiology*, 316(2):F328–F331, February 2019.

[79] Anita T. Layton and Volker Vallon. SGLT2 inhibition in a kidney with reduced nephron number: modeling and analysis of solute transport and metabolism. *American Journal of Physiology-Renal Physiology*, 314(5):F969–F984, May 2018.

[80] Anita T. Layton, Volker Vallon, and Aurélie Edwards. A computational model for simulating solute transport and oxygen consumption along the nephrons. *American journal of physiology. Renal physiology*, 311(6):F1378–F1390, 2016. Place: United States Publisher: American Physiological Society.

[81] Anita T. Layton, Volker Vallon, and Aurélie Edwards. Predicted consequences of diabetes and SGLT inhibition on transport and oxygen consumption along a rat nephron. *American Journal of Physiology-Renal Physiology*, 310(11):F1269–F1283, June 2016.

[82] Jessica Leete and Anita T. Layton. Sex-specific long-term blood pressure regulation: Modeling and analysis. *Computers in biology and medicine*, 104:139–148, 2019. Place: United States Publisher: Elsevier Ltd.

[83] Qianyi Li, Alicia A. McDonough, Harold E. Layton, and Anita T. Layton. Functional implications of sexual dimorphism of transporter patterns along the rat proximal tubule: modeling and analysis. *American journal of physiology. Renal physiology*, 315(3):F692–F700, 2018. Place: United States Publisher: American Physiological Society.

[84] M. D. Lindheimer and A. I. Katz. Kidney function in the pregnant rat. *The Journal of laboratory and clinical medicine*, 78(4):633–641, 1971. Place: United States.

[85] Marshall D. Lindheimer, Adrian I. Katz, Bruce M. Koeppen, Nelson G. Ordonez, and Suzanne Oparil. Kidney Function and Sodium Handling in the Pregnant Spontaneously Hypertensive Rat. *Hypertension (Dallas, Tex. 1979)*, 5(4):498–506, 1983. Place: United States Publisher: American Heart Association, Inc.

[86] Jamie O. Lo, John F. Mission, and Aaron B. Caughey. Hypertensive disease of pregnancy and maternal mortality. *Current Opinion in Obstetrics and Gynecology*, 25(2):124–132, April 2013.

[87] Eugenie R. Lumbers and Kirsty G. Pringle. Roles of the circulating renin-angiotensin-aldosterone system in human pregnancy. *American Journal of Physiology-Regulatory, Integrative and Comparative Physiology*, 306(2):R91–R101, January 2014. Publisher: American Physiological Society.

[88] Laura A Magee, Joel Singer, Terry Lee, Richard J McManus, Sarah Lay-Flurrie, Evelyne Rey, Lucy C Chappell, Jenny Myers, Alexander G Logan, and Peter von Dadelszen. Are blood pressure level and variability related to pregnancy outcome? Analysis of control of hypertension in pregnancy study data. *Pregnancy Hypertension*, 19:87–93, January 2020.

[89] Franck Mauvais-Jarvis, Noel Bairey Merz, Peter J Barnes, Roberta D Brinton, Juan-Jesus Carrero, Dawn L DeMeo, Geert J De Vries, C Neill Epperson, Ramaswamy Govindan, Sabra L Klein, Amedeo Lonardo, Pauline M Maki, Louise D McCullough, Vera Regitz-Zagrosek, Judith G Regensteiner, Joshua B Rubin, Kathryn Sandberg, and Ayako Suzuki. Sex and gender: modifiers of health, disease, and medicine. *The Lancet*, 396(10250):565–582, August 2020.

[90] Alicia A. McDonough and Jang H. Youn. Potassium Homeostasis: The Knowns, the Unknowns, and the Health Benefits. *Physiology*, 32(2):100–111, February 2017. Publisher: American Physiological Society.

[91] Harold Mcintyre, Patrick Catalano, Cuilin Zhang, Gernot Desoye, Elisabeth Mathiesen, and Peter Damm. Gestational diabetes mellitus. *Nature Reviews Disease Primers*, 5:47, July 2019.

[92] Katherine T Mills, Andrei Stefanescu, and Jiang He. The global epidemiology of hypertension. *Nature reviews. Nephrology*, 16(4):223–237, April 2020.

[93] S. K. Mujais, N. A. Nora, and Y. Chen. Regulation of the renal Na:K pump: role of progesterone. *Journal of the American Society of Nephrology*, 3(8):1488–1495, 1993. Place: United States.

[94] K. Munger and C. Baylis. Sex differences in renal hemodynamics in rats. *American Journal of Physiology-Renal Physiology*, 254(2):F223–F231, February 1988.

[95] Tina Napso, Hannah E. J. Yong, Jorge Lopez-Tello, and Amanda N. Sferruzzi-Perri. The Role of Placental Hormones in Mediating Maternal Adaptations to Support Pregnancy and Lactation. *Frontiers in Physiology*, 9:1091, August 2018.

[96] Nnabuike C. Ngene and Jagidesa Moodley. Physiology of blood pressure relevant to managing hypertension in pregnancy. *The Journal of Maternal-Fetal & Neonatal Medicine*, 32(8):1368–1377, April 2019.

[97] Mien T. X. Nguyen, Donna H. Lee, Eric Delpire, and Alicia A. McDonough. Differential regulation of $Na^+$ transporters along nephron during ANG II-dependent hypertension: distal stimulation counteracted by proximal inhibition. *American Journal of Physiology-Renal Physiology*, 305(4):F510–F519, August 2013.

[98] Ayodele Odutayo and Michelle Hladunewich. Obstetric Nephrology: Renal Hemodynamic and Metabolic Physiology in Normal Pregnancy. *Clinical Journal of the American Society of Nephrology*, 7(12):2073–2080, December 2012.

[99] M. Ohara, P. Y. Martin, D. L. Xu, J. St John, T. A. Pattison, J. K. Kim, and R. W. Schrier. Upregulation of aquaporin 2 water channel expression in pregnant rats. *The Journal of clinical investigation*, 101(5):1076–1083, 1998.

[100] O. Oudar, M. Elger, L. Bankir, D. Ganten, U. Ganten, and W. Kriz. Differences in rat kidney morphology between males, females and testosterone-treated females. *Renal Physiology and Biochemistry*, 14(3):92–102, June 1991.

[101] Seema Patel, Abdur Rauf, Haroon Khan, and Tareq Abu-Izneid. Renin-angiotensin-aldosterone (RAAS): The ubiquitous system for homeostasis and pathologies. *Biomedicine & Pharmacotherapy*, 94:317–325, October 2017.

[102] Rohit T. Rao and Ioannis P. Androulakis. Modeling the Sex Differences and Interindividual Variability in the Activity of the Hypothalamic-Pituitary-Adrenal Axis. *Endocrinology (Philadelphia)*, 158(11):4017–4037, 2017. Place: Washington, DC Publisher: Endocrine Society.

[103] Andrea Remuzzi, Stefania Puntorieri, Andrea Mazzoleni, and Giuseppe Remuzzi. Sex related differences in glomerular ultrafiltration and proteinuria in Munich-Wistar rats. *Kidney International*, 34(4):481–486, October 1988.

[104] Sofía P. Salas, Guillermo Marshall, Blanca L. Gutiérrez, and Pedro Rosso. Time Course of Maternal Plasma Volume and Hormonal Changes in Women With Preeclampsia or Fetal Growth Restriction. *Hypertension (Dallas, Tex. 1979)*, 47(2):203–208, 2006. Place: Philadelphia, PA, Hagerstown, MD Publisher: American Heart Association, Inc.

[105] Amel Salhi, Christine Lamouroux, Nikolay B. Pestov, Nikolaï N. Modyanov, Alain Doucet, and Gilles Crambert. A link between fertility and K+ homeostasis: role of the renal H,K-ATPase type 2. *Pflügers Archiv - European Journal of Physiology*, 465(8):1149–1158, August 2013.

[106] Silvi Shah. Hypertensive Disorders in Pregnancy. In Mala Sachdeva and Ilene Miller, editors, *Obstetric and Gynecologic Nephrology: Women's Health Issues in the Patient With Kidney Disease*, pages 11–23. Springer International Publishing, Cham, 2020.

[107] Baha M. Sibai. Diagnosis and Management of Gestational Hypertension and Preeclampsia. *Obstetrics & Gynecology*, 102(1):181–192, July 2003.

[108] Homer William Smith. *The kidney: structure and function in health and disease*. Oxford medical publications. Oxford University Press, New York, 1958. ISSN: 5100-3902.

[109] Melissa M. Stadt and Anita T. Layton. Adaptive changes in single-nephron GFR, tubular morphology, and transport in a pregnant rat nephron: modeling and analysis. *American Journal of Physiology-Renal Physiology*, 322(2):F121–F137, February 2022. Publisher: American Physiological Society.

[110] Sangita Swapnasrita, Aurélie Carlier, and Anita T. Layton. Sex-Specific Computational Models of Kidney Function in Patients With Diabetes. *Frontiers in Physiology*, 13, 2022.

[111] Gloria Valdés. Focus on today's evidence while keeping an eye on the future: lessons derived from hypertension in women. *Journal of Human Hypertension*, pages 1–5, January 2022. Publisher: Nature Publishing Group.

[112] Luciana C. Veiras, Adriana C. C. Girardi, Joshua Curry, Lei Pei, Donna L. Ralph, An Tran, Regiane C. Castelo-Branco, Nuria Pastor-Soler, Cristina T. Arranz, Alan S. L. Yu, and Alicia A. McDonough. Sexual Dimorphic Pattern of Renal Transporters and Electrolyte Homeostasis. *Journal of the American Society of Nephrology*, 28(12):3504–3517, 2017. Place: United States Publisher: American Society of Nephrology.

[113] Luciana C. Veiras, Brandon E. McFarlin, Donna L. Ralph, Vadym Buncha, Jessica Prescott, Borna S. Shirvani, Jillian C. McDonough, Darren Ha, Jorge Giani, Susan B. Gurley, Mykola Mamenko, and Alicia A. McDonough. Electrolyte and transporter responses to angiotensin II induced hypertension in female and male rats and mice. *Acta Physiologica (Oxford, England)*, 229(1):e13448, May 2020.

[114] Joseph G Verbalis. Disorders of body water homeostasis. *Best Practice & Research Clinical Endocrinology & Metabolism*, 17(4):471–503, December 2003.

[115] Arja Suzanne Vink, Sally-Ann B. Clur, Arthur A. M. Wilde, and Nico A. Blom. Effect of age and gender on the QTc-interval in healthy individuals and patients with long-QT syndrome. *Trends in Cardiovascular Medicine*, 28(1):64–75, January 2018.

[116] Carsten A. Wagner, Karin E. Finberg, Paul A. Stehberger, Richard P. Lifton, Gerhard H. Giebisch, Peter S. Aronson, and John P. Geibel. Regulation of the expression of the Cl-/anion exchanger pendrin in mouse kidney by acid-base status. *Kidney International*, 62(6):2109–2117, December 2002.

[117] A M Weinstein. A kinetically defined Na+/H+ antiporter within a mathematical model of the rat proximal tubule. *Journal of General Physiology*, 105(5):617–641, May 1995.

[118] Alan M. Weinstein. Mathematical models of renal fluid and electrolyte transport: acknowledging our uncertainty. *American Journal of Physiology-Renal Physiology*, 284(5):F871–F884, May 2003.

[119] Alan M. Weinstein. A mathematical model of the rat nephron: glucose transport. *American Journal of Physiology-Renal Physiology*, 308(10):F1098–F1118, May 2015.

[120] Alan M. Weinstein. A mathematical model of the rat kidney: $K^+$-induced natriuresis. *American Journal of Physiology-Renal Physiology*, 312(6):F925–F950, June 2017.

[121] Alan M. Weinstein. A mathematical model of the rat kidney. II. Antidiuresis. *American Journal of Physiology-Renal Physiology*, 318(4):F936–F955, April 2020.

[122] Alan M. Weinstein. A mathematical model of the rat kidney. IV. Whole kidney response to hyperkalemia. *American Journal of Physiology-Renal Physiology*, 322(2):F225–F244, February 2022.

[123] Alan M. Weinstein, Sheldon Weinbaum, Yi Duan, Zhaopeng Du, QingShang Yan, and Tong Wang. Flow-dependent transport in a mathematical model of rat proximal tubule. *American Journal of Physiology - Renal Physiology*, 292(4):1164–1181, 2007. Place: United States Publisher: American Physiological Society.

[124] A.M. Weinstein. Nonequilibrium thermodynamic model of the rat proximal tubule epithelium. *Biophysical Journal*, 44(2):153–170, November 1983.

[125] Crystal West, Zheng Zhang, Geoffrey Ecker, and Shyama M. E. Masilamani. Increased renal alpha-epithelial sodium channel (ENAC) protein and increased ENAC activity in normal pregnancy. *American journal of physiology. Regulatory, integrative and comparative physiology*, 299(5):R1326–R1332, 2010. Place: United States Publisher: American Physiological Society.

[126] Crystal A. West, Steven D. Beck, and Shyama M. E. Masilamani. Time course of renal sodium transport in the pregnant rat. *Current Research in Physiology*, 4:229–234, January 2021.

[127] Crystal A. West, Weiquing Han, Ningjun Li, and Shyama M. E. Masilamani. Renal epithelial sodium channel is critical for blood pressure maintenance and sodium balance in the normal late pregnant rat: Renal epithelial sodium channel blockade in late pregnancy. *Experimental physiology*, 99(5):816–823, 2014.

[128] Crystal A. West, Alicia A. McDonough, Shyama M. E. Masilamani, Jill W. Verlander, and Chris Baylis. Renal NCC is unchanged in the midpregnant rat and decreased in the late pregnant rat despite avid renal Na+ retention. *American journal of physiology. Renal physiology*, 309(1):F63–F70, 2015. Place: United States Publisher: American Physiological Society.

[129] Crystal A. West, Jennifer M. Sasser, and Chris Baylis. The enigma of continual plasma volume expansion in pregnancy: critical role of the renin-angiotensin-aldosterone system. *American Journal of Physiology-Renal Physiology*, 311(6):F1125–F1134, October 2016. Publisher: American Physiological Society.

[130] Crystal A. West, Jill W. Verlander, Susan M. Wall, and Chris Baylis. The chloride–bicarbonate exchanger pendrin is increased in the kidney of the pregnant rat. *Experimental physiology*, 100(10):1177–1186, 2015. Place: England Publisher: Wiley Subscription Services, Inc.

[131] Crystal A. West, Paul A. Welling, Jr West, Richard A. Coleman, Kit-Yan Cheng, Chao Chen, Jr DuBose, Jill W. Verlander, Chris Baylis, and Michelle L. Gumz. Renal and colonic potassium transporters in the pregnant rat. *American journal of physiology. Renal physiology*, 314(2):F251–F259, 2018. Place: United States Publisher: American Physiological Society.

[132] David A. West, Steven D. Beck, Aline M. A. de Souza, and Crystal A. West. Proteinase-activated receptor-2 (PAR2) on blood pressure and electrolyte handling in the late pregnant rat. *Experimental Physiology*, 106(6):1373–1379, 2021. _eprint: https://onlinelibrary.wiley.com/doi/pdf/10.1113/EP088170.

[133] Lei Yang, Yuanyuan Xu, Diego Gravotta, Gustavo Frindt, Alan M. Weinstein, and Lawrence G. Palmer. ENaC and ROMK channels in the connecting tubule regulate renal K+ secretion. *Journal of General Physiology*, 153(8):e202112902, June 2021.

[134] Jang H. Youn. Gut sensing of potassium intake and its role in potassium homeostasis. *Seminars in nephrology*, 33(3):248–256, May 2013.

[135] Jang H. Youn and Alicia A. McDonough. Recent Advances in Understanding Integrative Control of Potassium Homeostasis. *Annual review of physiology*, 71:381–401, 2009.